Mechanical and Tribological Properties of Nanoceramics Dispersion Strengthened 2205 Duplex Stainless Steel

by

MAHLATSE RAMAESELE MPHAHLELE

DISSERTATION

Submitted in fulfilment of the requirements for

MASTERS DEGREE

of

CHEMICAL ENGINEREERING TECHNOLOGY

in the

FACULTY OF ENGINEERING AND BUILT ENVIRONMENT

at the

UNIVERSITY OF JOHANNESBURG

SUPERVISOR: PROF. OLUBAMBI PETER A.

CO-SUPERVISOR: DR. IGE OLADEDJI O.

January, 2018

DECLARATION

I, the undersigned, hereby declare that this dissertation, which I herewith submit for the qualification of

MASTERS OF CHEMICAL ENGINEERING TECHNOLOGY

to the University of Johannesburg, Department of Chemical Engineering, is my own work apart from the recognised assistance of my supervisors, and has not previously been submitted by me to another institution to obtain a research degree.

Signature: ……...…..

Date: ……/……./…….....

DEDICATION

This work is dedicated to my late loving Mother, Mrs Leah Magalane Mphahlele, my dear Father Mr Monope Rolland Mphahlele, my sweet beautiful daughter Tshegofatso Moloko Hlaka, my entire family, and above all to the All Mighty God.

ACKNOWLEDGEMENT

Primarily I want to thank my Father in Heaven, The Omnipotent God. I am forever grateful for all that He has done for me and for His continued grace upon my life. It is not by might or power but by His Spirit to see me through this phase of my life. EMMANUEL.

I am thankful to my supervisor, Prof. Peter Apata Olubambi for encouraging me to pursue postgraduate studies. Words cannot express the gratitude for having the privilege of working with him. His amicable character and the love for his work are commendable and I am grateful I had the privilege to tap into them. I also appreciate his support, guidance, and advices.

I am grateful to my co-supervisor, Dr. Oladeji O. Ige for his guidance, wise and encouraging advices. I appreciate his patience with me and for always believing in me. His timely responses to matters regarding my research work is also acknowledged.

I specially thank my project partner and mentor, Mr. Samuel Ranti Oke for his in-puts to my research work. I also appreciate his guidance and advices. It has truly been an honour to work with him, I have learned so much from him.

I appreciate the Advanced Materials and Tribocorrosion Characterization Research Laboratory at the Department of Chemical, Metallurgical and Materials Engineering in Tshwane University of Technology for granting me access to their scanning electron microscope (SEM). Furthermore, I appreciate the assistance of Lawrence Bamidele and Pabi with the use of the SEM.

I thank all my colleagues (Mosima Maja, Segun Falodun, Akinribide Ojo, Victor and Scott) in the Centre of Nanoengineering and Tribocorrosion at the University of Johannesburg, for the various ways they assisted in my research experimental work.

I give special thanks to my loving family; dad, Monope Rolland Mphahlele and my siblings: Namedi Mphahlele, Ramatsimele Ferry Matabane, Leshiretje Alfred Mphahlele, Lebogang Mphahlele and Mmabatho Mphahlele as well as to my nieces and nephews for their continued support, prayers and well wishes with my studies. Special thanks to my **daughter** for her unconditional love and for always cheering me up.

My special thanks to the National Research Foundation (NRF), South Africa for the scholarship awarded me to pursue this MSc programme.

LIST OF JOURNAL ARTICLES AND CONFERENCE PRESENTATIONS

Journal Articles

[1] **Mphahlele, M.R.,** Oke, S.R., Ige, O.O., Falodun, O.E., Obadele, B.A. and Olubambi, P.A. (2017) Nanoindentation studies on the mechanical properties of TiN nanoceramics reinforced SAF 2205 fabricated via spark plasma sintering. Journal of Materials Research and Technology (Under review).

[2] Oke, S.R., Ige, O.O., Falodun, O.E., Obadele, B.A., **Mphahlele, M.R.** and Olubambi, P.A. (2017). Influence of sintering process parameters on corrosion and wear behaviour of SAF 2205 reinforced with nano-sized TiN. Materials Chemistry and Physics. 206,166-173

Conference Presentations

[3] **Mphahlele, M.R.,** Oke, S.R., Ige, O.O., Falodun, O.E., Obadele, B.A. and Olubambi, P.A. (2018) A Correlation Between Nano and Micro-Hardness Properties of TiN nanoparticles Strengthened SAF 2205. The 4th International Conference on Structural Nano Composites, 23-24 May, Berlin, Germany. (Accepted for oral presentation and Publication)

[4] **Mphahlele, M.R.,** Oke, S.R, Ige, O.O., Falodun, O.E., Obadele, B.A. and Olubambi, P.A. (2017) Nanoindentation studies on the elastic and plastic deformation properties of sintered SAF 2205 reinforced with TiN Nanoparticles. Proceedings of 14th International Conference on Fracture, June 18-23, 2017, Rhodes, Greece.

[5] **Mphahlele, M.R.,** Oke, S.R., Ige, O.O., Falodun, O.E., Obadele, B.A. and Olubambi, P.A. (2017) Wear Studies on nano TiN dispersed SAF 2205. Proceedings of the Microscopy Society of South Africa, Vol XLVII MSSA, ISBN: 978-0-620-78235-7.

[6] Oke, S.R., Ige, O.O., Falodun, O.E., Obadele, B.A., **Mphahlele, M.R**. and Olubambi, P.A. (2017). Influence of Sintering Temperature on Hardness and Wear Properties of TiN Nano Reinforced SAF 2205. In *IOP Conference Series: Materials Science and Engineering* 272 (1), 012030. IOP Publishing.

[7] Oke, S.R., Ige, O.O., Falodun, O.E., Obadele, B.A., **Mphahlele, M.R**. and Olubambi, P.A (2018). Dependence of wear and corrosion properties on holding time of spark plasma sintered SAF 2205 reinforced with TiN nanoparticles. Presented at the IEEE 9th International Conference on Mechanical and Intelligent Manufacturing Technologies, February 10-13, Cape town, South Africa. (Accepted for publication)

ABSTRACT

Conventional Duplex Stainless Steel used in industrial applications suffers degradation in wear and mechanical properties. A good approach to solve these problems is the dispersion of second phase nanoparticles into duplex stainless steel matrix to improve its strength and properties. Taking the advantage of the high hardness and high chemical stability of titanium nitride (TiN), efforts were made to disperse varying amounts of TiN nanoparticles into the matrices of SAF 2205 to enhance its properties. Hence the mechanical properties and tribological behaviour of the duplex stainless steel (SAF 2205 DSS) strengthened with varied amounts of titanium-based ceramics using nanoindentation system and tribometers were studied. The elastic and plastic deformation properties of the DSS composite materials were determined with a nanoindenter together with the wear behavior of the DSS samples using the strain-to-break (H/Er) and the plastic deformation (H^3/Er^2) parameters. Also the wear characteristics were estimated with a Tribometer, and Electron Microscopy-Energy Dispersive Spectroscopy (SEM-EDS) was employed to evaluate the morphology and chemistry of the wear scar of the DSS composite. The TiN nanoceramics reinforced SAF 2205 composites were fabricated using spark plasma sintering using optimized process parameters: sintering pressure (50MPa), sintering temperature (1150 ^oC), heating rate (100 ^oC/min) and sintering holding time (15 minutes). The TiN dispersions into the SAF were varied between 0 - 8 wt% at an interval of 2 wt%. Nanoindentation technique was used to access the plastic (H) properties, elastic (E) properties, the strain-to-break parameter (H/Er) and the resistance to plastic deformation parameter (H^3/Er^2) behaviour of the composites under loading and unloading conditions. The wear properties of coefficient of friction, wear loss, wear and specific wear rates under dry sliding conditions and varying loads and worn surface were investigated. The microstructures and worn surfaces of the composites were then evaluated using JEOL Scanning Electron Microscopy (FESEM, JSM-7600F). The results show that the TiN is evenly dispersed in the duplex matrix with a general tendency to locate itself at the grain boundaries. The mechanical properties improved considerably as the TiN content increased, resulting from grain boundary refinements and better dispersion strengthening mechanisms. The grain boundaries have better hardness and reduced young modulus compared to the grains. Furthermore, the ratios H/Er and H^3/Er^2 increased as the TiN composition increases which demonstrates that the nanocomposites wear resistance is favourable and it was in good correlation with the wear test data. The worn mechanism was a mixed mode of adhesive-abrasive at lower TiN composition but at higher TiN content, the adhesive mechanism prevails. This study established that increasing the addition of nanosized titanium nitride confers better microstructural properties, nanoindentation properties and wear behaviour on spark plasma sintered SAF 2205. Nanocomposite with DSS–6 % TiN reinforcement is recommended for industrial applications.

TABLE OF CONTENTS

LIST OF FIGURES

LIST OF TABLES

LIST OF ACRONYMS

A / Ac	Area / Contact Area
AFM	Atomic Force Microscopy
AM	Additive Manufacturing
ASTM	American Standard Testing Method
BH	Brinell Hardness
CoF	Coefficient of Friction
Cr	Chromium
D	Diameter
DSS	Duplex Stainless Steel
E / Er	Elastic Modulus / Reduced Elastic Modulus
EDS	Energy Dispersive Spectroscopy
FAST	Field Assisted Sintering
Fe	Iron
FGM	Functional Graded Materials
GNDs	Geometrically Necessary Dislocations
H / HIT	Hardness
HIP	Hot Isostatic Pressin
HSPS	Hybrid Spark Plasma Sintering
IAF	Indenter Area Function
ISE	Indentation Size Effects
ISO	International Organization for Standardization
KHN	Knoop Hardnes Number
L / P	Load
LENS	Laser Engineering Net Shaping

MIM	Metal Injection Moulding
MMC	Metal Matrix Composite
MMNC	Metal Matrix Nano-Composite
Ni	Nickel
PAM	Powder Additive Manufacturing
PECS	Pulsed Electric Current Sintering
PIM	Powder Injection Moulding
PMAX	Maximum Load
PREN	Pitting Resistance Equivalent
SEM	Scanning Electron Microscope
SLS/SLM	Selective Lase Sintering/Melting
SPS	Spark Plasma Sintering
SSDs	Statistically Stored Dislocations
UNHT	Ultra Nanoinder High Temperature
TAF	Tip Area Function
TEM	Transmission Electron Microscope
3DP	Three Dimensional Printing
TRB	Tribometer
TiN	Titanium Nitrite
VHN	Vickers Hardness Number
XRD	X-ray Diffraction

CHAPTER 1: INTRODUCTION

Severe process conditions existing in the mineral processing, pulp and paper, chemical, and oil industries demand the use of materials with good mechanical properties [Bhowmick and Nowell, 2014]. Amongst many materials, stainless steels are one of the most used engineering materials worldwide in the process industries. There are several prospective classes of stainless steels and are classified based on the characteristic crystallographic structure; namely the ferritic, austenitic, martensitic and duplex [Klar and Samal, 2007]. Duplex stainless steels are the most preferred to other stainless steels due to the characteristics that are of outmost interest in many applications [Dobrzanski *et al*., 2005]. These steels are available in different grades that are the lean, standard and superduplex, amongst which the standard grade is the most used [Charles, 2008].

Duplex steels are known to consist of dual phases, namely the austenite and ferrite phases. The combination of these two phases produces the type of steel with characteristics that supersede those of the austenitic and ferritic counterparts [Sotomayor *et al.*, 2013]. They possess good corrosion resistance in numerous environments; it is especially resistant to stress corrosion cracking and pitting corrosion [Saeidi *et al.*, 2016].

Besides excellent corrosion resistant properties, duplex stainless steels are widely employed in the process industries due to their ability to withstand high pressure, erosive and abrasive environments in process industries. They are often used in the manufacturing of pump, valves and impellers. Owing to their characteristics strength that is twice as much as that of the austenite [Marappan *et al.*, 2011], smaller pumps can be used in place of larger pumps made of other materials.

Despite the good mechanical properties duplex stainless steel (DSS) possesses, it however still suffers some limitations. DSS tend to wear off easily when subjected to high pressure abrasive medium as compared to the lean duplex grades [Aribo *et al.*, 2013]. As the result of the interaction of flow speeds, viscosity, particle shapes and types material etc. to the duplex steel surface of the structural component, the steels tend to wear off gradually [Lindgren *et al.*, 2015] and would eventually lead to failure of the components. Therefore, global focus has been directed towards improving the properties of these duplex steels. Amongst the varying efforts, the dispersions of secondary phases within the matrixes of duplex stainless steels has been observed as a very promising route for improving their strength.

Transition metal nitrides such as titanium nitride (TiN) have emerged as an effective ceramic material [Oyama, 1996] that holds high potential for improving the strength of duplex stainless steels if finely and evenly dispersed within their matrixes. The contribution of grain growth prevention, chemical stability, high hardness and elastic modulus of nitrogen and weight reduction and formability of titanium makes TiN to have excellent properties [Zhang *et al.*, 2016] such as outstanding strength and rigidity, good stability at high temperatures and excellent wear resistance [Guo *et al.*, 2015]. Although duplex stainless steels can be successfully manufactured using various techniques [Hanninen *et al.*, 2001] such as casting, powder metallurgy and the various metal forming processes, the powder metallurgy route stands the comparatively best option for producing duplex stainless steel components with well dispersed ceramics reinforcements.

The characteristics of the powder metallurgy products [Enneti *et al.*, 2012] such as the combination of chemical constituents, controlled porosity and microstructure as well as improved mechanical properties can be achieved through the use of enhanced powder feedstock and preparations. Furthermore, the use of powder metallurgy fabrication process can facilitate the production of intricate shapes that are not easily achieved with conventional fabrication methods [Voisin *et al.*, 2013]. Powder metallurgy also eliminates technical difficulties experienced using conventional methods when producing the same material [Dobrzanski *et al.*, 2005]. For instance, the novel powder metallurgy spark plasma sintering facilitates the production of ultrafine microstructure containing minimal pores and it has the advantage of short sintering time [Dong *et al.*, 2016].

There is always the need to assess the performance integrity of any newly developed materials in conditions typical of service life, despite robustness of the materials systems and processing technique adopted to fabricate it. It is therefore important to explore improved techniques for assessing the probable service performance of any developed materials. Amongst available materials testing methods, the nanoindentation testing system has become a widely used technique for ascertaining various mechanical properties of materials. Their use has grown significantly over the past two decades due to the advancements made to the systems [Wheeler *et al.*, 2015]. The attractive benefits of lower cost of sample manufacture and preparation, small device sizes, and higher speed are some of the features offered by the systems [Wheeler and Michler, 2013]. Nanoindentation uses smaller applied load in comparison to micro or macro hardness tester for determination of the plastic and elastic

properties of materials [Kralik and Nemecek, 2014]. Furthermore, for application such as in pumps, the tendency of the pumps to wear off makes it ideal to determine the wear behaviour of the produced materials. The ball/pin on disk tribometer is a widely used technique to determine the wear behaviour and the friction coefficient of materials. The technique allows for simulation of real-time wear behaviour of materials facilitating easy transition from lab-scale to industries. Furthermore, it offers the benefits of simplicity of use and reliable data.

Although the nanoindentation techniques has been widely used for mechanical property testing of various materials, the gap remains in the evaluation of the mechanical properties of TiN nanoparticle dispersion strengthened DSS. As there are limited studies on the application of nanoindentation on assessing the service performance of spark plasma sintered DSS reinforced with TiN nanoparticles, it was decided in this study to use nanoindentation technique to assess the various mechanical properties of these newly developed materials. It was also decided to explore using the conventional tribological testing to corroborate the wear properties that were estimated from the nanoindentation testing technique.

1.1 Research Problem

One huge limitation of DSS is the difficulty to machine it, as required with conventional production methods, due to their high toughness and low thermal conductivity [Paro *et al.*, 2001]. Post production methods usually result in irregular wear and deterioration of machined surface which influence negatively on the efficacy of the material and productivity [Krolczyk *et al*., 2014]. Alternatively, powder metallurgy spark plasma sintering facilitates the production of complex shapes and eliminates technical difficulties experienced using conventional methods when producing the same material [Dobrzanski *et al.*, 2005; Voisin *et al.*, 2013] and save costs as production time is much shorter than in conventional methods.

The DSS -TiN is a new material being developed which promises the extension of DSS materials to aggressive environments for use in pumps, impellers and pipeline structures. However, the properties of this material are not yet known, which brings about the objective for this research. Studies on nanoindentation and tribology techniques for testing this type of material are not reported. Nevertheless, several researchers used nanoindentation on the biphasic duplex steel [Guo *et al.*, 2013; Gadelrab *et al.*, 2012; Schwarm *et al.*, 2017].

The problem faced by mechanical testing is that conventional methods of testing require big samples and they only provide the overall mechanical properties of the samples. As a result, it is not possible to determine the individual mechanical properties and the possibility of

understanding the influence of the grain boundary and the different phases of DSS using conventional methods. Therefore, conventional method of testing is subjective and do not account for the role of the grain boundary and the phases towards the materials performance. Fortunately, the concept of nanoindentation allows testing of constituent phases and grain boundaries. The results can therefore be used to estimate the general properties of the material.

Another major challenge in mechanical testing using nanoindentation is the sensitivity of the nanoindentation system, because of the small applied loads any small vibrations caused by movements and noise coming from either people or transportation in close proximity to the system can interfere with the tests. The interference usually manifests in pop-in or pop-out behaviour in the test data on graphs. However, ensuring that there is minimal movement and noise in the testing area can produce reliable test data.

In respect to surface integrity, both the tribology (most challenges in tribology are associated with surface integrity) and nanoindentation systems requires the sample to be flat as the indenter moves the distance pre-determined in the set-up stage and assumes that the sample is flat throughout. Also, care should be taken as to the amount of stress is applied during the preparation of the samples as this can affect the performance of the structural component by inducing fatigue and stress corrosion cracking behaviour [Zhou *et al.*, 2016].

1.2 Aim and Objectives

The research mainly aims to study the mechanical properties and the tribological behaviour of the duplex stainless steel (SAF 2205 DSS) strengthened with varied amounts of titanium-based ceramics using nanoindentation system and tribometer, respectively. The stated aim would be achieved through the following objectives:

1. Study the elastic and plastic deformation properties of the SAF 2205 composite materials using a Nanoindenter.
2. Estimate the wear behavior of the SAF 2205 samples using the strain-to-break (H/Er) and the plastic deformation (H^3/Er^2) parameters.
3. Determine the wear behavior of the SAF 2205 composites using a Tribometer.
4. Study the morphology and the chemistry of the wear scar using Electron Microscopy-Energy Dispersive Spectroscopy (SEM-EDS).

1.3 Justification for the Research

DSS 2205 -TiN is a new material being developed, therefore, their properties are not yet known. Moreover, studies on nanoindentation and tribology as methods for testing the mechanical and wear properties of this type of material are not reported. Owing to the fact that nanoindentation technique has only gained recognition in the last twenty years, there is not much literature available in determining the mechanical properties of spark plasma sintered DSS reinforced with TiN. Therefore, this study aimed at addressing the gap.

The use of nanoindentation technique will enable the determination of the intrinsic nano-scale and micro-scale properties of constituent and combined phases of DSS that are unobtainable using the conventional materials testing techniques. Furthermore, information from nanoindentation studies can be easily obtained and directly correlated with SPS techniques for developing and fabricating bulk nanostructured DSS with improved engineering properties.

Moreover, this study will make it possible to extend the applications of the duplex grades to very aggressive environments. This development is also economically viable as it will cut cost to industries as the need to replace the structural components will be minimised due to the extended life span of the duplex stainless steel. Additionally, the strength to weight ratio of the duplex will allow smaller pumps to be used saving space and consequently saving energy as less power will be required to run industrial processes.

1.4 Scope of the Work

The scope of this work involved using the novel testing technology in the literature to determine the mechanical and wear properties of duplex stainless steel that have been reinforced with titanium nitride with the objective to improve its performance in pumps, impellers and pipelines. The as received samples were mechanically prepared and etched using Carpenter's etchant and characterised using optical microscopy, scanning electron microscope (SEM) and electron dispersive spectroscopy (EDS). The prepared samples were tested for mechanical properties in terms of hardness and elastic modulus with a nanoindenter. The coefficient of friction and wear behaviour were determined using a tribometer. The wear intensity was validated using the SEM and the chemistry of the wear scar was evaluated using EDS.

1.5 Structure of the Dissertation

Chapter 1 presents an introduction to the research study, research problems, Justification of the research study, aim and objectives and the scope of the research study. **Chapter 2** gives a literature review of metal matrices of duplex stainless steel and titanium nitride, powder metallurgy production methods and tribology as a method to test the wear and friction properties. It also present the evolving field of nanoindentation as a system to determine mechanical properties of materials, particularly the metal matrix nanocomposite (MMNC) of duplex stainless steel (DSS) and titanium based ceramics as a focus for this research study. **Chapter 3** presents the experimental approach that outlines the materials, fabrication method, characterisation methods and testing methods used for this study. **Chapter 4** gives the microstructure, plastic, elastic properties, wear and worn surface analysis of the spark plasma sintered SAF 2205 evaluated using the nanoindentation and ball on disc wear techniques were discussed. Additionally, it gives the strain-to-break, plastic deformation parameters were used to estimate the resistance of the composites to wear in comparison to the coefficient of friction, wear volume and wear rate analyses. **Chapter 5** the conclusions drawn from the results obtained from the research study and recommendations made are presented here. Recommendations for further studies were suggested. **Chapter 6** contains references used for this work.

CHAPTER 2: LITERATURE REVIEW

2.1. Introduction

This chapter gives an overview of metal matrices of duplex stainless steel and titanium nitride, powder metallurgy production methods and tribology as a method to test the wear and friction properties. It also presents the evolving field of nanoindentation as a system to determine mechanical properties of materials, particularly the MMNC of duplex stainless steel (DSS) and titanium based ceramics as a focus for this research study.

2.2. Metal Matrix Nanocomposites (MMNCS)

Metal matrix nanocomposites (MMNCs) are composite materials which combines ductile metal or alloy matrix with ceramic reinforcement of nano size. Recently, nano-dispersion matrices have gained popularity over traditional metal matrix composites (MMCs) due to their attractive characteristics [Oke *et al.*, 2017] contributed by the combination of both the ductile metal and ceramic reinforcement. They are characterised by high density, hardness, specific modulus, strength-to-weight ratio, fatigue strength, temperature stability, great wear resistance, and corrosion resistance [Saheb *et al.*, 2014; Saxena *et al.*, 2017]. Compared to MMCs, MMNCs have proven to show better mechanical and wear properties due to the size effect of the nanoreinforcement [Mouawad *et al.*, 2014].

2.3. Duplex Stainless Steels and their Shortcomings

Duplex stainless steels are a special class of steel that have been in existence for about nine decades and have been of much interest for producers and users of stainless steel in the last three decades due to the advances in steelmaking techniques [Charles, 2008]. Duplex steels exist as the biphasic microstructure of the body-centred cubic (BCC) ferrite/alpha iron and face centred cubic (FCC) austenite/gamma iron phase in approximate equal volume ratios [Saeidin *et al.*, 2016], Figure 2.1. The popularity of these steel arise from the combined characteristics offered by the two phases.

Generally, duplex stainless steels are characterised by high strength-to-weight ratio. The high strength in duplex steel is largely contributed by the ferrite phase [Dobrzanski *et al.*, 2005; Sahu *et al.*, 2009]. The duplex steel is widely known to have strength that is about twice as much as its counterparts [Saeidi *et al.*, 2016]. As a result, thinner sections can be used for weight savings, making it financially and ecologically viable [Donik *et al.*, 2009]. Weight saving is an important aspect in this era where shrinkage of component size is viable due to

the limitation of space resulting from high population density and overwhelming increase in industrialisation of land.

In contrast, the austenite phase in duplex contributes towards its toughness [Saeidi *et al.*, 2016; Dobrzanski *et al.*, 2005]. Toughness is described as the ability of a material to absorb energy and plastically deform without fracturing. Therefore, the good toughness of the duplex steel plays a huge role in maximising the mechanical properties of the material [Saeidi *et al.*, 2016; Dobrzanski *et al.*, 2005]. As a result, failure that is usually very severe in pumps, valves and impellers is greatly minimized.

Furthermore, the material offers good corrosion resistance in wide range of environments due to the presence of austenite phase [Saeidi *et al.*, 2016]. It is particularly resistant to stress corrosion cracking largely due to the ferrite content although the chemistry of the exposure and the ratio balance of the two phase plays a primary role [Bhattacharya and Singh, 2007] and localized corrosion due to high Chromium, Molybdenum and Nitrogen additions [Alvarez-Armas, 2008; Loto, 2017]. Since there is no standardized measure of corrosion resistance, the most appropriate way is to use Pitting Resistance Equivalent Number [www.utokumpu.org] (Table 2.1 shows how DSS compares with its counterparts) which can be denoted as follows: PREN = %Cr +3.3×%Mo + 16×%N [Charles, 2008].

It has been reported that the biphasic stainless steels have proven to be an alternative to their competitors based on the aforementioned advantages [Balancin *et al.*, 2013]. With the recent focus to improve the duplex stainless steel gaining remarkable momentum, the future of duplex family is even more promising.

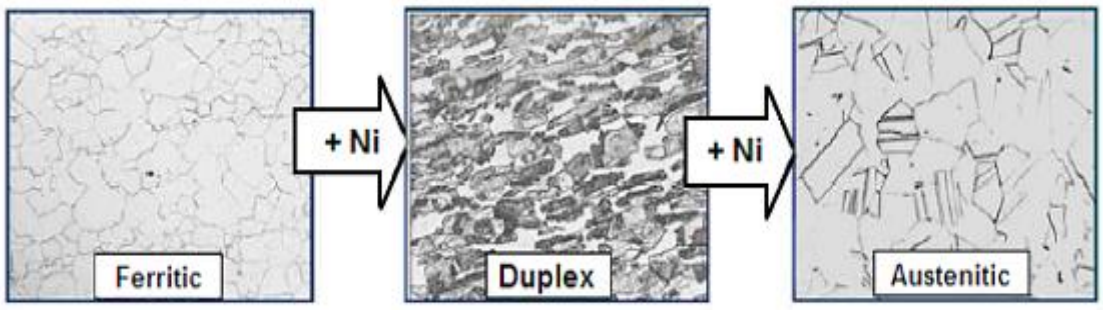

Figure 2.1: Schematic diagram of the Austenite, Ferrite and DSS microstructure [Yunan *et al.*, 2009].

2.3.1. Duplex Stainless Steel Grades

Duplex steels come in different grades (Table 2.1) according to their alloying elements [Lasebikan *et al.*, 2013] that also contribute to the overall performance of the steels. Naturally, between the austenitic and the ferritic areas, we obtain a mixture of ferrite and austenite microstructure; known as the duplex area (Figure 2.2). The duplex steel contains approximate 50% ferrite and 50% austenite phases by volume [Chail and Kangas, 2016]. They are categorised as the lean, standard, super and hyper duplex type. The standard duplex stainless steel known as SAF 2205 is the most used amongst the duplex grades [Charles, 2008].

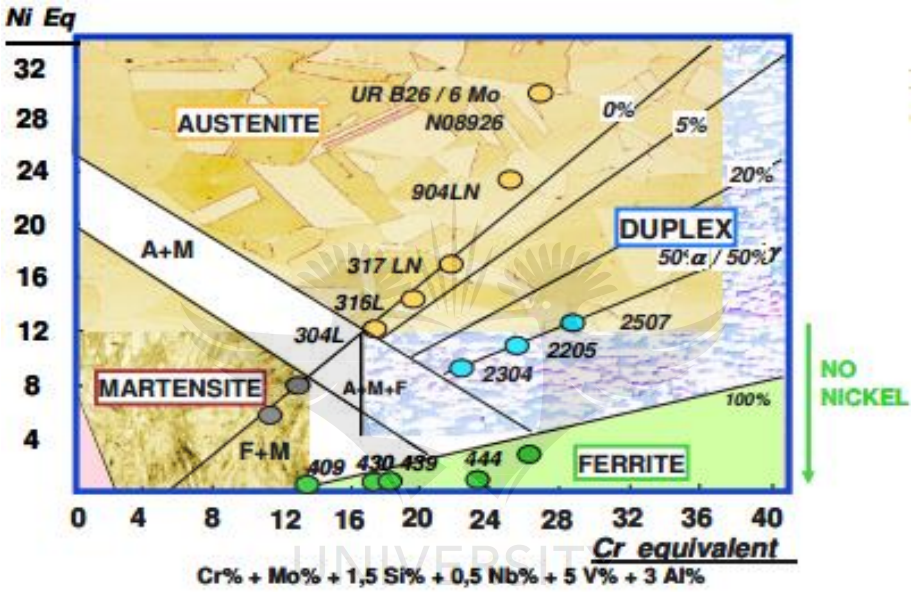

Figure 2.2: Schaeffler diagram [Charles, 2008].

Table 2.1: Typical composition of duplex stainless steel

		Alloying Elements Compositions (wt%)							
Duplex Grades	**UNS No.**	**C**	**Cr**	**Ni**	**Mo**	**N**	**Mn**	**Cu**	**PREN**
Lean 2101	S32101	0.04	21-22	1.3-1.7	0.1-0.8	0.2-0.25	4.0-6.0	0.1-0.8	25-27
Standard 2205	S32205	0.3	22-23	4.5-6.5	3.0-3.5	0.14-0.2	2.0		35-36
Super 2507	S32705	0.03	24-26	6.0-8.0	3.0-5.0	0.24-0.32	1.2	0.5	40-43

2.3.1.1. Lean Duplex

Lean duplex forms part of the first family of duplex stainless steel grades that have lower additions of the pricey molybdenum and nickel. For this type of steel, phase stability is achieved through the addition of manganese, one of the austenitic stabilizing elements [Charles, 2008; Zhao *et al.*, 2017]. Lean duplex stainless steel such as 2101 and 2304

contains no deliberate Molybdenum addition with nickel content of less than 3 wt%. Due to lower alloying content, the chance of forming sigma and alpha phases at high temperature is minimized [Dille *et al.*, 2017].

2.3.1.2. Standard Duplex

The standard duplex usually referred to as SAF 2205 is the most preferred type of duplex amongst the duplex steel family [Chan and Tjong, 2014]. The steel accounts for more than 80% of duplex use globally [Charles, 2008]. The steel is of the type 22Cr 5Ni 3Mo 017N having the corrosion resistance of which lies between AISI 316 and 6 wt% Mo + N superaustenitic grades. Therefore, the standard duplex steel balances both the benefit of low price and impact toughness compared to the other grades of duplex stainless steel [Saxena *et al.*, 2017].

2.3.1.3. Super Duplex

Super duplex stainless steel denotes the highly alloyed and high performance duplex steel containing 25-26 wt% Chromium and increased Molybdenum and Nitrogen. However, the high levels of alloys make the steel susceptible to formation of intermetallic phases [Michalska and Sozanska, 2006]. The amount of the alloying elements is sufficient to produce a pitting resistance equivalent (PREN) of more than 40 [Olsson, 2005]. An example of this type of duplex grade is the duplex 2507.

2.3.1.4. Hyper Duplex

Hyper duplex is a type of duplex stainless steel that is highly alloyed and especially developed for extra high strength and excellent corrosion resistance and structure stability [Chail and Kangas, 2016]. However, hyper duplex stainless steel experience the highest forming of secondary phases, sigma (Σ) and alpha prime (σ′) as the amount of precipitations of this phases increases with increased amounts of ferrite stabilizing elements particularly chromium and molybdenum [Stradomski and Dyja, 2009]. The uniqueness of these materials is in its high nitrogen contents which are up to about 0.5 wt% and its exceptional pitting resistance equivalent number (PRE)-values which are as high as 50, without compromising on the fabricability. It should also be reckoned with that the driving force of this type of steel is its higher chromium additions and partial replacement of molybdenum, to accomplish stabilisation of the grade with reduced sensitivity to intergranular phase precipitations when heated [Charles, 2008].

2.3.2. Phase Precipitation in DSS

Production processes or use of duplex stainless steel unavoidably introduces disadvantages as a result of the alloying elements added to the steel [Pohl *et al.*, 2007]. Although these additions are aimed to enhance the performances of the material, they also encourage microstructural instability of the material [Escriba *et al.*, 2009]. These instabilities usually occur when the steel is subjected to elevated temperatures which result in intermetallic phase precipitation [Sahu *et al.*, 2009], Figure 2.3.

Unfortunately, the precipitations compromise the materials competency [Fargas *et al.*, 2013]. Phase precipitation in duplex occurs at temperatures above 300°C and the rate of precipitation is highest at around temperatures of 450°C, which is rightfully termed the 450°C embrittlement [Pittsburgh, 2014], and it significantly affects the ductility, toughness and the corrosion resistance of DSS [Topolska and Labanowski, 2009]. The most critical of the precipitations, is the formation of sigma phase at 650 -950 °C [Pohl *et al.*, 2007; Sieurin and Sandstrom, 2006] and occurs in ferrite, where ferrite changes into sigma and austenite. It was also stated that at 1200 -1400 °C, sigma changes to tertiary austenite and enables separation from other austenitic phases with a different generation mechanism [Pohl *et al.*, 2007].

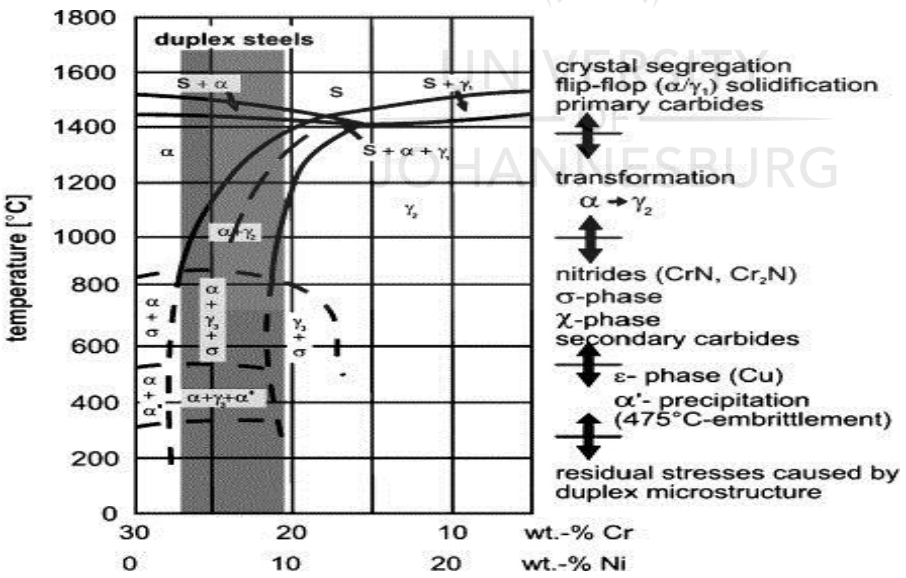

Figure 2.3: Pseudo-binary Fe-Cr-Ni phase diagram at 70% Fe [Pohl *et al.*, 2007].

Σ and Chi (χ) phases (Figure 2.4) are most likely to form in steels that contain high chromium and high molybdenum and they have high affinity to precipitate at the high energy regions such as the grain boundaries and interfaces of the DSS microstructure [Saeidi *et al.*, 2016;

Zucato *et al.*, 2002]. However, by increasing the cooling rate during solidification the volumetric fraction of the Σ phase can be minimized significantly [Saeidi *et al.*, 2016].

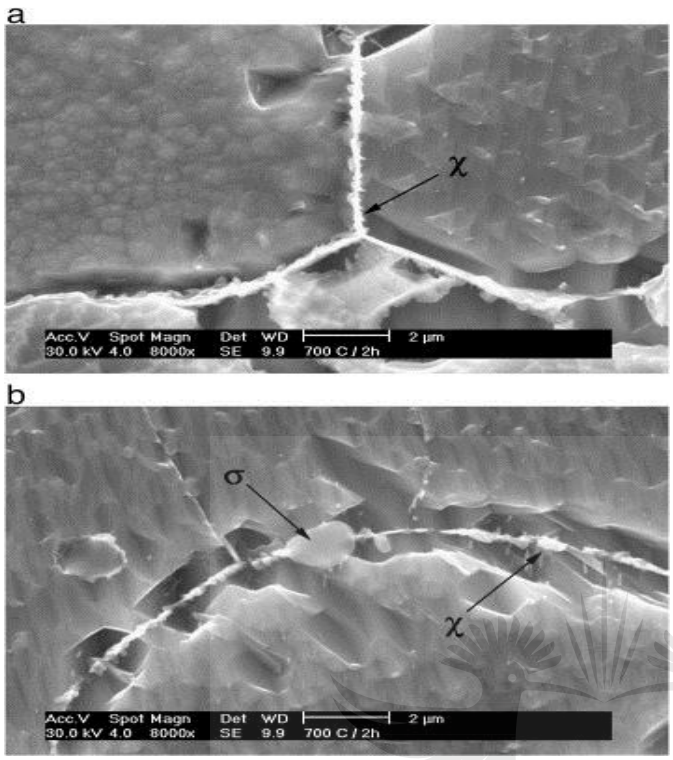

Figure 2.4: Microstructure of DSS with (a) χ phase and (b) σ and χ phases [Escriba et al., 2009].

2.3.3. Application of Duplex Stainless Steels

Most of the applications of duplex stainless steels concerns very harsh environments including corrosive, erosive, wear environments [Fargas *et al.*, 2013]. Duplex steels are used largely by the oil and gas, automobile, chemical, mining and mineral processing industries [Sahu *et al.*, 2009]. The steels are particularly preferred compared to austenitic steels due to a smaller amount of nickel content making duplex steels affordable considering the price volatility of nickel [Charles, 2008].

In the aforementioned industries, duplex materials are likely to be found as structural components such as turbines, boiler tubes, pressure vessels, automobile exhausts, motor engines, catalytic heat exchangers, and combustion systems [Bhowmick and Nowell, 2014; Rokanopoulou and Papadimitriou, 2011; El-Sayed *et al.*, 2009]. However, some producers of steels in fabricating pumps, valves and impellers using duplex stainless steels due to the difficulties associated with the final stages of fabrication or machining [Krolczyk *et al.*, 2015], have showed little interest.

As process designs are continuously being advanced to meet the escalating global demands in aforementioned industries; high wear resistant and hardness properties of materials have become of primary concern [Krolczyk *et al.*, 2015]. The extremities of the conditions existing in these industries are detrimental and over some period of time, structural components such as pumps, impellers (Figure 2.5), valves and pipes tend to wear off gradually which then leads to failure of the structures.

Figure 2.5: Worn out impeller [Courtesy of Turbine Francis].

2.4. Ceramic Materials as Reinforcement

Ceramics are inorganic and non-metallic materials, usually present in a form of crystalline oxide, nitride or carbide material. Ceramic materials are available in a large range either in crystalline or amorphous form; however, they are generally characterized by high hardness, high modulus of elasticity, high melting temperature, chemical resistance and low ductility [Black and Kohser, 2012].

Saxena *et al.*, 2017, studied the effect of ceramic reinforcement on the properties of metal matrix nanocomposites produced by powder metallurgy technique. It was found that the addition of ceramic reinforcement improved the density, hardness, wear, deformation and corrosion properties. Several researches [Saxena *et al.*, 2017; Pan *et al.*, 2016] has been done on the effect of ceramic reinforcement, however, the effect of transition metal ceramics on duplex stainless steel has received little attention. The gap has therefore brought about the research in question which is focused on investigating the mechanical properties of duplex stainless steel reinforced with titanium nitride.

2.4.1. Titanium Nitride

Reports have highlighted that the modification of the microstructures and phases within duplex stainless steels would be very effective in improving their overall corrosion resistance and mechanical properties required in service [El-Sayed *et al.*, 2009]. For this reason, the properties of DSS may be improved by reinforcing Titanium Nitride (TiN) and with duplex stainless steel through spark plasma sintering technique.

TiN has the potential to improve the strength and hardness properties of duplex structure based on its characteristics. This transition metal has greater affinity for carbon than chromium, therefore, titanium carbides are formed in preference to chromium carbide and thus localised depletion of chromium is prevented. It favourably produces fine carbides and grain size which are suitable for micro-alloying [Manda, 2015]. TiN is also characterized by good tribological and anti-wear properties, as well as acceptable biocompatibility and chemical inertness [Cui *et al.*, 2017]. Conversely, Nitrogen has an effective nickel-substituting potential for austenite formation [El-Sayed, 2009]. Nitrogen preferentially partitions to the austenite due to the increased solubility in the phase, and also concentrates at the metal-passive film interface [Gun, 1997]. Increased Nitrogen improves the corrosion and temperature stability of duplex structure [Petterson and Jernkontorent, 2013; Charles and Chemelle, 2011], creep and localised corrosion resistance properties [Baeslack *et al.*, 1979].

Nitrogen also assists in controlling the chemical balance between austenite formers and ferrite formers and hence the ferrite/austenite ratio [Brammer and Hughes, 1988]. Nitrogen delays the formation of intermetallics to allow processing and fabrication; however, it does not prevent the formation of those intermetallics. In simpler form it acts as an agent to offset the tendency to form sigma phase in duplex stainless steel [Alvarez-Armas, 2008; Loto, 2017].

2.5. Powder Metallurgy Fabrication Methods

Powder metallurgy enables the production of duplex stainless steels by several methods [Han *et al.*, 2011]. The use of powder metallurgy technology to produce duplex steels makes it possible to efficiently control their chemical and the phase composition as well as eliminating a number of difficulties (Figure 2.6) that are present during the production of DSS using conventional fabrication methods [Dobrzanski *et al.*, 2005]. More importantly the powder metallurgy process can be used to fabricate complex shapes [Chong, 1995].

Depending on the application, several methods are offered through powder metallurgy to obtain desired duplex stainless steel product. The methods include using pre-alloyed powder; mixing an austenite powder with a ferritic stabilising element powder such as Si, Al, Mo, Ti, Zr, Cr, W and V [Karoly *et al.*, 2015]. This is done so that the ferrite phase could diffuse in the austenitic phase and cause its destabilization to produce the dual microstructure; or by premixing the ferrite and austenitic powder in comparable proportion [Han *et al.*, 2011]. In the latter procedure, the starting powder ration and the sintering atmosphere are of outmost importance as they determine the final microstructure [Oke et al., 2017].

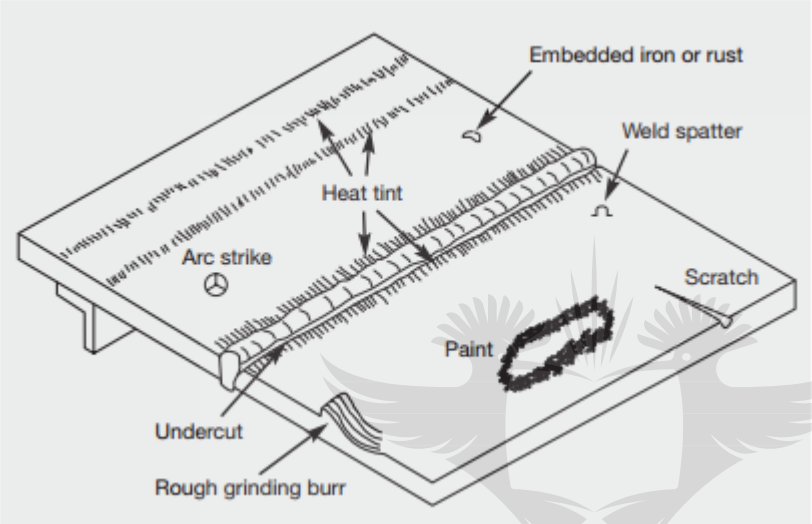

Figure 2.6: Typical fabrication defects or surface conditions that may be encountered with conventional production methods [Courtesy of Nickel Institute].

2.5.1. Powder Metal Injection Moulding

Powder or metal injection molding (PIM/MIM) has been used for fabrication of near net shape parts from various materials including stainless steels [Chong, 1995]. Through PIM increased design flexibility, excellent properties, and good surface quality is achievable. Because of its net shape forming capabilities it is regarded as a cost saving fabrication process [Wu *et al.*, 2015]. Moreover, the technique offers the advantage of obtaining components with complex shape. Importantly is that the PIM technology favours all fundamental studies of sintering.

PIM requires that the spherical powder particles and the right amount of a binder be mixed together for a feedstock [Sotomayor *et al.*, 2015]. The feedstock is then injected into a mould to obtain the green body. Thereafter, the brown body is obtained by removing the binder which was initially added to allow the mixture to flow with ease. The brown part which

retains the net shape is then sintered to obtain fully dense material. The duplex stainless steel produced this way comprises of good strength and ductility comparable to those obtained in cast and wrought products.

The properties of PIM parts tend to be higher than those of other PM due to the finer initial powder used [Wu *et al.*, 2015]. Therefore, the final products have higher sintered density and a more uniform microstructure. However, the possibility to obtain fully-dense material parts rely significantly on the amount of the initial powder and appropriate processing and sintering parameters [Wu *et al.*, 2015; Sotomayor *et al.*, 2011].

2.5.2. Powder Additive Manufacturing

Additive manufacturing (AM) is defined as a process of adding different materials from 3D model data by layers, using thermal heat [Lima and Sankare, 2014]. The technology offers the opportunity to manufacture innovative new products in shorter production time and also reduce waste material during finishing processes [Yilzmaz and Ugla, 2016]. However, the properties of the components prepared this way have to be known before application, there's uncertainty in the properties of the final product as they don't usually coincide with those fabricated by conventional methods [Skiba *et al.*, 2009].

Additive manufacturing is categorised into three groups: solid-based, liquid-based and powder-based. For powder-based AM, the processes are the Selective Laser Sintering (SLS) or Selective Laser Melting (SLM), Three-Dimensional printing (3DP) and Laser Engineering Net Shaping (LENS). For SLS/SLM process, layers are created by melting powder or partially melting powder by using laser or electron beam [Cormier and West, 2004]. Whereas for LENS and 3DP, layers are created from powders onto which a traversing ink jet head prints a bonding agent. However, for both LENS and 3DP processes, post processing is required [Utela *et al.*, 2008].

Through the modification of process parameters, the possibility to create a wide range of unique, anisotropic microstructures that are otherwise difficult or impossible to manufacture by other means arise [Popovich *et al.*, 2016]. The ability to blend different feedstock powders offers the creation of custom materials and the potential to vary the material composition to fabricate high-performance, functionally graded materials (FGM). The technique can be used to produce complex metal matrix composites (MMC). However, duplex stainless steels are

challenging to produce in this way. The challenges are mainly associated with the heat transfer that results in the imbalance in the ferrite to austenite ratio and the precipitation of intermetallic phases [Elmer *et al.*, 2007].

2.5.3. Hot Isostatic Pressing

The hot isostatic pressing (HIP) is a densification process. The HIP process is a fabrication method used to produce numerous class of materials such as ceramics and metallic alloys including steel components with simple or complex shapes. The principle of the technique, as shown in Figure 2.7, involves simultaneous application of external pressure and temperature [Zimmerman and Toops, 2008]. HIP process leads to high densified material consisting of finer microstructure and isotropic features [Sequeira and Santos, 2016].

However, Hot Pressing may sometime require long heat-up (±5 °C/min) which lead to relatively slow cycle time, and this encourages grain growth [Saheb *et al.*, 2014; Kessel *et al.*, 2009]**.** According to Antona and Mapelli, 2013, the mechanical performances of HIP products depend on the distribution, morphology and volume fraction of porosity having a detrimental effect on properties like fracture toughness, fatigue resistance and tensile strength.

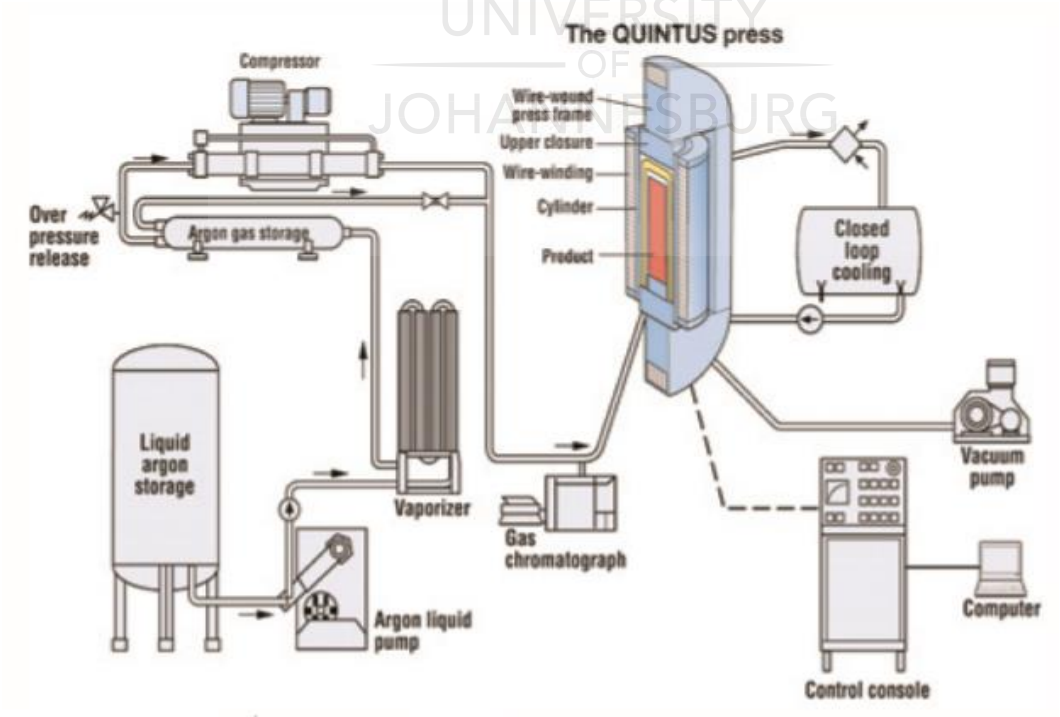

Figure 2.7: Schematic diagram of Hot Isostatic Pressing [Zimmerman and Toops, 2008]

2.5.4. Spark Plasma Sintering

Spark plasma sintering (SPS), also known as field assisted sintering (FAST) and pulsed electric current sintering (PECS) is an advanced powder metallurgy sintering technique that combines high heating rate with high pressure for an effective rapid consolidation of fully dense materials, Figure 2.8, [Mouawad et al., 2014; Wang et al., 2017]. It is however, less effective in sintering some classes of materials such as non-conductive materials and larger samples to produce final product with controlled and homogenized stoichiometry, microstructure and phases [Enneti *et al.*, 2012].

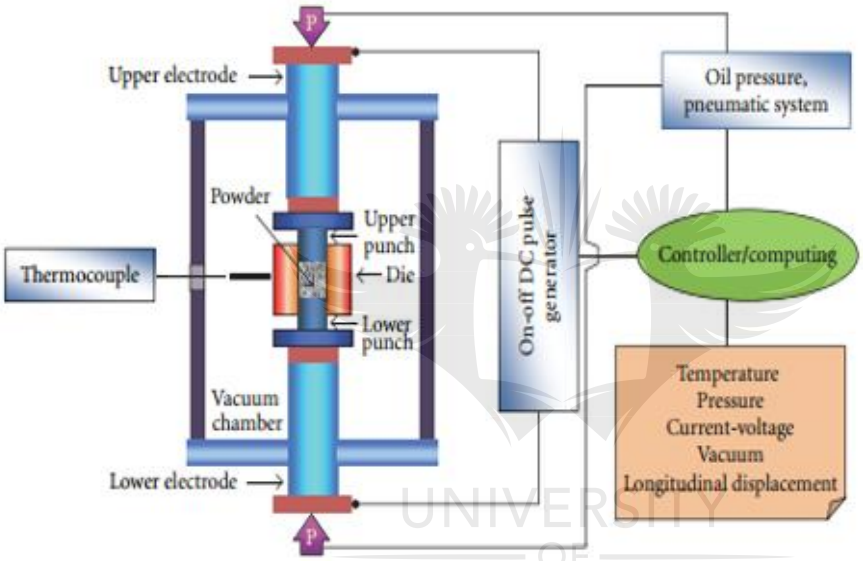

Figure 2.8: Schematic diagram of SPS process [Saheb *et al.*, 2014].

2.5.5. Hybrid Spark Plasma Sintering

Hybrid spark plasma sintering (HSPS) is a modified type of spark plasma sintering. Since SPS and Hot Press are limited in producing fully dense large samples with homogenized stoichiometry and microsture [Suarez *et al.*, 2013], Hybrid SPS has been developed to bridge the shortcomings of the two techniques. Hence, the technique combines the benefits of two different heating modes (Figure 2.9) which are the induction/resistance heating offered by hot isostatic pressing and pulsed direct heating offered by spark plasma sintering [www.fct-systeme]. Shongwe *et al.*, 2016, stated that this combination eliminates radial thermal gradient which are often experienced when fabricating larger samples using either the hot isostatic or spark plasma sintering. As a result, homogeneous radial densification is obtainable through the use of HSPS in shorter production time.

Usually for the purpose of testing for mechanical properties, the larger sample (Figure 2.10a), is cut into smaller sample sizes (Figure 2.10b) which are easier to handle during testing, especially those that concern nanosize.

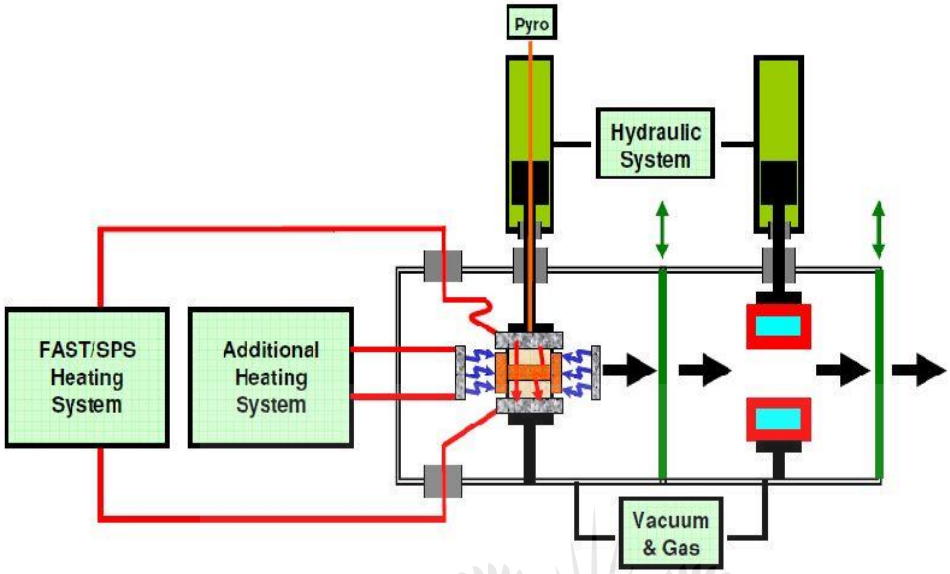

Figure 2.9: Schematic diagram of Hybrid Spark Plasma Sintering equipment [Kessel *et al.*, 2010].

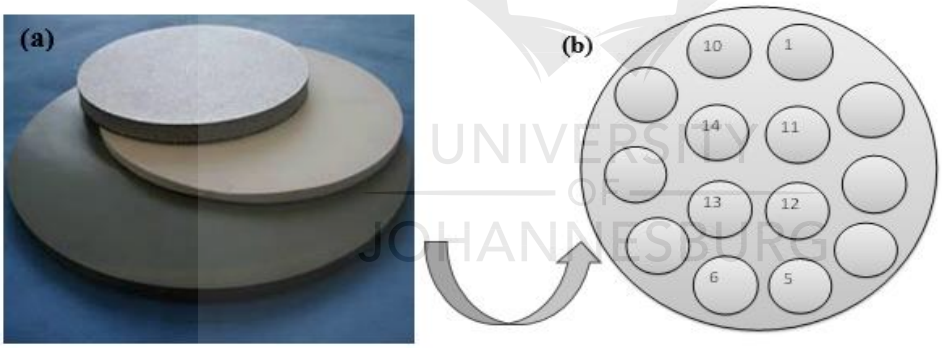

Figure 2.10: (a) Largest (400mm) binder-less WC sample produced by Hybrid-SPS [Kessel *et al.*, 2010] (b) An illustration of small sample sizes cut out of big sample size.

2.6. Mechanical Property Testing Methods

Upon the development of the potential material for any applications, it is essential to accurately determine the properties of the materials so that the designs are safe for the applications. A variety of mechanical property tests methods have been used by producers, researchers and consumers previously [Wang and Rokhlin, 2005; Dowling, 2012; Schwarm *et al.*, 2017]. Indentation tests are common amongst them as hardness and elastic modulus are

usually primary mechanical properties to be tested for a number of applications and materials [Schuh, 2006].

Indentation methods have since evolved over the past years with indentation size continuously shrinking in scale. The indentation techniques are suitably grouped into macro-indentation, microindentation, nanoindentation and even picoindentation with respect to the corresponding size range [Schuh, 2006]. By increasing the load on the indenter into the sample, the penetration depth is increased progressively producing transition stages classified according to the characterisation indentation size as shown in Figure 2.11.

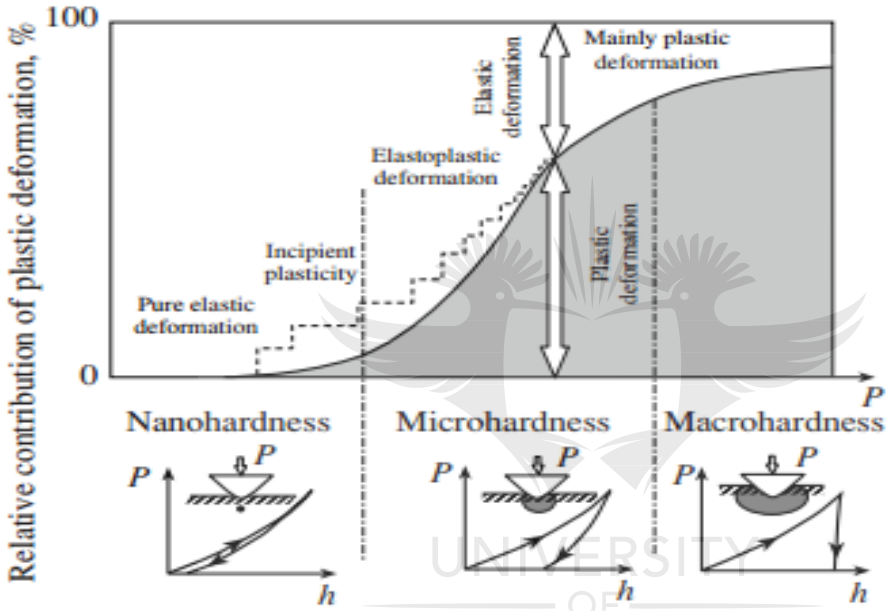

Figure 2.11: Schematic diagram illustrating different indentation scales [Golovin, 2008].

2.6.1. Conventional Hardness Testing Methods

Hardness is one of the most commonly tested mechanical properties for the purpose of quality control, usually because it has close relation to other mechanical properties such as strength, ductility, and fatigue resistance [Broitman, 2017]. Hardness is defined as the ability of the material to resist deformation under applied load. Hence, the principle of hardness testing is based on the load penetration relationship. The penetration is measured either by depth or area, which is then translated to a hardness value [Stone, 2006].

The most commonly used conventional indentation hardness tests are the Brinell, Rockwell, Knoop and Vickers Hardness testers. These conventional hardness testing techniques are based on the use of large samples, which consumes large amounts of materials to be produced

[Stefan *et al.*, 2015]. Furthermore, the imprint of the indent has to be large enough to be measured with naked eyes to enable calculation of the hardness value and for microhardness testers the indents are usually observed optically. The aforementioned limitations have pushed for new innovative techniques to be developed to bridge the limitations of the conventional hardness testing methods [Schuh, 2006].

2.6.1.1. Brinell

The Brinell test (Figure 2.12) is used primarily for inhomogeneous materials such as forgings and castings, particularly cast iron. Brinell testing uses larger indenters (e.g. 10 mm) and heavier loads (e.g. 3000 kg) to minimize localized feature effects such as graphite flakes or voids in castings. In Brinell test, a ball (D=mm) is used to produce an indent (d=mm) on the material under an applied load (P). The Brinell hardness number is calculated as follows [Leu, 2011; Wang and Rokhlin, 2005]:

$$BH = \frac{P}{Ac} = \frac{2P}{\pi D(D-\sqrt{D^2-d^2}} \quad (1)$$

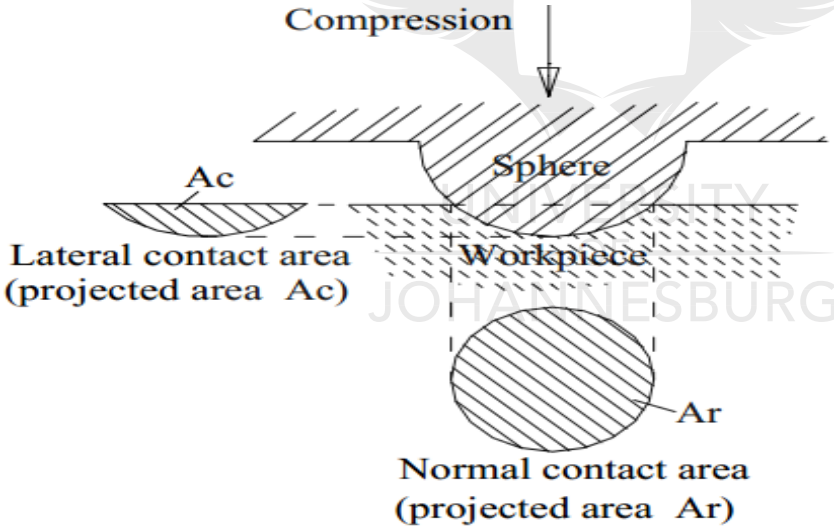

Figure 2.12: Brinell Indentation model [Leu, 2011].

2.6.1.2. Rockwell

The Rockwell hardness test as shown in the model in Figure 2.13 is used widely used for metal products [Song *et al.*,1998], both ferrous and nonferrous materials, which have been annealed, hardened, case hardened or tempered. Common indenters for Rockwell testing include diamonds and steel or carbide. The applied testing loads for Rockwell tests range from 15kg to 150kg. The test involves applying low loads of 10kgf (98.1N) followed by a

higher load. The function of the low load is to eliminate errors such as backlas and surface imperfections in measuring the penetration depth [Broitman, 2017]. The high load is removed while still holding the low load. The hardness is calculated using the equation [Song *et al.*,1998]:

$$HR = N - 500h \quad (2)$$

Where h(mm) is the difference of the two penetration depth measurements. N is a constant and it depends on the type of indenter used: 100 for spheroconical and 130 for a ball.

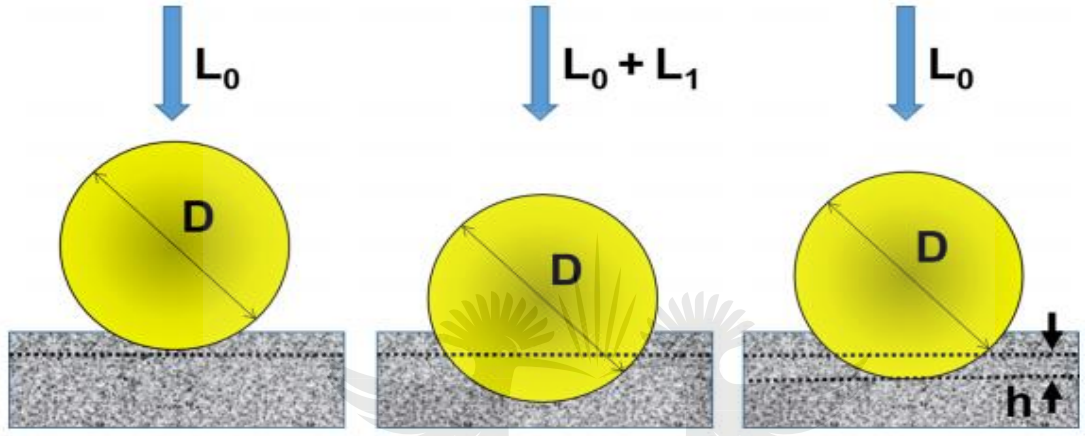

Figure 2.13: Rockwell macohardness test model [Broitman, 2017].

2.6.1.3. Knoop and Vickers

Knoop and Vickers hardness testers form part of microhardness testing and uses loads ranging from 1gram to 1kg and requires a properly prepared surface. These methods are easy, quick, and require small polished area of specimen surface for testing. These tests involve applying a given load onto the surface of a test specimen via a pyramidal diamond indenter. The imprints of the indents are measured optically requiring accurate measurement of the indentation boundaries, especially when using lighter loads which usually not precise enough [Guillonnean *et al.*, 2013]. The accuracy of the measurement however, can be limited by the resolution and elastic recovery of the material, therefore resulting in uncertainty in the measured indentation size which then affect the reliability of the hardness results [Shahdad *et al.*, 2007].

The Knoop and Vickers indenters have different aspect ratios (Figure 2.14 a and b). Vickers indenters are more symmetric and better suited for better suited for more precise measurements of layers or for measurements at specific depths. Vickers hardness test uses a

square-based pyramid indenter for which the angle, ψ, between the two opposite sides is equal to 136^0 [Guillonnean *et al.*, 2013].

$$VHN = \frac{P}{A_{TAC}} = \frac{P}{\frac{d^2}{2}.\sin(\frac{\psi}{2})} = 1.854\left(\frac{P}{d^2}\right) \quad (3)$$

Where VHN is Vickers microhardness value, P is the load applied (N), A_{TAC} is the true contact area and d is the diagonal of the indent (mm).

For Knoop hardness test, a lozenge-based pyramid with θ angle between the two opposite faces being 172.5^0 and the angle φ between the other 2 being 130^0. The hardness value is calculated by [Stone, 2006; Shahdad *et al.*, 2007]:

$$KHN = \frac{P}{A_{PAC}} = \frac{P}{d^2\left[\cot\frac{\theta}{2}\tan(\frac{\varphi}{2})\right]} = 14.230\left(\frac{P}{L^2}\right) \quad (4)$$

Where KHN is Knoop microhardness value, P is the load applied (N), A_{pac} is the projected contact area and d is the length of the largest diagonal of the indent (µm).

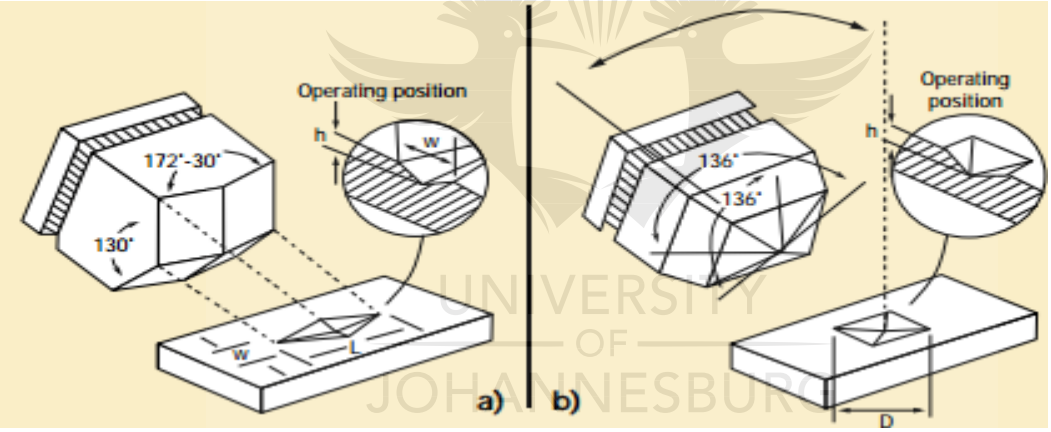

Figure 2.14: (a) Knoop and (b) Vickers Hardness Indenters [Stone, 2006].

2.6.2. Nanoindentation

Nanoindentation test is a universally used method to probe the mechanical properties of materials. Over the past twenty years nanoindentation has gained momentous recognition (Figure 2.15), and this is due to the improvement made to the instrumentation providing better experimental techniques [Phani and Oliver, 2016; Wheeler *et al.*, 2015; Trenkle *et al.*, 2010]. Furthermore, the simplicity of the sample requirements that are a clean and a flat surface has made it a well sought after technique [Wheeler *et al.*, 2015].

The main driving force towards the development of scaled-down equipment such as nanoindentation is that in conventional hardness testing, a hard tip is pressed into the material

and the residual indentation size is measured optically using different kinds of microscopes [Moser *et al.*, 2007]. The size of such an indentation mark has to be big enough usually in the range of micrometers in order to be measurable in an optical microscope. This is not practical for nanostructured materials as the size of such an indent could exceed the sample size or the film thickness. This limitation in testing of small samples has led to development of variety of depth-sensing hardness testing systems that are constantly being improved [Moser *et al.*, 2007].

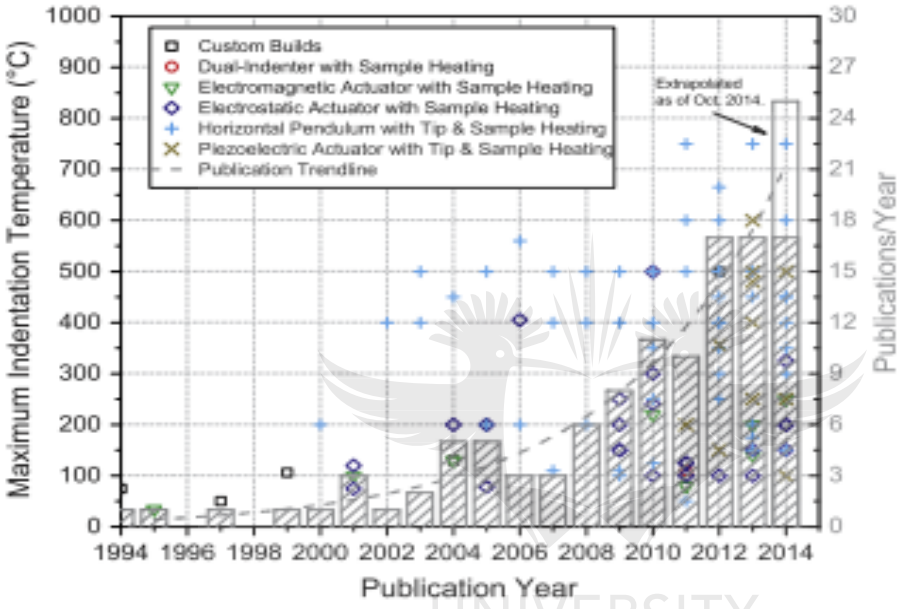

Figure 2.15: Maximum published indentation temperatures for various system configurations and publications per year in recent years [Wheeler *et al.*, 2015].

Nanoindentation is a well-suited method to obtain mechanical properties with high lateral and depth resolution [Koch *et al.*, 2015]. The topical capabilities of the technique make nanoindentation one of the most used instruments. Amongst many of the advancement to the system, it is the ability to carry out indentation testing at temperatures up to 800^0C with similar thermal drift occurring with tests conducted at room temperature [Wheeler *et al.*, 2015].

In as much that indentation can now be conducted in real service conditions, the system also offers high spatial resolution and accurate positioning of the indenter. This advancement makes it possible to image the sample surface prior to testing, to choose the position of the indentation with high lateral accuracy, and to image the residual imprint afterwards [Moser *et al.*, 2007].

The technique can effectively be used for the assessment of micromechanical behaviour of multiple phases within the material microstructure [Kralik and Nemecek, 2014] and obtaining reliable mechanical property measurements from microscale amounts of material, including thin films, single grains, and individual phases of various heterogeneous system [Trenkle *et al.*, 2010]. In addition, it can be utilised to probe physical phenomena in materials, such as dislocation nucleation, shear band activation and phase transformations due to the high sensitivity of nanoindentation [Trenkle *et al.*, 2010]. Proper understanding of mechanical properties of a materials including multi-phase structured material is very important for an advanced material design and application. However, being a relatively new technique, sufficient information is lacking.

2.6.2.1. Influences on the Nanoindentation Data

Material hardness is a multifunctional physical property and it depends on a large number of factors. Indentation hardness value also depends on the test used for the measurement. Smaller indentation hardness measurements usually eliminate or reduce the influences on the hardness value which are common in larger indentation measurement [Broitman, 2017]. However, the benefits of the shrinkage in scale of the indentation measurement magnify other influences on the hardness values.

(i) Indentation Size Effect

Indentations at shallow depths using the nanoindenter introduce the multiscale material behaviour known as the indentation size effect (ISE). There are two classical theories in indentation research classified by indentation scale size [Costinescu *et al.*, 2011]. Namely, the continuum mechanics in which typical length scales of components and deformation are larger than millimetres, and the other is the strain gradient plasticity theory where the characteristic length scales are very small.

It has often been found that the hardness and other relating mechanical properties on the surface of the material are often different to those within different depths of the material [Voyiadjis and Peters, 2009]. That is at small indentation depths h, the material appears to be harder than at larger indentation depths. Materials with high dislocation densities are known to be prone to ISE, crystalline materials [Li and Ngan, 2003] sometimes contain dislocation densities that can exceed 10^{16} m^{-2}. Voyiadjis and Peters, 2009, elucidated on the ISE effect, which is when the hardness of the material decrease for increasing indentation depth, and an

increase in hardness when increasing indentation depth and when further increasing the indentation depth the hardness decrease whereas in other instances a decrease in hardness for the smallest indentation can be observed.

According to Costinescu *et al.*, 2011, the presence of ISE in metals is as a result of the contribution by statistically stored dislocations (SSDs) and geometrically necessary dislocations (GNDs) and their interactions. The SSDs are dislocations moving through the material and trapping each other in a random way and the GNDs are dislocations that are required for compatible deformation within the polycrystal. Therefore, the inhomogeneous deformation of the material results from dislocation storage and the size effects arising from an increase in strain gradients inherent in non-uniform deformation modes [Song *et al.*, 2017]. As the material is being deformed the SSDs are constantly moving and lead to the emerging of GNDs that cause additional hardening by acting as obstacles to the SSDs [Voyiadjis and Peters, 2009]. The effects of GNDs are especially prominent when the characteristic length of deformation becomes sufficiently small.

(ii) Pop-in

According to Song *et al*., 2017, the popping is classified as a burst of plastic deformation which can either be as a cause of stress drops or strain jumps. The stress drops result when the indentation test is conducted under displacement control mode while strain jumps results when load control mode is used. The discontinuous plastic deformation in load controlled indentation mode is commonly labelled as pop-in.

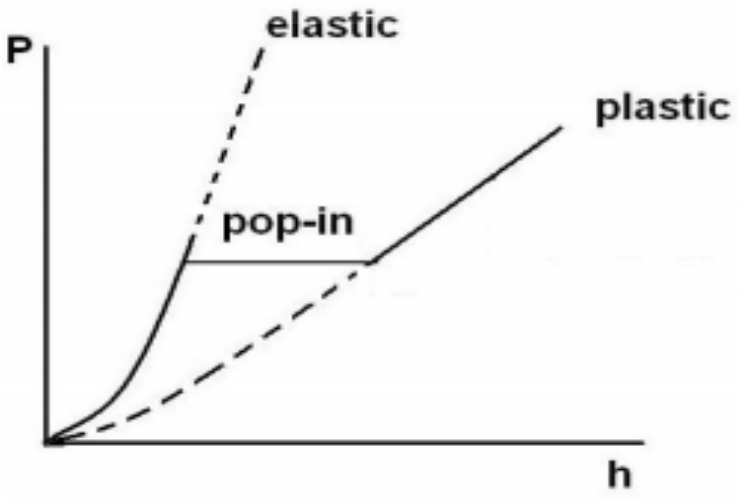

Figure 2.16: Schematic of pop-in [Wang, 2012].

Pop-in is a transition from elasticity and plasticity (Figure 2.16) of the material in the deformation processes [Wang, 2012]. The first transition is the primary pop-in which is represented as a large jump in displacement and the subsequent pop-in events displaying small displacement jumps. Fortunately, the effect of pop-ins can be drastically reduced with proper surface preparation which eliminates absorbed oxide layer, contaminations and scratches.

(iii) Noise

Noise is typically picked up by nanoindentation systems as vibration and is displayed as irregular pattern it the load-displacement curve. The sensitivity of the system is due to the small scale of the mechanism (indenter tip and applied load) of the system. High noise indicates high variability in the measured deformation rate, which may present obstacles to reliably extracting data from test results. To obtain reliable test results, several independent indentations points are performed and an average is taken to minimize the influence of noises [Blau and Shaffer, 2005]. Obligatory, the nanoinder system is also stationed on a table designed to eliminate vibrations.

2.6.2.2. Nanoindentation Measurement Modes

Nanoindentation system provides different modes of performing indentation tests. Different modes are used depending on the type of test the user intends to run. Also the information the user needs to extract will determine the mode to be used. For the purpose of this research study grid indentation and user-defined modes will be discussed in this chapter. The mentioned testing methods enables the indentation testing of the individual phases of materials with multiple phases [Kralik and Nemecek, 2014].

(i) Grid Indentation Test

Grid indentation test offers the possibility to measure the different phases in a composite material. The test is carried out by making cross sections on the sample making indentation imprints on each of the cross section as shown in Figure 2.17. The overall indentation data are combined to give average results.

The capabilities of grid indentation include the assessment of both elastic and hardness and volume fraction estimates from load-displacement diagrams measured from the impression of a sharp tip. Although SEM-EDS have proved to be able of deriving single grain properties

but they require measurements of each indent which is time consuming. The main motive for carrying out grid indentation is its ability to provide estimates on the statistical distribution of phases' properties on a sample rather than strict measurement of a single phase properties.

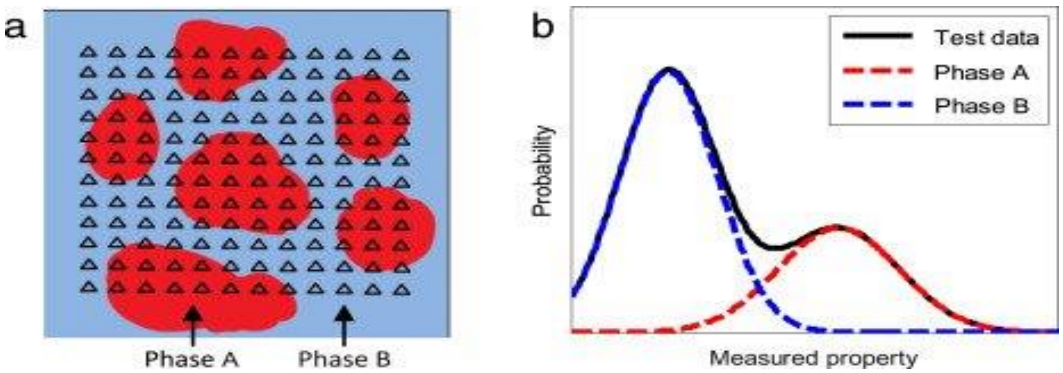

Figure 2.17: Schematic of grid indentation test on heterogenous material [Vasconcelos *et al.*, 2016].

(ii) User-defined Mode

The user defined mode as described in the UNHT manual allows the user to create specific indentation profile by combining loadings, holds and unloading. Each segment can be independently programmed for various load/unload rates or hold times. Indentations can be performed on the same spot. Main application is for materials that require measurements at different temperatures therefore provides stabilization times before other segments of indentation cycle / for segments with different loading rates within the same cycle.

2.6.2.3. Indenter Tip Geometry

There are numerous geometries available of the indenters for a variety of applications, as shown in Table 2.2. The five main types are the Berkovich, Vickers, Cube-corner, Cone and Sphere. The tip end of the indenter can be made sharp, flat, or rounded to a cylindrical or spherical shape to suit the application. Standard nanoindentation indenters and custom indenters with applicable geometry are accepted if the relevant indenter dimensions and angles conform to the ISO 14577-22 standard [www.iso.org] which is an internationally accepted standard is governing the tolerances associated with microindenter and nanoindenter, delivering confidence in accuracy and repeatability of the test.

The spherical is well suited for probing mechanical properties on micro electromagnetic systems and for determining yield strength, workhardening as the indenter initiates elastic

contact and then produces elastic–plastic contact at higher loads. However, the application of spherical indenter is the fact that it is very difficult to obtain a precise sphere with a diameter of less than 100 mm made of diamond [Li and Bushan, 2001].

The three-sided pyramidal indenter, the cube corner indenter, is ideally used to determine the fracture toughness of the material at relatively small scale [Cuardado *et al.*, 2012]. The primary reason for this application is that it can displace more than three times the volume of the Berkovich indenter at the same load, thereby producing much higher stresses and strains in the vicinity of the contact and reducing the cracking threshold [Li and Bhushan, 2001; Li *et al.*, 1997]. The three-sided Berkovich and the Vickers indenter are essentially used for similar applications. However, the Berkovich is preferred to the four-sided Vickers hardness tester for probing properties such as hardness and elastic modulus at the smallest possible scales. This is because the three-sided Berkovich can be easily ground to a sharp point. Also it is not easily damaged and can be manufactured without difficulties [Li and Bhushan, 2001].

Table 2.2: Indenter Geometries and their applications [www.toyo.co.jp]

	Berkovich	Vickers	Cube-Corner	Cone (angle ψ)	Sphere (radius R)
Features					
Shape	3-sided pyramid	4-sided pyramid	3-sided pyramid w/ perpendicular faces	Conical	Spherical
Applications	Bulk Materials, Thin Films, Polymers, Scratch Testing, Wear Testing, MEMS, Imaging	Bulk Materials, Films and Foils, Scratch Testing, Wear Testing	Thin Films, Scratch Testing, Fracture Toughness, Wear Testing, MEMS, Imaging	Modeling, Scratch Testing, Wear Testing, Imaging, MEMS	MEMS
Available as Traceable Standard	Yes	Yes	Yes	No	No
Parameter					
Centerline-to-face angle, α A	65.3°	68°	35.2644°	—	—
Area (projected), A(d)	$24.56d^2$	$24.504d^2$	$2.5981d^2$	πa^2	πa^2
Volume-depth relation, V(d)	$8.1873d^3$	$8.1681d^3$	$0.8657d^3$	—	—
Projected area/face area, A/A_f	0.908	0.927	0.5774	—	—
Equivalent cone angle, ψ	70.32°	70.2996°	42.28°	ψ	—
Contact radius, a	—	—	—	d tan ψ	$(2Rd-d^2)^{1/2}$

2.6.2.4. Mechanical Properties Derived from Nanoindentation Experiments

Nanoindentation has become the preferred method for determining mechanical properties on wide range of materials such as metals, glass, ceramics and even on materials that were previously considered to be difficult to analyse such as thin films and oxidizing materials, in

small volumes [Wheeler *et al.*, 2015]. Several mechanical properties can be derived from nanoindentation testing; these include elastic modulus, hardness, strain-hardening exponents, fracture toughness, and viscoelastic properties of materials [phani and Oliver, 2016; Wheeler *et al.*, 2015; Kralik and Nemecek, 2014].

The indentation load-displacement data derived can be used to determine mechanical properties even when the indentations are too small to be imaged conveniently [Oliver and Phaar, 1992]. The two mechanical properties measured most frequently using load and depth sensing indentation techniques are the elastic modulus, E, and the hardness, H [Oliver and Phaar, 1992]. The universally accepted approach offered by Oliver and Phaar (Oliver-Phaar method) has structured and motivated the domains of indentation and can be used to accurately determine H, E and S (stiffness) [Golovin, 2008].

(i) Hardness and Elastic Modulus

Hardness and elastic modulus values are extracted by nanoindentation based on the Oliver and Phaar method [Wheeler *et al.*, 2015]. Unlike conventional hardness tests, the residual impression left on the surface of the material does not need to be measured as the uniform geometry of the indenter tip combined with precise displacement sensing equipment with nanometer resolution is used to calculate the contact area during indentation as a function of load. The resulting load-displacement curves are then used to quantify the hardness of the material, HIT, which is defined as the ratio of the maximum load, PMAX, over the contact area, A; $A=C_0h^2$. [Kheradmand *et al.*, 2016]

$$H = \frac{Pmax}{A} \tag{5}$$

Monclús *et al*., 2014, stated that the contact area between the indenter and the sample can be determined from the contact depth and the calibrated indenter geometry, typically referred to as the indenter area function (IAF). In order to determine the IAF, two methods can be adopted: (i) an indirect calibration, by indenting a reference material exhibiting known elastic properties (e.g., fused quartz) and (ii) a direct measurement of tip area by metrological atomic force microscopy (AFM) of the tip. The latter is the recommended direct method of obtaining the IAF by the ASTM E2546-07 [ASTM International, 2007] and the ISO 14577 standard [Saheb *et al.*, 2014].

In addition to hardness measurements, indentation techniques are also commonly used to determine the elastic modulus of the material being tested. During indentation, the initial contact between the indenter and sample surface can be considered elastic. As the load increases, plastic flow and yielding occurs beneath the material in contact with the indenter [Schuh *et al.*, 2006]. Once the maximum load is attained, the slope of the unloading curve measured from the tangent of PMAX can be analyzed to calculate the elastic modulus of the sample material [wang and Rokhlin, 2005], Figure 2.18.

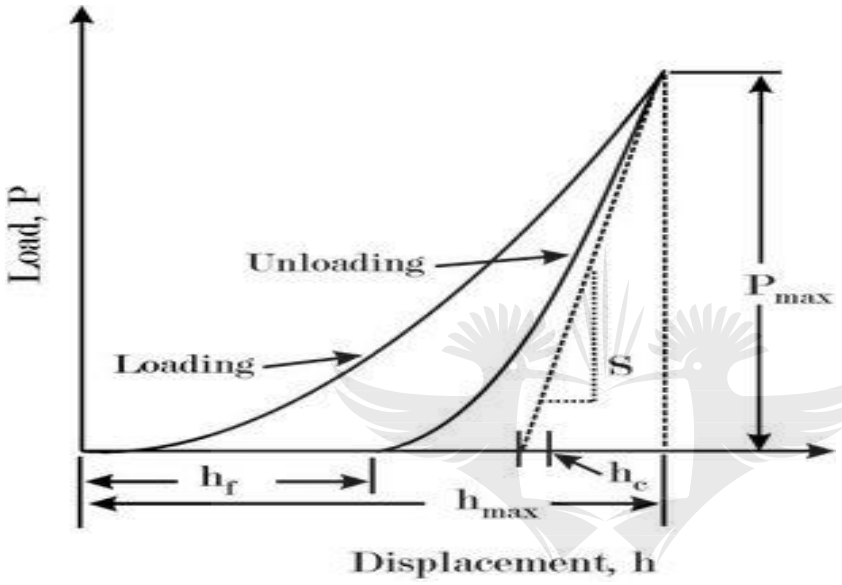

Figure 2.18: Typical load-unload curve [Kheradmand *et al.*, 2016].

Golovin, 2008, elucidated on the load-displacement graph and from it can be understood that hysteresis loss energy, which is equal to the area between the loading and unloading curves (Figure 2.19), is an important source of information on the inelastic deformation of the surface of the material upon indentation. The indentation modulus is determined using the slope of unloading curve at maximum load and they are related by the following expression [Monclús *et al.*, 2014]:

$$E_r = \frac{\sqrt{\pi}}{2\beta} \times \frac{S}{\sqrt{Ap}} \quad (6)$$

Where Er is the reduced modulus, which accounts for the fact that elastic deformation occurs in both the sample and indenter. S is the initial unloading stiffness, i.e., the slope (dP/dh) of the line in tangent to the initial unloading curve in the load-displacement plot. Moreover, β is a correction factor correlated to the indenter geometry (β=1.034) for a Berkovich indenter.

According Wheeler and Michler, 2013, in order to minimize the effect of possible creep on the slope of the unloading curve. S can be determined using a linear approximation to the high load portion of unloading curve (from 98% load to 40% load), which assumes that the contact area remains constant for the initial unloading of the materials [Wang *et al.*, 2015]. This reduced modulus is the convolution of both the indenter and sample elastically deforming during contact according to the relation [Wheeler *et al.*, 2015];

$$\frac{1}{E}=\frac{(1-v_s^2)}{E_s}+\frac{(1-v_i^2)}{E_i} \quad (7)$$

Where E_i, ν_i and E_s, ν_s are the Young's modulus and Poisson's ratio of the indenter and sample, respectively. This equation demonstrates necessity of accurate knowledge of the indenter properties in order to apply instrumented indentation to measure the mechanical properties of a sample.

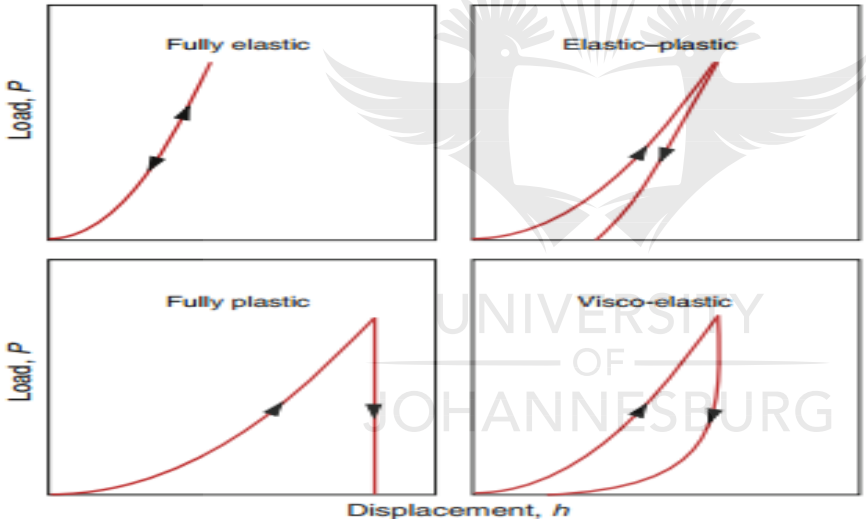

Figure 2.19: Load P versus indenter displacement h for various idealised material types [Lawn and Cook, 2012].

2.6.2.5 Indenter Calibration

Indenter tips in perfect cases are taken to encompass an axisymmetric shape, however, that is not usually the case. The commonly used Berkovich indenter is an equivalent axisymmetric cone modelled through the Oliver and Pharr approach [Tadjiev *et al.*, 2010]. Furthermore, for tests at shallow indentation depths (<1μm), the deformation of the specimen depends largely on the actual shape of indenter tip which also greatly influence the calculated parameters of the material as they depend significantly on the contact area function [Wang and Rokhlin, 2005].

Therefore, calibration of the indenter is important especially due to the reason that real tip shape will deviate from its ideal geometry to some extent. The same is experienced even by a new indenter and importantly is for the achieved data to be reproducible with different machines [Mencik, 2007; Herrmann *et al.*, 2000]. Another reason that the need to calibrate the indenter on a regular basis is tip contamination which is common when indentation tests are carried out on hard sample and metals that readily oxidise at high temperature (≥200°C) [Wheeler *et al.*, 2015].

Tadjiev *et al.*, 2010, explained how the calibration is carried out. It was mentioned in their report that Fused silica is a commonly used standard material for the calibration of the indenter as it has a known certified elastic modulus value which remains constant with depth [Gao and Liu, 2017]. They also stated that the test result gives an area size imprint the calibrated indenter should make. Indenter calibration is advised to be performed for new tip or when testing at shallow depth. Furthermore, it was mentioned that the main reason for calibration rises due to the fact that nanoindentation results are based on a calibrated tip area function (TAF) which differs from conventional indentation where the results are based on imaging of the residual indent which presents challenges and also impractical for very low load indents which are common with nanoindentation. One way of calibrating the indenter is by the applying the following equation [Oliver and Phaar, 1992]:

$$r_c = \frac{S}{2\beta E_r} \tag{8}$$

2.6.2.6 Indenter Maintenance

Effective use of equipment yielding precise and accurate results of the process depends largely on the good maintenance of the equipment. The indentation process naturally produces debris that may damage the indenter and contaminating particles that may add an unknown factor to the indenter producing erroneous data in results. Monclus *et al.*, 2014, reckons the importance of monitoring the tip shape during indentation, as tip wear and contamination from chemical reactions, especially at high temperature, can degrade tips very fast, when indenting metals and ceramics, sometimes even at relatively moderate temperatures.

Proper handling of the nanoindenter reduces the frequency of cleaning the indenter. However, in cases where the indenter is contaminated, proper cleaning is mandatory and can be carried

out with aid of stereo microscope by rubbing the diamond with a cotton swab soaked with isopropyl alcohol and drying it with pressurized air [Wheeler *et al.*, 2015] as shown in Figure 2.20.

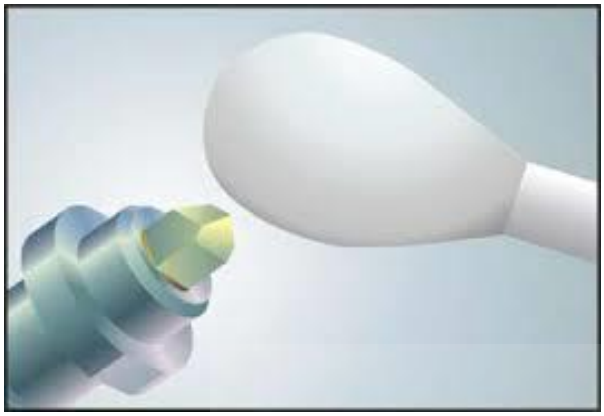

Figure 2.20: Indenter cleaning by cotton swap [www.microstartech.com]

2.6.3 Tribology

Tribology is defined as the study of interacting surfaces in relative motion. The concept of tribology is interested in the friction coefficient and the wear properties of the material. The phenomena of tribology depend largely on the load, sliding velocity, surface characteristics and the mechanical properties of the contact materials [Kakas *et al.*, 2009]. Moreover, tribology offers potential for deeper understanding of fundamental wear phenomena like ploughing, micro-breaking or adhesion occurring under operating conditions [Varga *et al.*, 2017].

2.6.3.1 Principles of Tribology

The wear tests can be carried out under dry or wet sliding condition on a pin-on-disc or ball-on-disk tribometers (Figure 2.21), in respect to the ASTM G99-05 standard [ASTM International, 2005]. In cases where excessive wear is a concern, lubrication and or engineering processes are reasonable options for reducing the wear of materials [Rokanopoulou and Papadimitrou, 2011].

During dry test, a directly driven ball is rotated against the specimen, which is mounted on a dead-weight load lever. The wear scar produced on the specimen surface is assumed to reproduce the spherical geometry of the ball. From tribology tests, the friction coefficient and wear behaviour of the material can be obtained.

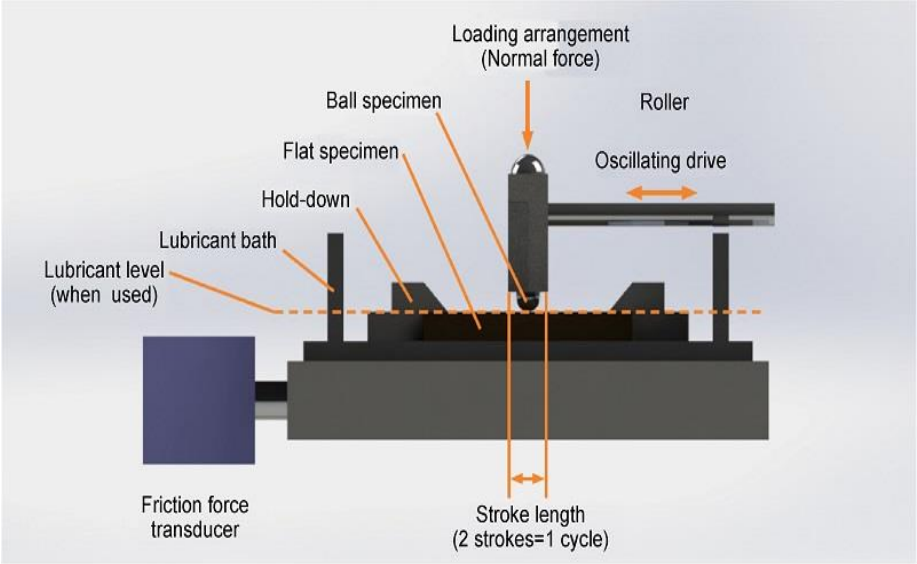

Figure 2.21: Schematic diagram of the ball on disk tribometers [Dohda *et al.*, 2015].

2.6.3.2 Friction

Friction is defined as the resistance to motion of a body in relation to another. The motion could either be sliding or rolling under tangential force over a stationery body [Hutchings and Shipway, 2017]. Nuruzzaman and Mohammad, 2012, stated that variation of friction depends on several factors such as the normal load, geometry of the contacting bodies, relative surface motion, sliding velocity, surface roughness of the rubbing surfaces, surface cleanliness, type of material, system rigidity, temperature stick-slip, humidity, lubrication and vibration. They further argued that the third law of friction which states that friction is independent of velocity in not generally valid. On the contrary, the study was in agreement with the third law of friction and it reported that friction is independent of apparent contact area and the sliding speed [Menezes *et al.*, 2013]. The ratio between the frictional force F_t and the normal load F_n is known as the coefficient of friction which follows Amonton's Law and is usually denoted by the symbol μ [Menezes *et al.*, 2013]:

$$\mu = \frac{F_t}{F_n} \tag{9}$$

For most materials where the sliding test is conducted in normal air conditions, the coefficient of friction usually lies in the range of 0.1 and 1 [Hutchings and Shipway, 2017]. Friction between static and dynamic body depends on numerous factors [Dubois and Esther, 2014], either in wet and dry test:

- Mechanical parameters such as contact pressure, plastic strain, strain rate, sliding velocities, material yield stress,
- Physical parameters such as roughness, temperature, viscosity and lubricant film thickness,
- Chemical parameters such as surface energy, presence of oxides, chemical reactions between lubricant and metallic surfaces

2.6.3.3 Wear

Wear is a major problem impacting significantly on the growth of the economy and the sustainability of the environment in applications involving abrasive and erosive wear, such as pumps and pipelines especially in slurry transportation [Ojala et al., 2016]. Wear is defined as the progressive loss of material from solid surface caused by the relative motion between that surface and a contacting substance. Wear is regarded as a system response rather than a material's property.

It is usually expected that high friction results in high wear rate, however, this is a wrong assumption as different conditions and different materials may yield contrary wear rates. For instance, Interfaces with solid lubricants and polymers usually yield low friction, however high wear. Whereas, ceramics show moderate friction with extremely low wear and in other cases friction and wear might be corresponded [Choudhury and Gupta, 2017].

To derive wear data, the following equations are used [Wen and Huang, 2012]:

i. Height of the worn cap

$$h = R - \sqrt{R^2} - \frac{d^2}{4} \quad (10)$$

ii. Volume of the worn cap

$$V = \frac{1}{3}\pi h^2(3R - h) \quad (11)$$

iii. Wear rate

$$wear\ rate_{sample} = \frac{V}{LF_n} \quad (12)$$

In general, minimal wear rates will be obtained with a hard material with smooth surface but the costs of preparation often dictate the choice of material and finish within acceptable tribological performance limits [Bellemans *et al.*, 2005]. It should also be taken into

consideration that for most materials, wear rate in unlubricated sliding applications vary with operating conditions and time [Zmitrowics, 2006].

2.6.3.4 Parameters Influencing Friction and Wear Characteristics

Tribology mechanisms are complex and involve a number of interactions amongst the mechanical parameters such as contact pressure, sliding velocity, lubrication; surface chemical effects such as metal oxidation and dissolution, adsorption of organic molecules present in the body fluids; and materials properties such as composition, microstructure, hardness; that determine wear [Munoz *et al.*, 2011]. Discussed here are the following parameters: material surface, environment, sliding speed and normal load.

(i) Material Surface

The material's surface finish is important as it greatly influences the friction and wear characteristics of most materials [Hanief and Wani, 2016], therefore, influencing the performance of the components. Roughness is the main concern in material surface finish where tribology is concerned [Masouros *et al.*, 1977]. Roughness is defined as irregularities in the surface texture that are inherent in the production process. Material's surface roughness exerts an influence on the contact of the sliding body on the counterface. Moreover, the surface roughness, beside misalignment of the components, can generate some vibration which contributes to the noise [Lundberg, 2014].

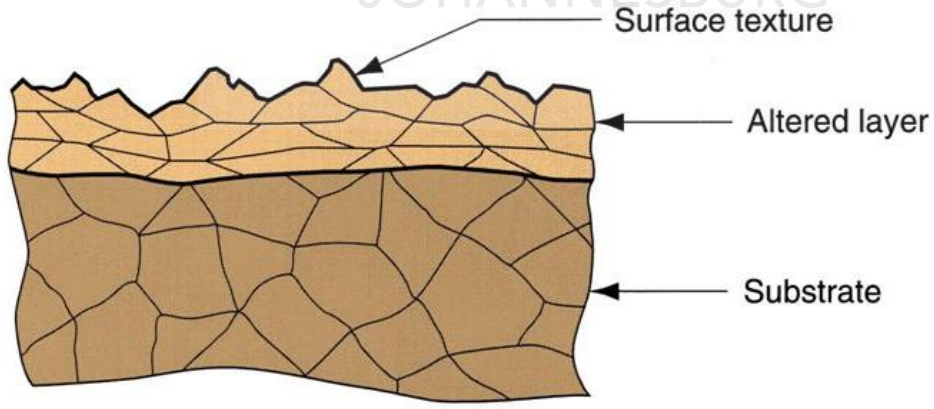

Figure 2.22: A typical engineering surface [Grooves, 2007].

Engineering surfaces (Figure 2.22) are also covered with asperities that usually have random height distribution and they are mostly covered with contaminants [Lu, 2008]. Most of these

surface contaminants consist of oxide layers that form on the clean material surface exposed to air, through the adsorption of molecules of oxygen and water vapour [Moore and Hopkins, 2013]. All of these contributions to the surface of the material should be considered as they significantly influence the tribological behaviour of materials.

(ii) Environment

Tribology material should exhibit some resistance to the environmental effect to be considered for the application in order to cut cost of replacement or maintenance. Highly chemical resistant materials would therefore be suitable for application in acids, alkalis and solvents. Usually neglected is the effects of humidity on the effect of friction and wear [Lancaster, 1990].

The points of contact (junctions) between contact areas of two bodies in tribosystem are major initiators of friction and wear. These regions of contact are commonly separated by adsorbed contaminant film (boundary film) from the environment [Rabinovich and Totten, 2006; Bowden and tabor, 1950], which may be broken down by tangential movement under normal load. It has been noted that high humidity on smooth surfaces increased adhesion through surface tension forces, however for surfaces with high roughness the effect of high humidity is insignificant [Zhang and Meng, 2015].

A review reported that at low load wear rate was low because the force was insufficient to remove the film, however at higher load there was a transition from the break of the film to real contact of the surface which resulted in high wear [Lancaster, 1990]. Moreover, the load to initiate the transition increased with increasing relative humidity which suggested that water vapour facilitated the formation of a more protective oxide. However, above the transition the wear rates were noted to be greater at high humidity which suggested that the adsorption of oxides impeded the aggregation and transfer of metallic debris.

(iii) Sliding Speed

Sliding speed is an important factor in tribology. It has been indicated that the coefficient of friction decreased with an increase in the sliding speed due to stick-slip phenomena [Moore and Hopkins, 2013]. The phenomena arise upon relative sliding of one rough surface against the other, when the kinetic friction is lower than the static friction [Bengisu and Akay, 1999]. At low speeds, friction is mostly due to local adhesion and shearing of contacting asperities.

These interactions of frictional resistance generates surface heating, however at low speed the heating generated is not sufficient to have great effect [Kennedy, 2001].

At high sliding speed the flash temperature phenomena is induced. According to Straffelini et al. [Straffelini *et al.*, 2002], in steels, if the flash temperature is about 400°C or higher and the sliding velocity is more than 1m/s, sliding wear is by oxidation and it is described by the Quinn theory. However, at lower sliding velocity, oxidation effects are absent, and the sliding wear process is dominated by plasticity.

Straffelini *et al.*, 2002, studied the effect of sliding speed (varied between 0.2 and 1.2m/s) on austenitic 304L and duplex 2205 stainless steels. It was found that the wear behaviour was characterised by sliding-distance transition, from delamination (transitional stage) to tribo-oxidation (regime stage) with reduction in wear rate. Moreover, it was also noted that the duration of the transitional stage increased as sliding velocity was increased and that the transition was more difficult in duplex 2205 than in 304L steel due to the presence of higher thickness of the protective oxide-rich scales than in 304L due to high chromium content in duplex 2205 steel.

(iv) Applied Load

Amongst the many factors including the ones mentioned earlier, beside the sliding velocity, the applied load plays a significant role in the friction of materials [Nuruzzaman and Mohammad, 2012]. Under different rage of normal load, different wear mechanisms are involved however, others are more prominent than the others in different situations. For instance, Jie *et al.*, 2016, in their studies involving dry sliding tests on Mg-Gd-Zn-Zr alloys they found that the wear mechanisms of abrasion, plastic deformation, oxidation, adhesion and delamination were detected. However, abrasion dominated the wear mechanism under the low load; whereas, adhesion dominated the wear mechanism under intermediate load, and under high load, plastic deformation had an effect on the wear rate.

Nuruzzaman and Mohammad, 2012, studied the effect of normal load and sliding velocity on friction coefficient of aluminium sliding against different pin materials. It was found that the friction coefficient increased with the increase in normal load and sliding velocity for all the tested pairs and that the magnitude of the friction coefficient varied for different pairs of material depending on normal load and sliding speed.

2.6.3.5 Wear Modes

As mentioned earlier, tribology concerns the study of contacting bodies under the influence of applied load. The bodies involved interact in different ways depending on several factors including the type of load, the type of motion, the type of environment and the characteristics of the contacting bodies. This interaction of bodies introduces several wear mechanism (Figure 2.23) and none of these mechanism can exist in isolation however, one may dominate. Discussed here are the four commonly experienced wear mechanisms.

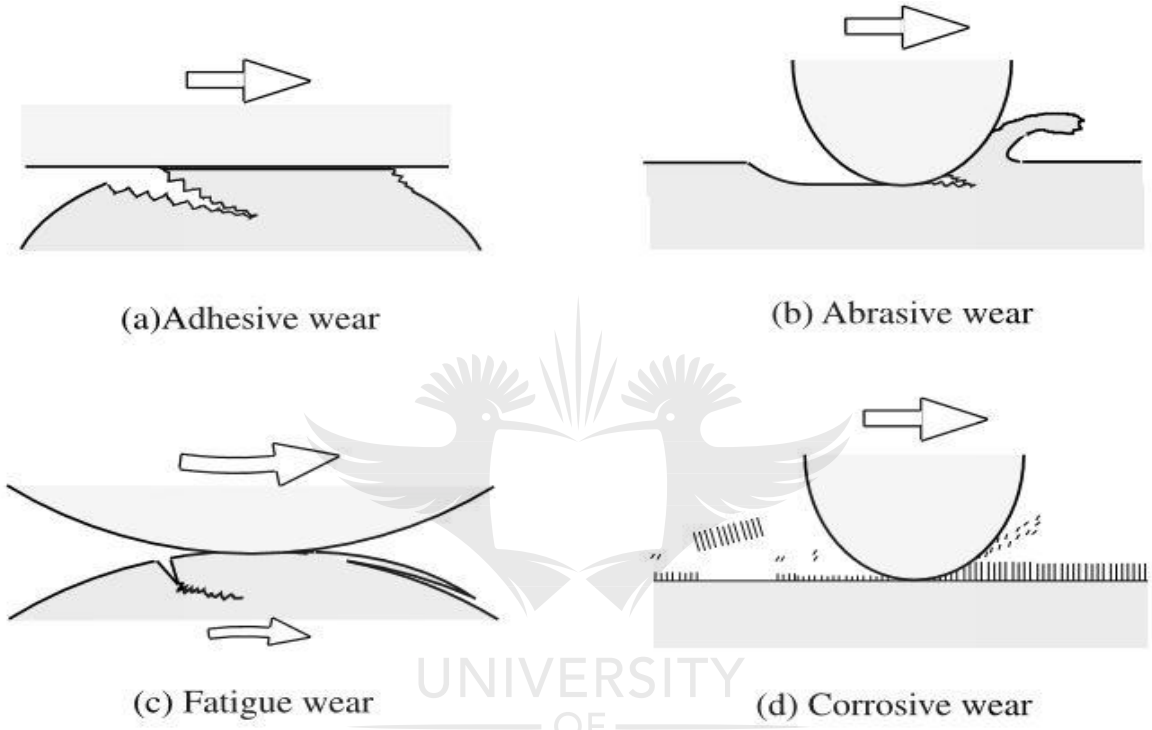

Figure 2.23: Schematic diagram of wear modes [Kado and Adachi, 2001].

(i) Adhesive Wear

Adhesive wear occurs when two surfaces in contact interact and form adhesive junctions at the interface. According to Dowson *et al*., 1992, there are several steps leading to the formation of adhesive-wear particles which can be identified as follows:

(i) deformation of the contacting asperities;
(ii) removal of the surface films;
(iii) formation of the adhesive junction;
(iv) failure of the junctions and transfer of material;
(v) modification of transferred fragments;
(vi) removal of transferred fragments and creation of loose wear particles.

Adhesive wear is influenced by the following parameters characterizing the bodies in contact [Masouros *et al.*, 1977]:

(i) electronic structure;
(ii) crystal structure;
(iii) crystal orientation;
(iv) cohesive strength.

(ii) Abrasive Wear

Abrasive wear is the most occurring and a severe form of wear [kovarikova *et al.*, 2009]. This type of wear arises when under applied load a harder asperities of a material penetrate the softer material surface producing plastic deformations through the actions of ploughing and cutting [Rahnejat, 2010]. In abrasive wear, if wear involves a harder material sliding on a softer material, the process is called two-body wear and if wear occurs by debris rolling between two other bodies then the process is called three-body wear [Wu *et al.*, 2014].

The amount of abrasive wear a material undergoes is governed by the extent of work-hardening it can undergo, its ductility, strain distribution, crystal anisotropy and mechanical stability [Stolaeski, 1999]. For example, a hexagonal cubic material will resist abrasive wear better than face centred cubic and body centred cubic materials [Stolaeski, 1999; Buckley and Johnson, 1968].

(iii) Fatigue Wear

Fatigue wear emerge when cyclic load is continually applied on the material through sliding, rolling or slippage [Mahzoon *et al.*, 2012]. The stresses induced on the contacting surfaces eventually lead to failure of the material and is classified as a fatigue failure [Stewart and Ahmed, 2002]. Although fatigue wear is associated with rolling contacts because of the cycling nature of the load, it also occurs in sliding contacts as the asperities of the contacting bodies are subjected to cyclic stress which over time they concentrate and leads to the generation and propagation of cracks [Barber and Ciavarella, 2009; Yust, 1985]. A number of steps leading to the generation of wear particles can be identified [Idriss and Erkki, 2014]:

- transmission of stresses at contact points;
- growth of plastic deformation per cycle;
- subsurface void and crack nucleation;

- crack formation and propagation;
- creation of wear particles.

(iv) Corrosive Wear

In highly chemical reactive materials, it is likely for friction between contacting materials to initiate chemical reaction. The environment and its active interaction with the materials in contact [Lancaster, 1990] mainly influence the severity of wear by chemical reactions induced by friction. The process of corrosion wear involves the contacting surfaces interacting with the environment, creating reaction products that are deposited on the surfaces [Wood, 2007]. The reaction products are then removed due to crack formation and abrasion, further exposing the underlying material to more corrosive environment [Dowson *et al*., 1992].

2.7. Summary

The future prospect for duplex stainless steel use in valves, pumps and impellers is a promising one, depending on the success of the optimisation of the duplex steel for an improved wear tolerance. The use of titanium nitride as an instrument to combat the limitations experienced by duplex steel could be a solution to many users of pumps, impellers, and valves. Nanoindentation and tribology ball on disk techniques could be useful in achieving the validation of the reinforced duplex steel for safety in the intended designs and applications.

CHAPTER 3: EXPERIMETAL APPROACH

This chapter presents the methodology flow diagram, materials and methods used in the research study.

3.1 Methodology Flow Diagram

This experimental procedure of this study was sectioned into three stages in order to achieve the aim and objectives. The fabricated composites with varying amounts of TiN nanoparticles were microstructurally evaluated. The second stage involved assessing the mechanical properties vis-à-vis nanoindentation and micro hardness testing. Also the samples were further subjected to wear using a tribometer and the worn surfaces were examined to determine the extent of damage. The methodology adopted is as presented in the flow diagram in Figure 3.1.

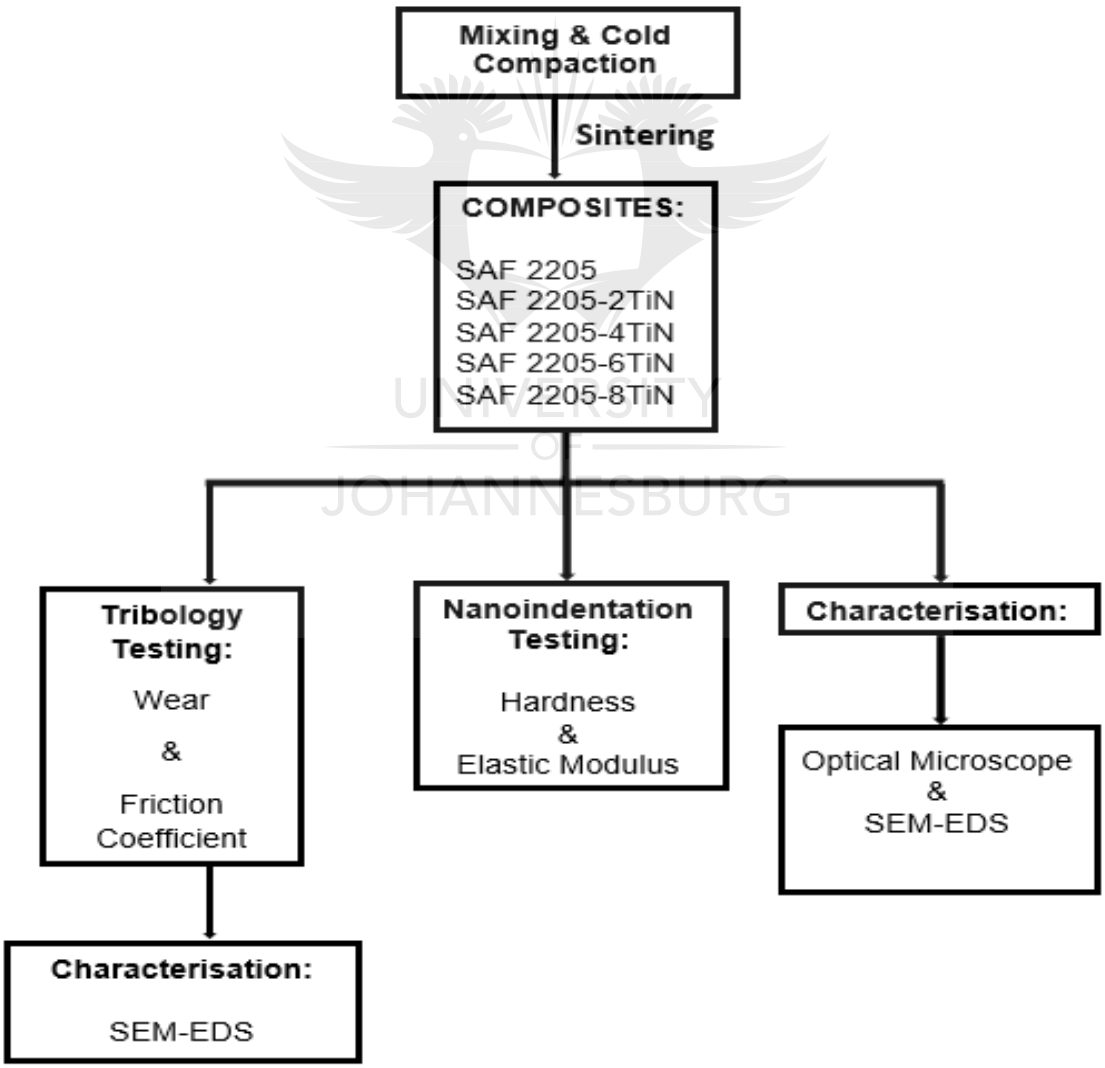

Figure 3.1. Methodology flow diagram

3.2 Materials

The starting powders utilized for this study were SAF 2205 duplex grade, (average particle size 22 µm, 96 % pure) supplied by Sandvik Osprey Ltd, UK and TiN (average particle size of 20 nm, 97 % purity) supplied by Nanostructured & Amorphous Materials, Inc. USA. The TiN dispersions into the DSS were in the order of 2, 4, 6 and 8 wt%. The chemical compositions of the powders are presented in Table 3.1. The following reagents were used in this study: de-ionized water, acetone, colloidal silica suspension (0.03 microns) and Carpenters reagent.

Table 3.1: Chemical composition of SAF 2205 and TiN (wt %)

Elements	C	Si	Mn	P	S	Cr	Ni	Mo	N	Ti	Fe
SAF 2205	≤0.03	≤1.0	≤2.0	≤0.03	≤0.015	22	5	3.2	0.18	-	Bal
TiN	0.03	<0.003	-	-	-	-	<0.001	-	21.91	77.83	<0.001

3.3 Method

3.3.1. Mixing of powders

Rule of mixture was used to calculate the appropriate amount of individual powders. The powders were mixed using a turbula mixer (T2F) for 6 hours at 72 rpm to ensure homogeneity.

3.3.2. Sintering

The mixed powders were sintered using an automated spark plasma sintering machine (model HHPD-25, FCT GmbH Germany). The composites were sintered in vacuum with pressure of 50MPa, sintering temperature of 1150 ^{o}C, heating rate of 100 ^{o}C/min and sintering holding time of 15 min (optimized sintering process parameters from our previous study). Graphite sheets were used to shield the powders from the die, upper and lower punches to ensure easy removal. The sintered products were sand blasted to remove the graphite contaminations on the surface of the products.

3.3.3. Microstructural Evaluation

For microstructural evaluation, nanocomposite samples were metallographically prepared by grinding with silicon carbide papers followed by polishing with colloidal silica suspension to flat mirror finished surfaces. The polished specimens were then etched using the Carpenters

reagent. The microstructures of the nanocomposites were then evaluated using an Optical Microscopy (ZEISS, AxioCam ICc 5) and JEOL Scanning Electron Microscopy (FESEM, JSM-7600F).

3.3.4. Evaluation of mechanical Properties

3.3.4.1. Nanoindentation

All nanoindentation tests were performed with Anton Paar ultra-Nanoindenter (UNHT) fitted with a diamond Berkovich indenter (Figure 3.2). The indentation experiments were run under force control mode as explained in [Mosima *et al.*, 2018], were an indentation test is ran under constant load to reach possible maximum depth.

(i) User Defined Profile

The indentation experiments were run to reach the peak force of 1mN using the user defined profile to make the indents. A minimum of 7 indents were made on the grains and the grain boundary for all the samples. The user defined profile allows the user to select where the indents should be, with the assistance of a built-in microscope offering three sets of magnification head making it possible to indent separately on the grains and the grain boundaries.

Figure 3.2. UNHT nanoindentation system

(ii) Grid Indentation (Advanced Matrix Profile)

UNHT nanoindenter was also used to perform an array of 10×10 indents with the separation distance of 20µm between indents covering the area containing the austenite phase, ferrite phase and the grain boundary. The maximum force for every indent was about 2mN. The loading cycle consisted with loading up to the peak force in 6s and a pause of 10s followed by unloading in 6s.

3.3.4.2. Micro hardness Testing

Micro hardness measurements of the materials were performed using a digital micro hardness tester (INNOVATEST Falcon 500) as shown in Figure 3.3. A profile of a minimum of 10 indents at different locations was made on each phase (austenite and ferrite) and the grain boundary. The applied load was kept at 10g for all the tests for a peak-load time of 30s. The indent's diagonals were measured optically to give hardness values of the materials with an accuracy of ±0.1µm.

Figure 3.3. Micro hardness tester

3.3.5. Tribology

All wear tests were carried out using a ball-on-disk tribometer, in respect to the ASTM G99-05 [American Society for Testing and Materials; 2005], a standard test method for wear testing with ball/pin-on-disk tribometers. These wear tests were carried out at ambient temperature under dry sliding condition using an Anton Paar Tribometer (TRB) (Figure 3.4). The relative humidity was kept at 50%. A hardened steel was used as a counterface material

for all tests. The tests were carried out for about 600 cycles covering distance of 11.31m, 22.62m and 33.93m for the load of 1N (3mm radius), 3N (6mm radius) and 5N (9mm radius), respectively. The samples were weighed before and after each test using a sensitive four digits analytical weighing balance. The wear volumes were determine using the weighed mass of the samples.

Figure 3.4. TRB tribometer system.

3.3.6. Analysis of the Wear Surface

The morphology of the worn sample surfaces was examined using the FESEM, JSM-7600F (Figure 3.5). The chemistry of the worn sample surface was evaluated using the energy dispersive spectroscopy (EDS).

Figure 3.5. SEM system [www.futurelabs.co.in].

CHAPTER 4: RESULTS AND DISCUSSIONS

In this section, the microstructure, plastic and elastic properties, wear and worn surface analysis of the spark plasma sintered duplex stainless steel (SAF 2205-TiN) evaluated using the optical and secondary electron microscopes, nanoindentation and ball on disc wear techniques were presented and discussed. The strain-to-break, plastic deformation parameters were used to estimate the resistance of the composites to wear in comparison to the coefficient of friction, wear volume and wear rate analyses.

4.1 Microstructural Properties: Introduction

The fundamental understanding of microstructural properties is to gain information on the chemistry of the material, shape, size distribution and phases present [Musil *et al.*, 2001]. These acquired understanding may potentially facilitate a better correlation of the microstructural properties to the physical and mechanical properties of the sintered material and ultimately lead to informed decision making based on performance, economic feasibility and availability as well as deciding on whether further analysis are required or process methods and parameters need to be modified [Asgari and Mohammadi, 2018].

A study worth mentioning is that by Sotomayor *et al.*, 2013. In their work, microstructural study of DSS obtained by powder injection molding, which is a form of powder metallurgy fabrication process, was conducted. By means of SEM-EDS, XRD and EBSD, they were able to identify the morphology and chemistry of the microstructure, the identification of phases and the transformation and or stability of the phases, respectively. From their findings, it was established that in a heterogeneous system where particles with different composition are present and diffusion phenomena becomes significantly important, thorough examination of the microstructure after processing should be obligatory.

4.1.1 Microstructural Properties: Results

The optical and Scanning Electron Microscopy (SEM) images of sintered Duplex stainless steel with varied amounts of nano TiN particle additions are presented in Figures. 4.1 and 4.2 respectively. The biphasic austenite-ferrite microstructure obtained by sintering is complex and different to those observed in conventional duplex SS [Oke *et al.*, 2017; Campos *et al.*, 2003; Cao *et al.*, 2013]. The microstructure is a function not only of the chemical composition of the powders, but also of the spark plasma sintering process parameters [Oke et al., 2017, Mariappan *et al.*, 2013; Dobrzank *et al.*, 2005]. The microstructure of the TiN

nanoparticles reinforced duplex SS showed the existence of three distinct phases consisting of a austenite, ferrite and grain boundaries dominated TiN particles. The TiN particles were noted to increase with TiN reinforcements (Figure 4.1) with a general tendency of the reinforcing TiN phase to locate itself at the vicinity of grain boundaries in the matrix. The presence of TiN particles at the grains does not appear to promote significant grain growth as observed in the SEM images. Evidently, TiN along the grain boundaries acts as an effective force in pinning these boundaries, thus avoiding grain boundary (GBr) migration. Previous researches [Charles, 2011] have found that nitrogen inhibits grain growth during the thermal processing of Fe powders.

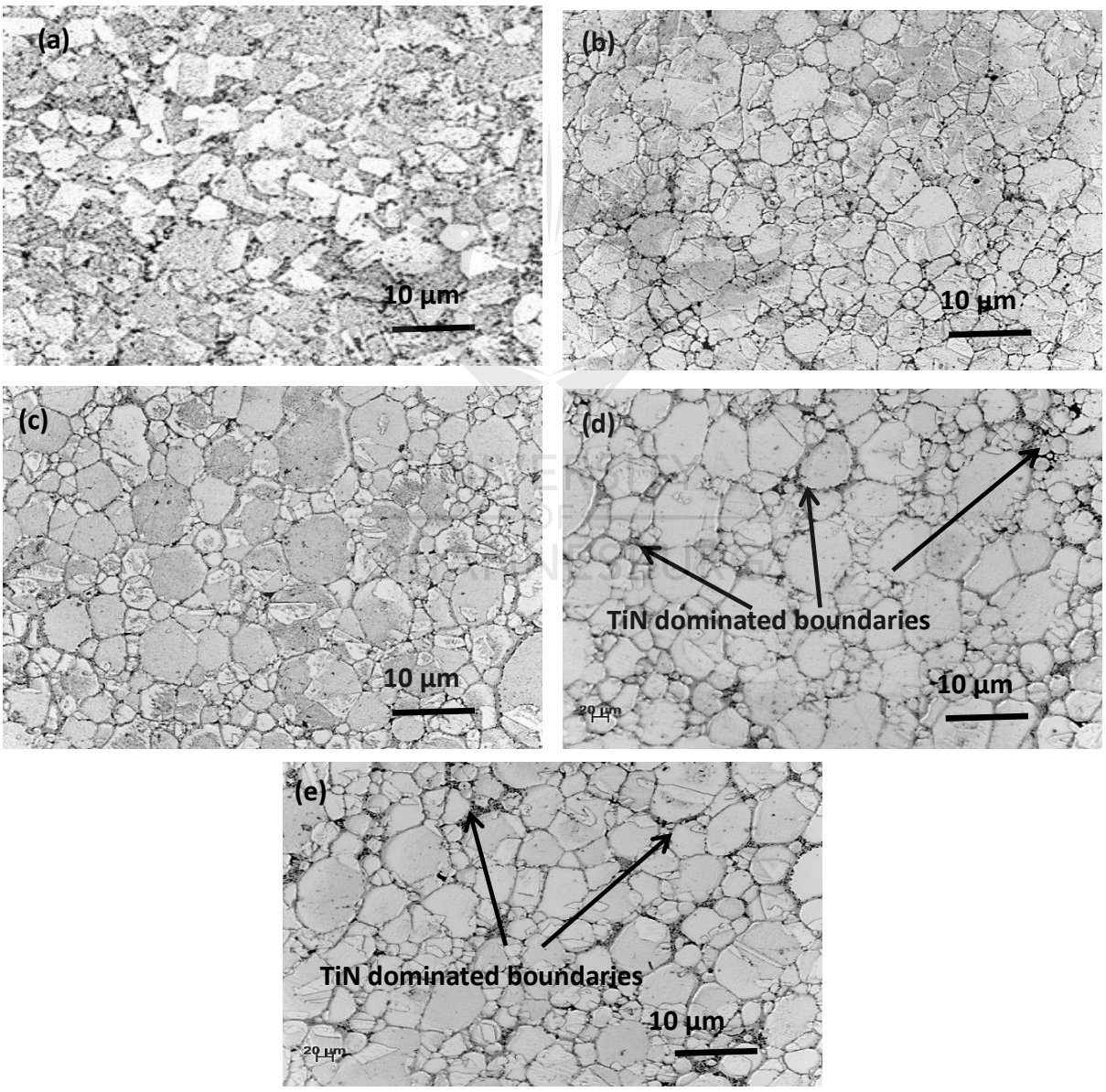

Figure 4.1. Optical microstructure showing the effect of TiN on the microstructure: (a) SAF 2205 (b) SAF 2205-2TiN (c) SAF 2205-4TiN (d) SAF2205-6TiN (e) SAF 2205-8TiN

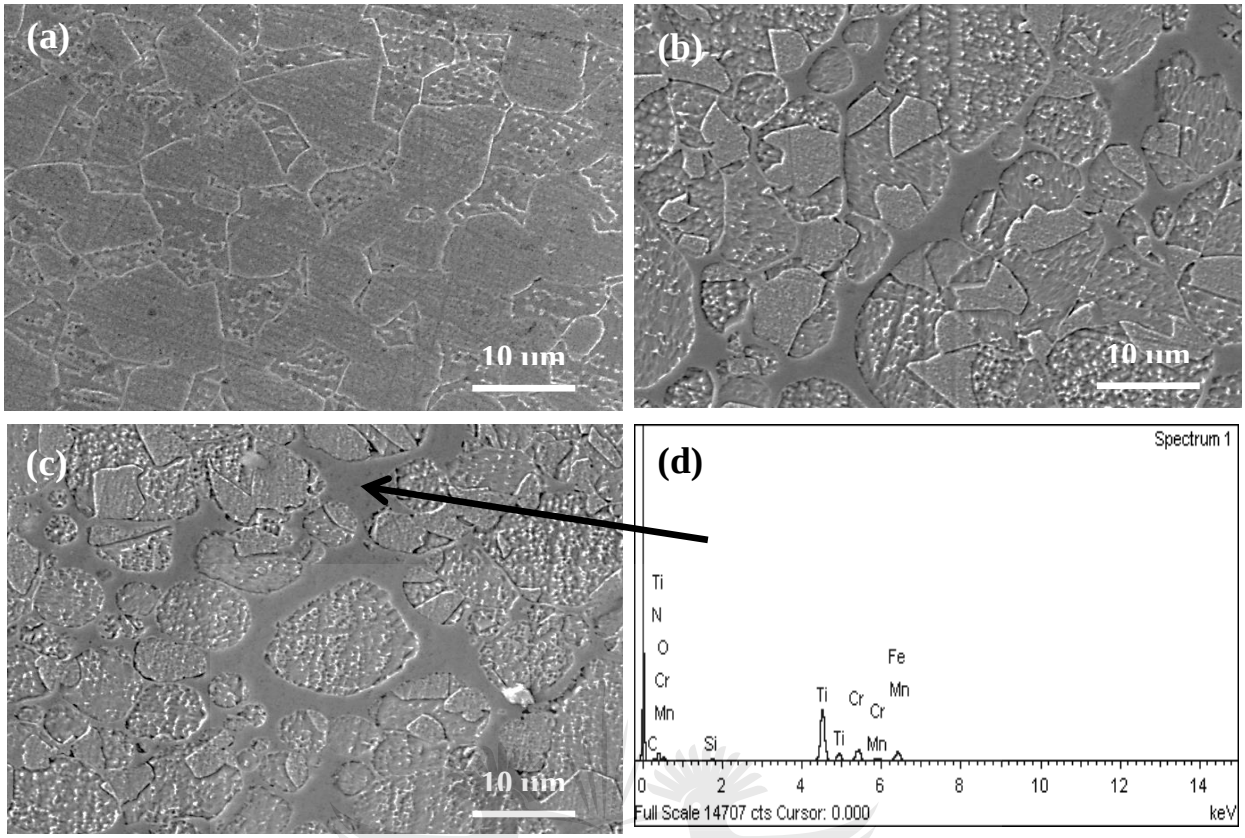

Figure 4.2. Scanning electron micrographs (SE): (a) SAF 2205 (b) SAF 2205-6TiN. (c) SAF 2205-8TiN. (d) EDX showing presence of TiN.

4.2 Mechanical Properties

Another important aspect upon the development of the potential material for any applications is the accurate determination of the materials' properties. Proper understanding of mechanical properties of a materials including multi-phase structured material such as duplex stainless steel is very important for an advanced material design and application. Not only is it customary for safety but also economically it is viable, to avoid probable costs of poor quality. Amongst many methods available for testing mechanical properties, hardness and elastic modulus are usually primary [Schuh, 2006].

4.2.1 Hardness Properties

It is undisputed that hardness is a multifunctional property and therefore is one of the most commonly tested mechanical properties due to the potential it hold to reveal, understand or open channels to estimate other mechanical properties [Broitman, 2017]. In the studies by Musil *et al.*, 2002, the hardness property of the nanocomposite coatings was correlateted with the elastic modulus (E) and elastic recovery (W_e) as well as the resistance to plastic deformation (H^3/Er^2) material. On the other hand, Ehtemam-Haghighi, Cao and Zhang, 2016,

in addition to E, H3/Er2, and We they correlated H to H/Er (ability to resist strain to failure), U_p/U_{tot} (plasticity index) of Ti based alloys.

4.2.1.1 Micro-Hardness Properties in Relation to Nanohardness

Figure 4.3 and Table 4.1 shows the results of average micro and nano hardness values obtained from different TiN reinforced SAF 2205 matrix composites. It is observed that the addition of nano particles of TiN to the steel matrix led to significant increase in the micro and nanohardness of composites. In both the cases all composites samples displayed improved hardness compared to that of the unreinforced stainless steel. The lowest micro and nano hardness values were measured as 293.13 VHN and 4.86 GPa respectively for SAF 2205, and the highest hardness values were measured as 476.18 VHN and 16.17 GPa for steel matrix composite with 8% reinforced TiN. Both micro and nanohardness tests displayed similar trends in the increment of hardness values of composites with reference to the unreinforced steel. The increase in hardness values in both cases can be attributed to the high hardness, good dispersion and strengthening effect of TiN nano particles in the steel. It has been reported that good dispersion of reinforcements aids the improvement the interfacial bonding between steel matrix and reinforcements [Chen *et al.*, 2015; Guan *et al.*, 2018]. It is also important to state that the reinforcements could sufficiently resist plastic deformation during indentation.

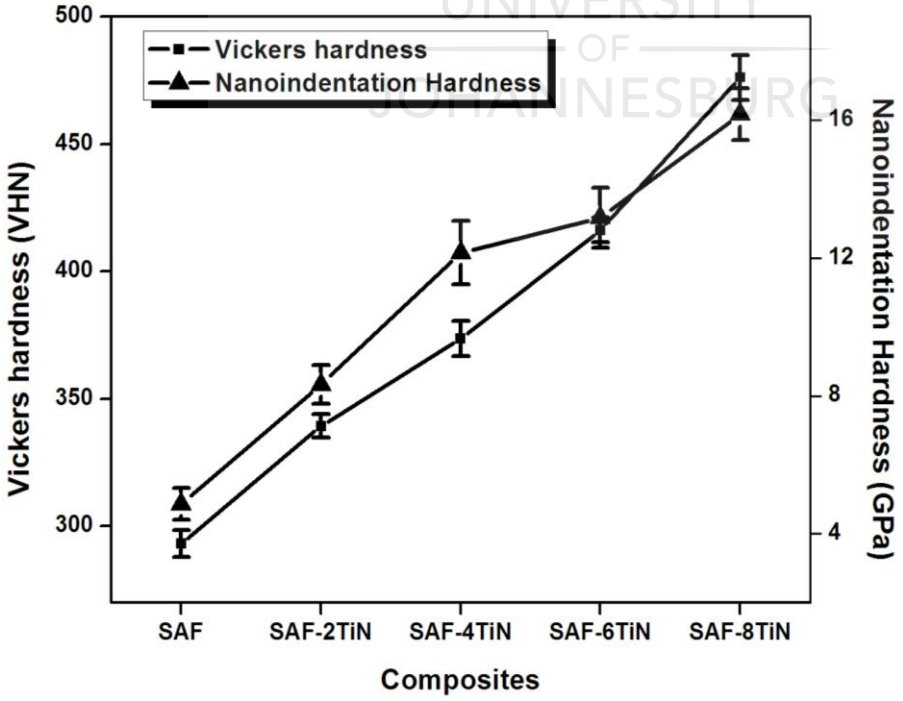

Figure 4.3: Micro and nanoindentation hardness plots of SAF 2205 and its composites.

Table 4.1: Micro and nanohardness values of SAF 2205 and composites

S/N	Composites	Vickers hardness (VHN)	Nanoindentation Hardness (GPa)
1	SAF 2205	293.13	5.35
2	SAF 2205-2TiN	339.32	8.33
3	SAF 2205-4TiN	373.71	12.15
4	SAF 2205-6TiN	416.32	13.17
5	SAF 2205-8TiN	476.18	16.17

4.2.1.2 A correlation between micro-hardness and nano-hardness

The plot of the measured average Vickers hardness as a function of corresponding nano-hardness for the stainless steel composite is presented in Fig. 4.4. A significant linear relationship is observed to exist between Vickers hardness and nano-hardness. Therefore, line regression can be used to model the linear relationship between Vickers hardness and nano-hardness. The value of the correlation coefficient obtained indicates that the linear relationship is reliable enough to be used to model the relationship of Vickers hardness and nano-hardness for SAF 2205/TiN composites.

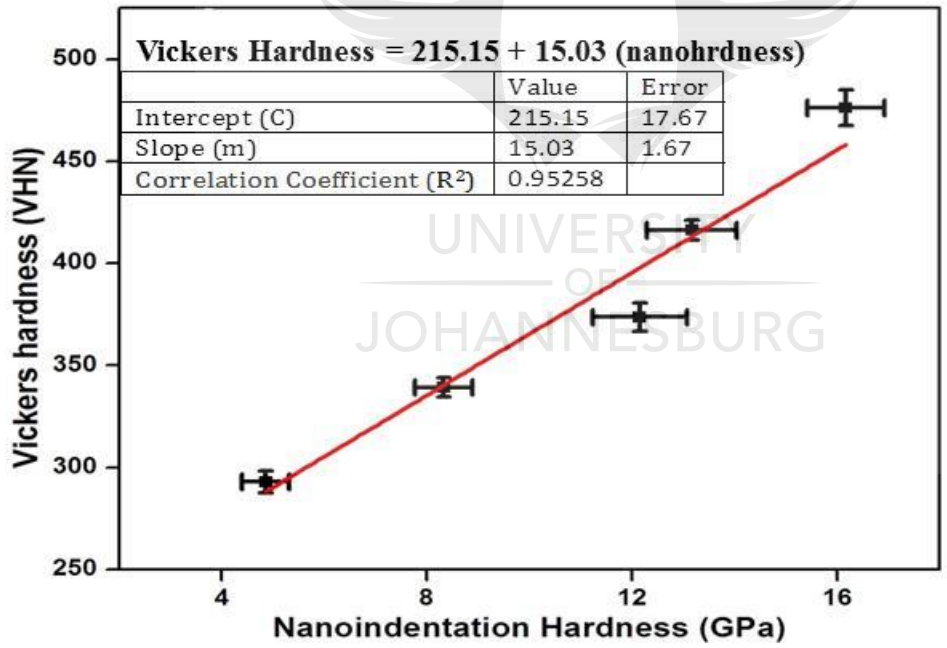

Figure 4.4. The Vickers hardness plot as a function of corresponding nano-hardness with increase in TiN nanoparticles.

The deviation in linear fit as noted in Fig. 4.4 is possibly from the influence of pile-up or sink-in effect occurred during the hardness measurement [9]. The established correlation between Vickers hardness and nano-hardness (HV = 215.15 + 15.03Hnano) indicates that

there is no difference in behavior for the Vickers hardness and nano-hardness, both of which were obtained from an indentation on materials with an indenter. Yang et al. [9] has established the correlation between Vickers and nanohardness, the authors reported a linear relationship and no significant difference in Vickers and nanohardness. They concluded that the only difference between Vickers hardness and nano-hardness is the definition.

4.2.1.3 Nanohardness Properties of fabricated composites

(i) Load-displacement graph and Load-time graph

Representative nanoindentation behaviours of the TiN dispersion strengthened SAF 2205 composites are presented in Figures. 4.5 and 4.6. Nano indents were taken separately on the grains and the TiN dominated grain boundaries. The loading and unloading curves at maximum load 1MN at grains and grain boundaries for the different grade of composites are presented in Figure 4.5. A smooth loading, holding at maximum load and unloading curve without evidence of pop-in effects (an assumption that existing dislocations inside the stressed area of the samples take part continuously in plastic deformation and no sudden displacement jump occurs) is evident as shown in Figure 4.5. Though similar loading and unloading behaviour was observed within grains and at grain boundaries, indentation depths at grain boundaries were noticed to be lower.

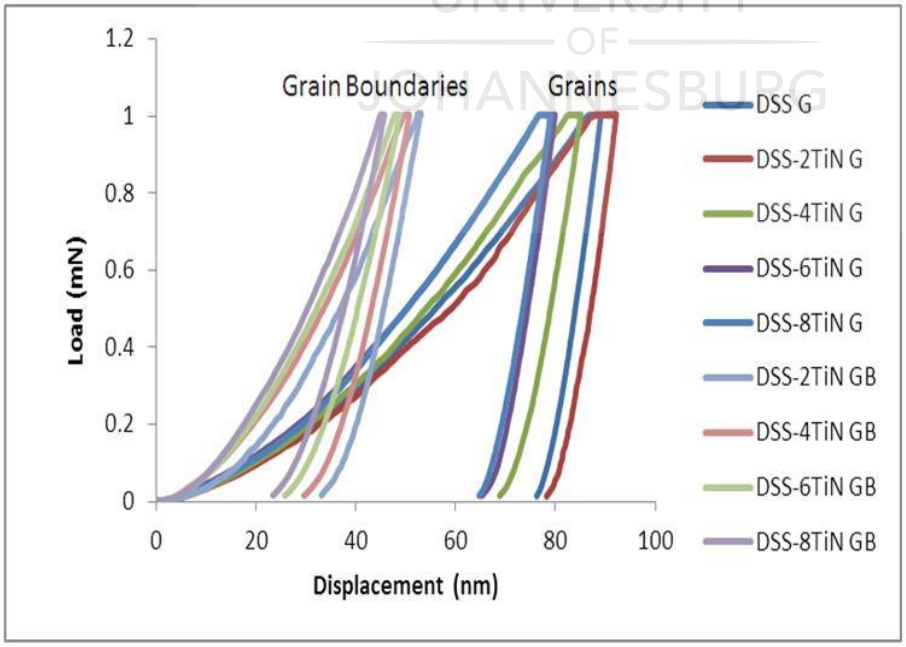

Figure 4.5. Load-displacement curves showing penetration depth at grains and grain boundaries of SAF 2205-TiN.

The behaviour at the grain boundaries could be attributed to addition of nano particles of TiN which dominates the grain boundaries as shown in Figure 4.2b. It was also obvious that the indentation depths decreased with increased addition of TiN at the grain boundaries. This is also owed to the strengthening effect played by TiN at the grain boundaries by blocking dislocation motion in the composite material. The large penetration depths at the grains are due to high energy dissipated in the composites as a result of plastic deformation [Yan *et al.*, 2016; Li and Bhushan, 2001]. The variation of penetration depth with increase in TiN content at the grain is expected due to strengthening through load transfer between the SAF 2205 matrix and the segregated TiN reinforcements. Load transfer is largely dependent on the bond integrity at the reinforcement-metal matrix interfaces [Yan *et al.*, 2016; Sadeghpour *et al.*, 2014; Oliver and Pharr, 1992].

The penetration depth as a function of time at grains and grain boundaries are shown in Figure 4.6. Excessive plastic deformation is apparent in the nano structured composites in the first 10 min both at grains and grain boundaries. The penetration depth on the grain boundaries ranges from 20 nm to 35 nm while on the grains it ranges from 65nm to 80nm. The extent of penetration at the grain boundaries could be attributed to the resistance to deformation posed by the nano-sized TiN. At this stage the phases tend to attain a stable configuration to resist the penetration effect of the indenter. The excessive deformation is followed by no plastic deformation behaviour characterized by a constant penetration depth irrespective of time, an indication that the nano sized composites are totally resistant to plastic deformation at 1 mN. The decrease in penetration depth is as a result of unloading.

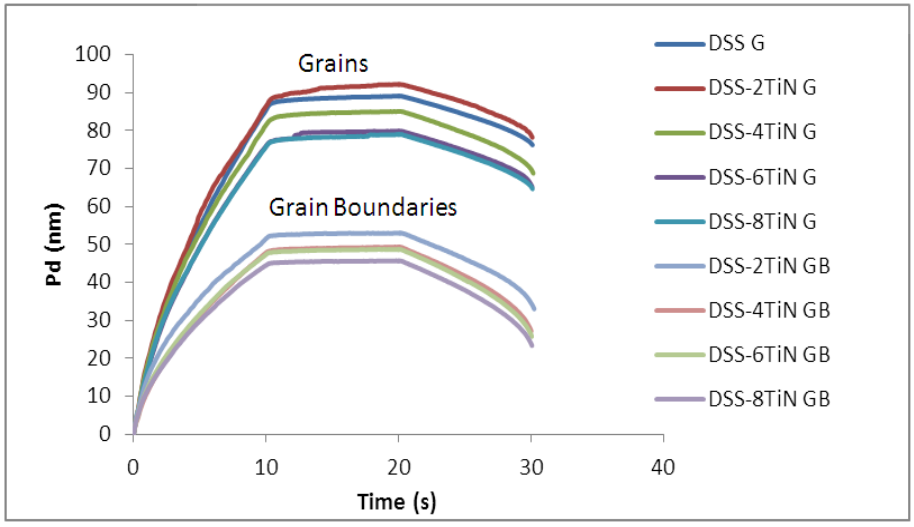

Figure 4.6. Penetration depth against time at grains and grain boundaries of SAF 2205-TiN.

(ii) Hardness Properties

The values of hardness (H) of the investigated samples at grains and grain boundaries as calculated from the load-displacement curves are presented in Figures 4.7. Figure 4.7 showed that the grain boundary hardness increased linearly with increasing TiN concentration, while the relationship is sinusoidal for grain – the unreinforced SAF 2205 sample have higher hardness than the one with 2% TiN and continued to increase for 4% TiN after which it dropped for 6% TiN while the maximum hardness values was obtained for SAF 2205-8TiN. Also, it was noticed that there are huge differences in the hardness values for grain and grain boundaries for all the samples.

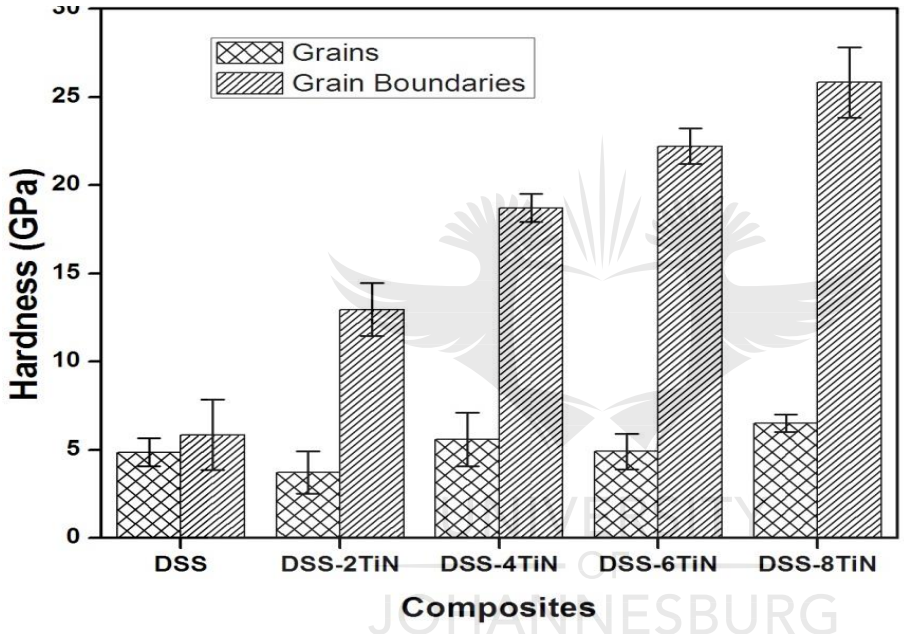

Figure 4.7. Hardness results of SAF 2205/TiN at grains and grain boundaries

4.2.2 Modulus of Elasticity: Introduction

According to Han *et al.*, 2012, Elastic modulus of materials is one of the important mechanical properties especially in applied and fundamental fields. It should also be noted that different hardness can exhibit the different modulus of elasticity. Therefore a very hard material with high plastic deformation (low H^3/Er^2) or a very elastic material with high resistance to plastic deformation (high H^3/Er^2) can be formed [Musil *et al.*, 2001].

4.2.2.1 Modulus of Elasticity: Results

From Figure 4.8, it is evident that variations of the elastic modulus increased with increase in TiN content of the duplex stainless steel at the TiN dominated grain boundaries with the

duplex steel reinforced with 8 % TiN having the highest elastic modulus of 325.05 GPa. However, the elastic modulus at ferrite/austenite grains was noted to decrease with the addition of TiN up to 4 %. Further increase in the TiN content raised the elastic modulus. The variation of elastic modulus at the grains could be as a result of the difference in hardness and elastic modulus of ferrite and austenite.

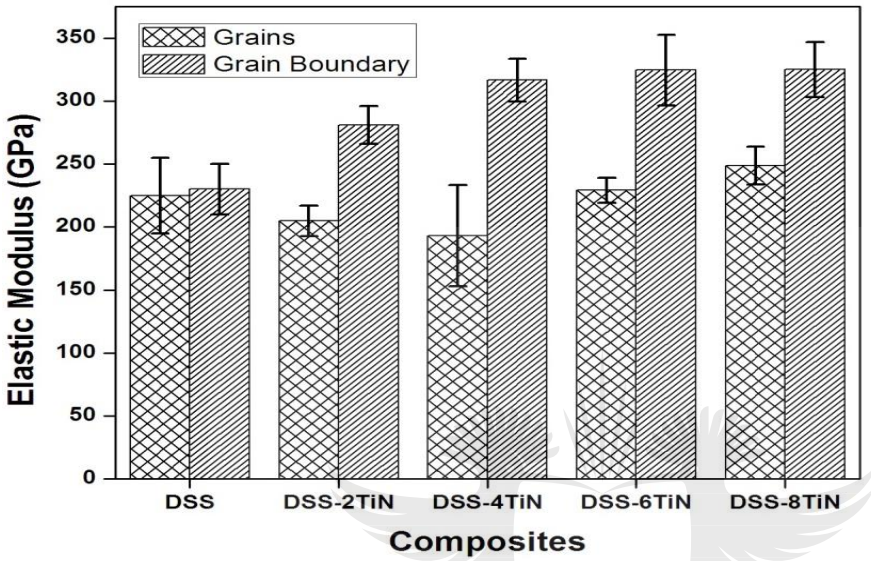

Figure 4.8. Young modulus results of SAF 2205/TiN at grains and grain boundaries.

4.2.3 Mean hardness and Modulus of Elasticity

The mean values of hardness (H) and modulus of elasticity (E) of the investigated samples at grains and grain boundaries as calculated from the load-displacement curves are presented in Figure 4.9 and Table 4.2.

Table 4.2. Average hardness and elastic modulus values at grains and grain boundaries

Samples	Grain		Grain boundary	
	Hardness (GPa)	Elastic Modulus (GPa)	Hardness (GPa)	Elastic Modulus (GPa)
SAF 2205	4.86	224.96	5.84	226.07
SAF 2205-2TiN	3.72	204.85	12.94	280.97
SAF 2205-4TiN	5.59	193.06	18.71	316.67
SAF 2205-6TiN	4.91	229.21	22.21	324.52
SAF 2205-8TiN	6.51	248.88	25.83	325.05

Noticeably, the grain boundaries exhibits a rather large H and E_r compared to the grains. The H and E_r were also noted to increase with increase in TiN content at both the grain and grain

boundaries. The steel grade reinforced with 8 % nano sized TiN had the highest H and Er. It may be argued that dispersion/grain boundary hardening and matrix/reinforcement load transfer effects could be responsible for such pronounced difference in hardness between the grains and grain boundaries. It is worth mentioning that TiN is known to be a hard ceramic phase [Angerer *et al.*, 2005]. With increase in TiN content, the role of grain boundaries in blocking dislocation propagation becomes more and more pronounced, resulting in an increased stress concentration at grain boundaries due to dislocation pile-up. Thus, higher applied stresses are needed to propagate dislocations through the material, resulting in a larger hardness [Musil *et al.*, 2002; Kiyohiro *et al.*, 2014]. The nature and orientation of the SAF 2205/TiN boundaries can also cause dislocations multiplication, due to this effect there is increase in dislocation density and dislocations tend to hinder the movement of other dislocations, eventually also leading to an increase of hardness [Abdi *et al.*, 2014]. Figure. 4.9 is the calculated average hardness and young modulus for both grains and grain boundaries increase as the TiN composition increased.

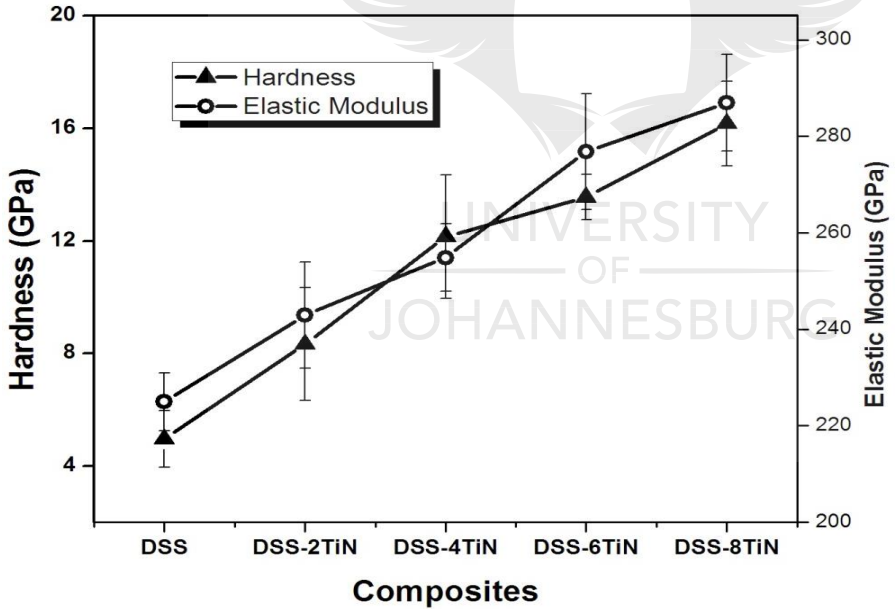

Figure 4.9. Average hardness and young modulus (grains and grain boundaries) results of SAF 2205/TiN.

4.2.4 Resistance to Elastic Strain to Failure and Resistance to Plastic Deformation

It has been established that the ability of a material to resist elastic strain which is described by the H/Er ratio is a measure of the material resistance to wear. The yield pressure (H^3/Er^2) is another important parameter that describes the ability of a material to resist plastic deformation [Sadeghpour *et al.*, 2014; Masanta *et al.*, 2011; Xu *et al.*, 2014]. Higher values

of H/Er and H^3/Er^2 ratios indicate better wear and resistance to plastic deformation respectively. The above parameters were used to estimate the anti-wear ability (associated with plastic deformation) of the nano-sized reinforced SAF 2205 composite.

The results of H/E_r and H^3/E_r^2 calculated from the H and E_r values for the different nano reinforced composites are presented in Figure 4.10 and Table 4.3. The ratios H/E_r and H^3/E_r^2 ratios were noted to increase with TiN content; this is expected due to high hardness as a result of increase in TiN content from 0 to 8%. It is noted that the H/E_r ratios were higher at the grain boundaries than the grains. Although the TiN phase is intrinsically harder than the ferrite and austenitic phase, its existence in the nano range at grain boundaries could effectively pose resistance to plastic deformation thus resulting in practically high H/Er ratios. In our instance, the existence of a two-phase microstructure (including the presence of nano TiN at boundaries) favours the increase of the wear resistance [Hynowska *et al.*, 2013; Leyland and Matthews, 2000].

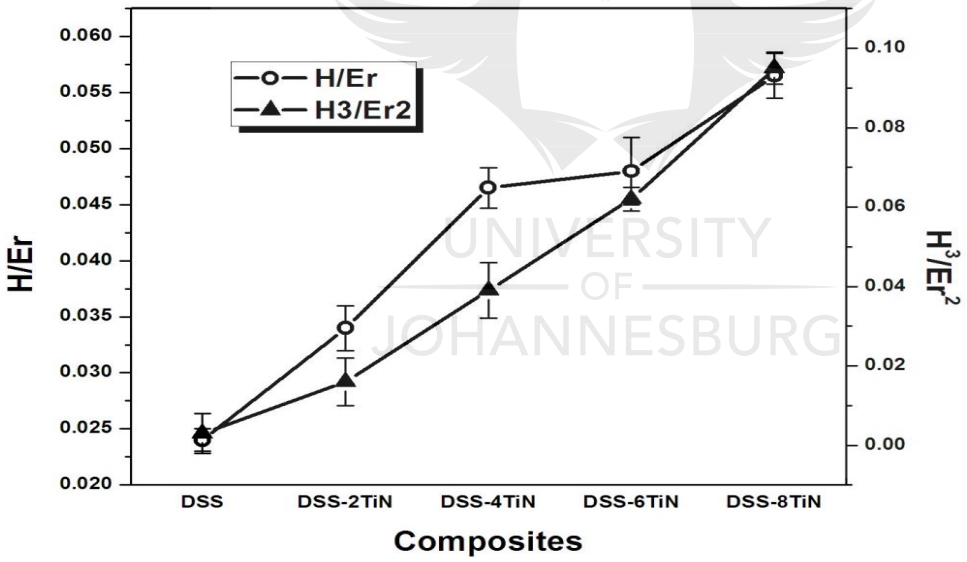

Figure 4.10: H/Er and H^3/Er^2 ratios of the SAF 2205 with varied TiN additions.

Table 4.3. Mean values of H/Er and H^3/Er^2

Samples	H/Er	H^3/Er^2
SAF 2205	0.024	0.003
SAF 2205-2TiN	0.034	0.016
SAF 2205-4TiN	0.0465	0.039
SAF 2205-6TiN	0.048	0.062
SAF 2205-8TiN	0.0565	0.095

4.3 Tribological Properties

Tribology testing reveals the behaviour of wear and coefficient of friction. Through the understanding of these two core aspects of tribology, deeper understanding of wear mechanisms phenomena occurring under operating conditions [Varga *et al.*, 2017] could be attained. Furthermore, the relationship between wear and friction of coefficient for that specific system could be understood as it may differ depending on the conditions and materials [Choudhury and Gupta, 2017].

Study on sliding wear of Austenitic and DSS stainless steels by Straffelini *et al.*, 2002, is a classical example in the context of this research work. Their experimental findings revealed the dependence of wear rate on sliding, frictional behaviour (depending on wear mechanisms), formation of tribo-oxidation layer due to the presence of Chromium and the evolution of surface temperature.

4.3.1 Coefficient of Friction

Figure 4.11 presents the coefficient of friction as a function of load for the nano TiN particles reinforced SAF 2205 stainless steel. It shows that the coefficient of friction decreases with increaseing load from 1 to 5N but tend to increase with increase in TiN content from 0 to 8 %. The reduction in the coefficient of friction value with increase in applied load could be as a result of slither (movement over surfaces) occurring between contact surfaces. When the applied load is increased from 1 to 3 N, an increase in contact temperature is evident due to increase in nominal area contact between pin and counter surface. The rise in contact temperature results in softening of the surface and thus more slipping action occurs between the contact surfaces thereby decreasing the coefficient of friction [Onuoba *et al.*, 2016; Zhang *et al.*, 2017; Jin and Plucknett, 2016]. Further increase in nominal load to 5 N was noted to advance the decrease in coefficient of friction. The further reduction in coefficient of friction can be attributed to the higher the shear rate at the load of 5 N. At this load, there is reduction in contact areas characterized by severe wearing of the sample surface, breaking and producing the chips. [Cao *et al.*, 2013] reported the formation of tribolayer as a result of severe wearing/deformation due to higher loads, it was explained that presence of such tribolayers could prevent the actual contact between mating surfaces there by further lowering the coefficient of friction. Researchers [Samarai *et al.*, 2012; Rao *et al.*, 2001] have presented similar results of reduction in coefficient of friction with increase in load for different alloys and composites. However, it is noted that increase in coefficient of friction

with increase in TiN nanoparticle addition is independent of the applied load. The increase in coefficient of friction with reinforcements could be attributed to the presence of hard TiN nanoparticles in the steel matrix. These uniformly dispersed reinforcements protrude from the softer duplex matrix and are pulled out during the contact. These pulled TiN particles slide at the contact surface thereby increasing the friction coefficient [Mousavi *et al.*, 2010].

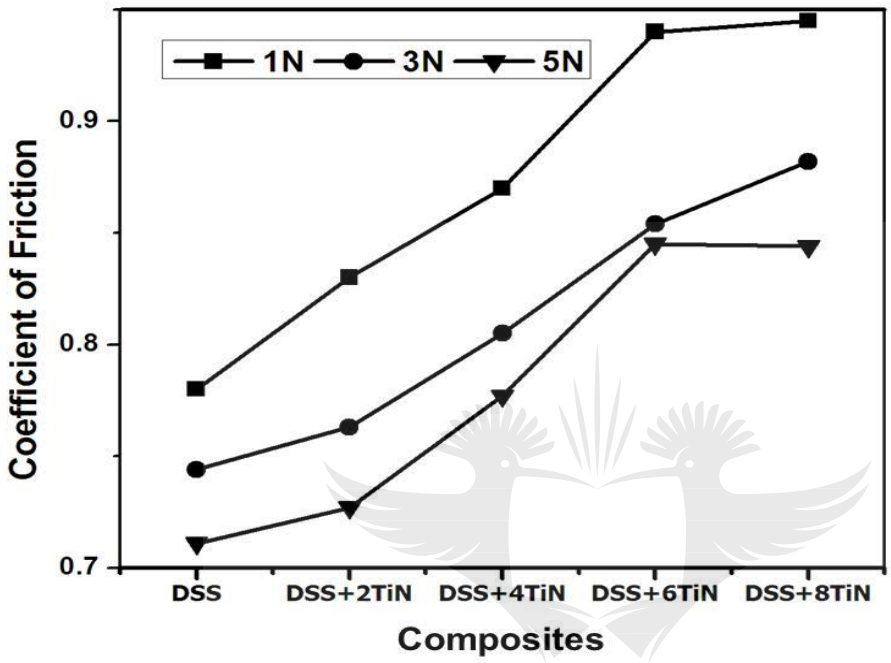

Figure 4.11. Mean value of coefficient of friction of SAF 2205 alloy and its composites as a function of applied load. Mean values were obtained from the total test duration in each case.

4.3.2 Wear Volume

The variation in wear volume of the TiN nanoparticles reinforced stainless steel composites for different loads for 1, 3 and 5 N is presented in Figure 4.12 and Table 4.4. It was observed that at lower load (1 N) there is a linear relationship between the volumetric loss and TiN concentration. The trend becomes parabolic as the load increased to 5 N. It is noted from Figure 4.12 that by increasing the TiN nanoparticles up to 6 weight percentage, the wear volume of the composites gradually decreases and the wear resistance of the composites increases irrespective of the load used. However, when the volume fraction of the TiN is increased further to 8 %wt, the volume loss of the composite was observed to increase. The volume loss of the duplex stainless steel matrix alloy was higher compared to that of the composites; this indicates better wear resistance with the addition of TiN nanoparticles.

It has been reported that an increase in the weight percentage of ceramic reinforcement improves the hardness of the composites which improves the wear resistance of the materials [Onuoha *et al.*, 2016; Zhang *et al.*, 2017; Wu *et al.*, 2018; Sulima *et al.*, 2014; Ni *et al.*, 2011]. The results were up to 6 % TiN reinforcement in agreement with the strain-to-break parameter (H/Er) and yield pressure (H^3/Er^2) results which were used to evaluate the antiwear capabilities in the previous section. Though, the H/Er and H^3/Er^2 ratios were highest for the reinforced stainless steel containing 8 % TiN, the wear resistance was inferior compared to other grades of composites. However, the decreasing tendency in wear resistance of the composites containing 8 % of TiN nanoparticles was attributed to the presence of voids, cracks, and agglomeration of nanoparticles. The presence of these defects in materials could act as effective weakening sites under load [Mallikarjuna *et al.*, 2017]. Furthermore, researchers [Chen *et al.*, 2015; Koppad *et al.*, 2013] have reported a reduction in the mechanical properties of nanoparticle reinforced composites when the volume fraction of nanoparticles in the composite exceeds 4 vol%. They argued that the reduction in mechanical properties of composites might be due to the agglomeration of nano-sized particles. It is imperative to state that the mechanical properties of MMCs have a great influence on wear resistance of the composites.

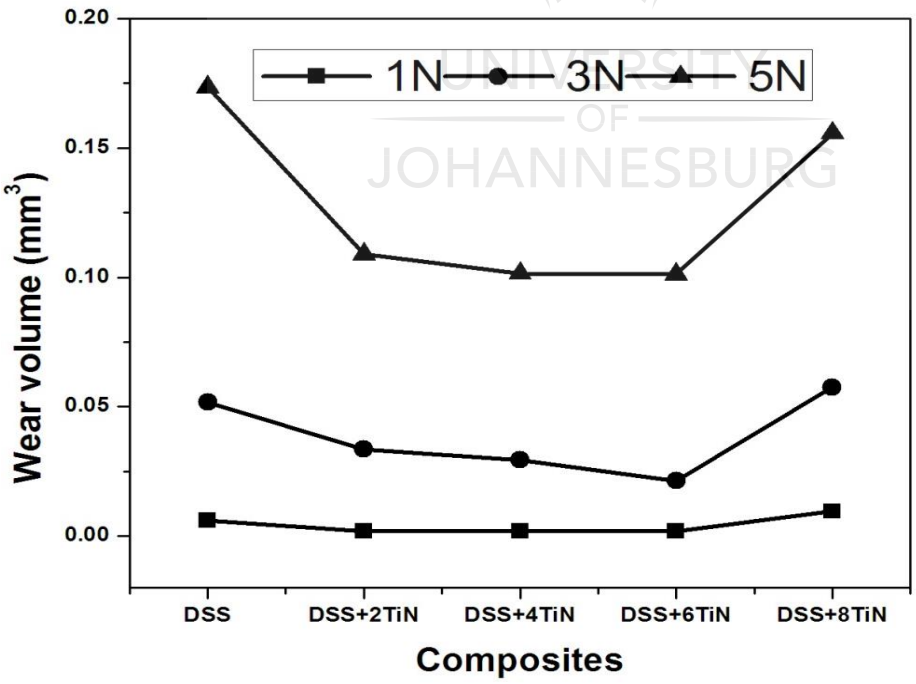

Figure 4.12. The volumetric wear loss as a function of TiN nanoceramic reinforcements

The volume of wear is also observed to increase when the load increases from 1 to 5 N for all the grades of stainless steel composite (Figure 4.13). It is clear that the volumetric loss increases with applied load in a nominally linear manner. This observation broadly complies with the Lancaster model, which states that the volumetric wear loss exhibits a linear dependency with applied load [Lancaster, 1967]. This abrading action of hard TiN nanoceramic particles increases when the applied load increases, which in turn increases the volume loss of the composites. Higher amount of stress due to increase in applied load acts on the ball and composite contact that leads to large plastic deformation of the composite surface. Composite containing 6 % TiN reinforcement exhibits better wear resistance compared to the matrix alloy and other grade of composites.

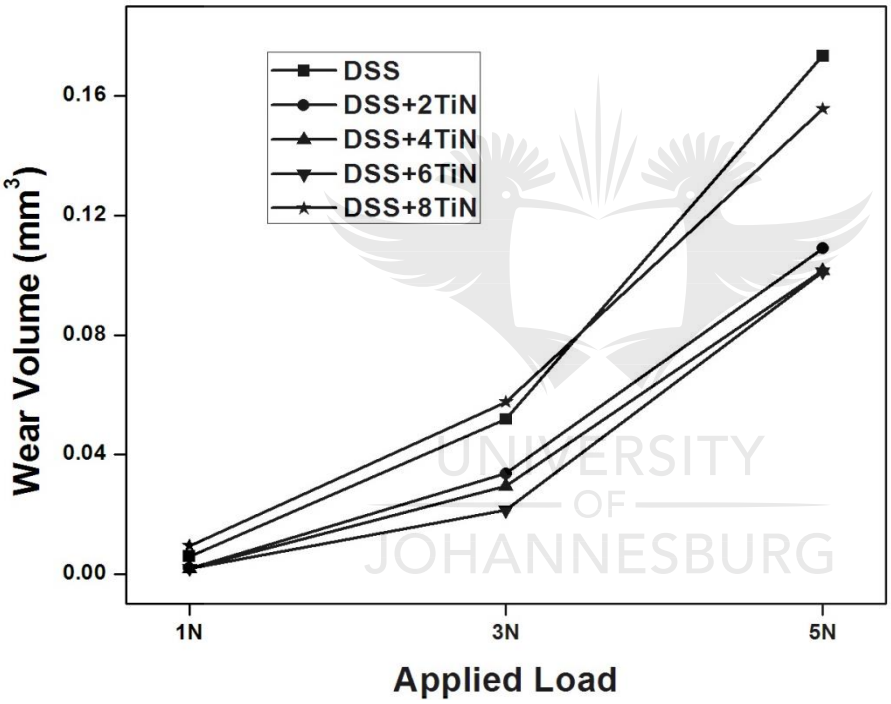

Figure 4.13. The volumetric wear loss of TiN–2205 stainless steel as a function of applied load.

Table 4.4: Volumetric wear loss values as a function of applied load

Composites	Wear volume (mm^3)		
	1N	3N	5N
SAF 2205	0.00598	0.05183	0.17343
SAF 2205-2TiN	0.00198	0.03368	0.10897
SAF 2205-4TiN	0.00197	0.0295	0.10148
SAF 2205-6TiN	0.00195	0.02146	0.10118
SAF 2205-8TiN	0.00958	0.05761	0.15569

4.3.3 Wear Rates

In engineering applications, wear and specific wear rates are very important parameters. Wear rate is independent of load applied and defined as volume loss per unit distance. Specific wear rate depends on applied load to cause wear; it is volume loss per unit meter per unit load. Their units are m^3/m and m^3/Nm respectively. Results of variation of wear and specific wear rate of pure sintered duplex stainless steel and its composites as a function applied load is shown in Figures 4.14, 4.15 and Tables 4.5 , 4.6 respectively. It is apparent that the wear and specific wear rates increases with the applied load but decreases with the incorporation of TiN nanoparticles into the stainless steel matrix up to 6 % reinforcement. The reduction of wear rates is an indication that the addition of TiN nanoparticles improved the wear resistance of composites compared to the unreinforced steel. Increasing the TiN content of the stainless steel results in an associated reduction in wear rate, this could be attributed to the high hardness/elastic modulus TiN phase. The TiN nanoparticles can resist plastic deformation, and offer additional resistance to the effective load applied. The extent of material removal from the steel surface, in the form of particle pull-out, decreases with increase in TiN content and is related to higher hardness of the TiN. At low loads and higher TiN content, the steel deformation and material removal is effectively minimised by the TiN grains, which form a contacting network that resists wear. The degree of plastic deformation is high at higher applied loads which promotes higher wear rates in all samples. The wear rates obtained in our study is comparable to those obtained in previous studies [Niu *et al.*, 2013].

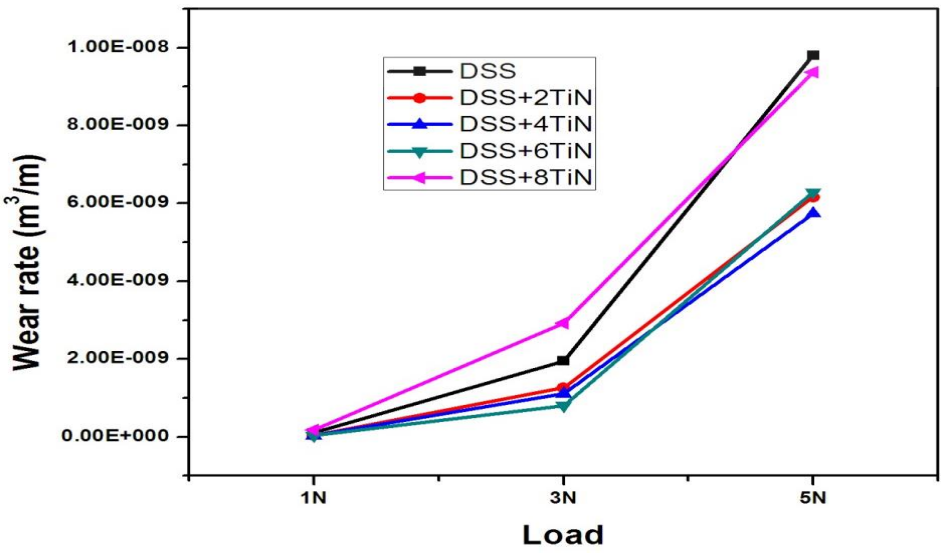

Figure 4.14. Variation of wear rate as a function of applied loads of the nano TiN reinforced SAF 2205 steel.

Table 4.5. Calculated wear rate values of the nano TiN reinforced SAF 2205 steel.

Composites	**Wear rate (m^3/m)**		
	1N	3N	5N
SAF 2205	1.12735E-10	1.9542E-09	9.80851E-09
SAF 2205-2TiN	3.7327E-11	1.26987E-09	6.16291E-09
SAF 2205-4TiN	3.71384E-11	1.11227E-09	5.7393E-09
SAF 2205-6TiN	3.67614E-11	8.09128E-10	6.2879E-09
SAF 2205-8TiN	1.80602E-10	2.92621E-09	9.37076E-09

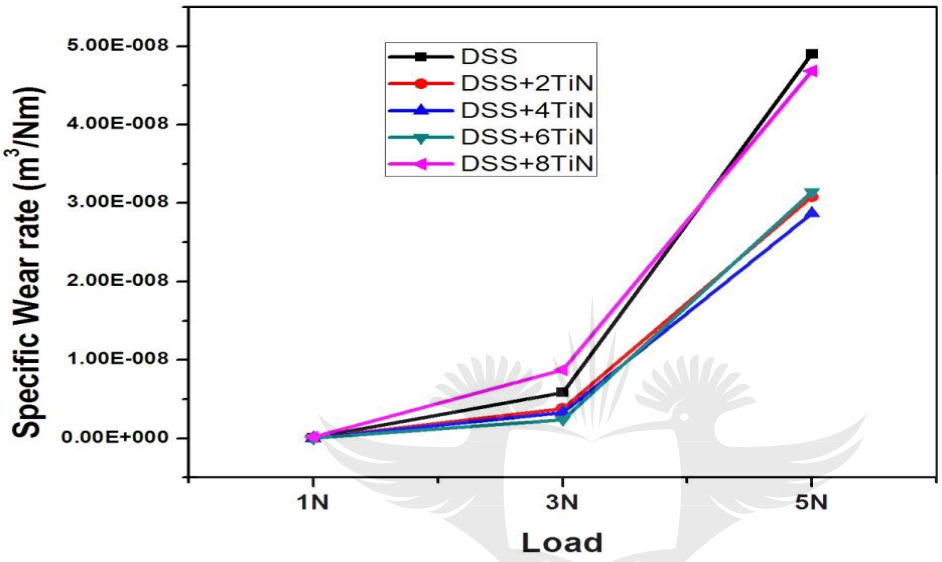

Figure 4.15. Variation of specific wear rates with loads of the nano TiN reinforced SAF 2205 steel.

Table 4.6. Calculated specific wear rate values of the nano TiN reinforced SAF 2205 steel.

Composites	**Specific wear rate (m^3/Nm)**		
	1N	3N	5N
SAF 2205	1.12735E-10	5.86259E-09	4.90425E-08
SAF 2205-2TiN	3.7327E-11	3.80961E-09	3.08145E-08
SAF 2205-4TiN	3.71384E-11	3.3368E-09	2.86965E-08
SAF 2205-6TiN	3.67614E-11	2.42738E-09	3.14395E-08
SAF 2205-8TiN	1.80602E-10	8.77862E-09	4.68538E-08

4.3.4 Microstructural Analysis of Wear Properties

4.3.4.1 Wear Tracts

The impact of nano TiN reinforcements and applied loads on the wear width of the SAF 2205 composites are presented and discussed in this section. Figure 4.16 presents secondary electron images of wear tracks showing variation in wear widths with wear loads for unreinforced steel samples. A detail of wear width values for all composites is presented in

Table 4.8. Lower and same magnification scale was selected in order to reveal the features and wear width profiles of the sintered samples. As can be seen in the Figure 4.16, the wear scars on the surfaces of the unreinforced stainless steel show progressive increase in wear track width with increase in load from 1 to 5 N because of the relatively ductility of steels. Upon increasing the normal load, the contact temperature is increased resulting in decreased strength of the steel.

Severe plastic deformations occurred on the steel ball surfaces, and larger new surfaces came into contact, thus resulting in a higher wear per unit load rate. Similar behaviour of increased wear track width with load (Table 4.7) is noted for all the composite grades irrespective of the amount of reinforcement, with the exception for SAF 2205 – 2TiN sample at 3 N and SAF 2205 – 6TiN at 5 N. Since wear width is a measure of the wear rate and has a direct relationship with the wear rate, it can be claimed that by increasing the wear width, the wear rate of the specimens will also increase [Iqbal *et al.*, 2017].

However, for each of the applied load the wear track widths were observed to increase with an increase in TiN reinforcement as presented in Table 4.8. Visual examination of the samples showed that the wear scar depths were shallow, but their widths were larger than that of the steel pair at each of the loads. The ceramic balls had much smaller plastic deformations due to their high hardness of the TiN. Wear rates per unit reinforcement irrespective of the applied loads were smaller for the composites than the steels.

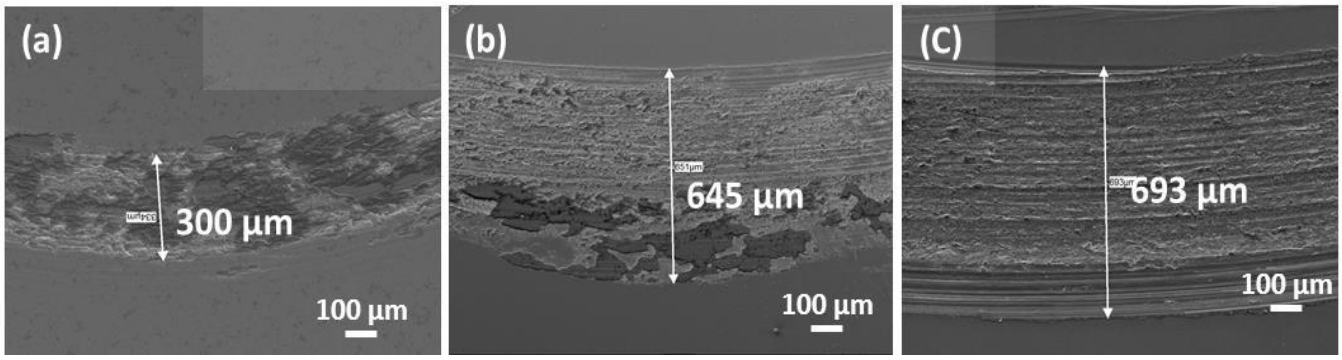

Figure 4.16. SEM images of the wear width configuration of unreinforced sintered stainless steel at (a) 1 N (b) 3 N and (c) 5 N.

Table 4.7. Summary of wear track widths of TiN nanoparticle reinforced SAF 2205 stainless steel under varying loads

Composites	1N (µm)	3N (µm)	5N (µm)
SAF 2205	300.0	645.0	693.0
SAF 2205-2TiN	347.0	572.0	900.0
SAF 2205-4TiN	404.0	669.0	1160.0
SAF 2205-6TiN	518.0	693.0	1220.0
SAF 2205-8TiN	649.0	780.0	1170.0

4.3.4.2 Wear Mechanism

In order to gain insight into the wear mechanisms of the specimens, the worn surfaces were examined by scanning electron micro-scope. Figure 4.17 show the micrographs of the worn tracks for the TiN reinforced steel samples at an applied load of 1 N. The wear tracks for the unreinforced (Figure 4.17a) and the stainless steel containing 2 vol% of TiN nanoparticles (Figure 1b) showed similar wear mechanisms. Figures. 4.17 (a & b) showed the presence of parallel grooves formed on the worn surface, which indicated that wear proceeded by an abrasive mechanism [Akbarpour and Alipour, 2017]. However, due to the relatively low hardness of these samples (Table 4.2), spalling chips formed during the wear process adhered to the steel surface. The adhesive wear component was established by the patches of material removal (Figure 4.17 (a & b)). Detailed evaluation of the wear track of the samples at 1 N applied load indicated a mixed mode of adhesive–abrasive wear mechanisms. Comparing Figs. 4.17 (a & b), it was evident that the extent of abrasive wear was more in the unreinforced stainless steel sample (Figure 4.17a) due to a comparatively lower coefficient of friction. The wear volumes and wear rates were high for these grades of composites because of the severe local plowing of the surface during the sliding test as discussed in previous sections.

On the other hand, by increasing the TiN nanoparticle content of the stainless steel composites as observed in Figures 4.17 (c and d), a dominant adhesive tribolayer of TiN forms on the surface [Jiang *et al.*, 2014], thereby smoothing and densifying the worn surface and resulting in shallower grooves (Figures 4.16 b). For these grades of composites, no significant plowing or fracturing is observed, and no protruding particles of TiN are formed on the worn surface. This could be attributed to the presence of increased TiN nanoparticles and limited stainless steel matrix flow during wear and due to the increase in hardness of these grades of composites [Sulima *et al.*, 2014]. The wear mechanism as compared with Figures 4.17 (a & b) shows a transition from adhesive–abrasive to predominantly adhesive

wear mechanism. The transition suggests that TiN particles exhibited excellent plowing effect and bonding with the matrix. The reinforcing TiN particles were noted to be homogenous with no evidence of crack during sliding, but show a marked tendency to adhere and undergo strain-hardening, thereby forming a tribolayer over the entire surface that enhances the wear resistance [Jiang *et al.*, 2014].

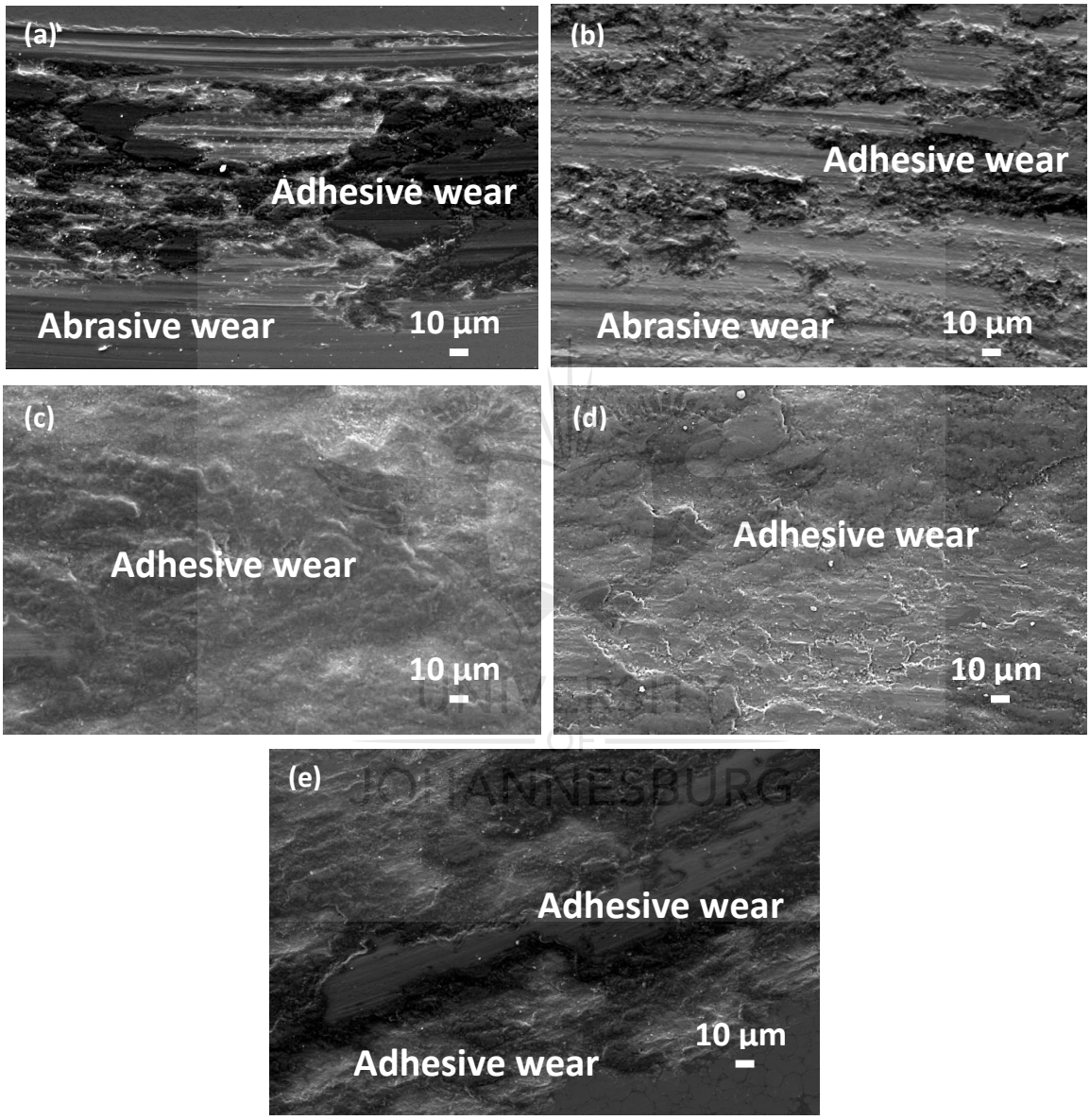

Figure 4.17. Secondary electron images showing wear tracks of composite under 1 N applied load (a) SAF 2205 (b) SAF 2205 + 2TiN (c) SAF 2205 + 4TiN (d) SAF 2205 + 6TiN (e) SAF 2205 + 8TiN

However, addition of excess amounts of TiN nanoparticles (8 vol%, Figure 4.17e) results in coarse microstructure which damage the TiN tribolayer and increase wear rate. This causes greater penetration of the ball on the composite surface, causing severe plastic deformation

and generation of substantial amount of debris. This degrades the wear resistance as discussed in the previous sections. This could be attributed to weak interface bonding between the duplex matrix and nanoceramic particles. Al-Mangour *et al.*, 2017, in their work reported that poor densification, thermal cracking, and high degree of coarsening of the microstructure may cause spalling of the tribolayer.

The SEM micrographs of the worn surface of the TiN nanoparticle reinforced stainless steel composites under 5 N applied load is presented in Figure 4.18. For the unreinforced stainless steel sample (Figure 4.18a), large plastic deformation is evidently observed on the worn region.

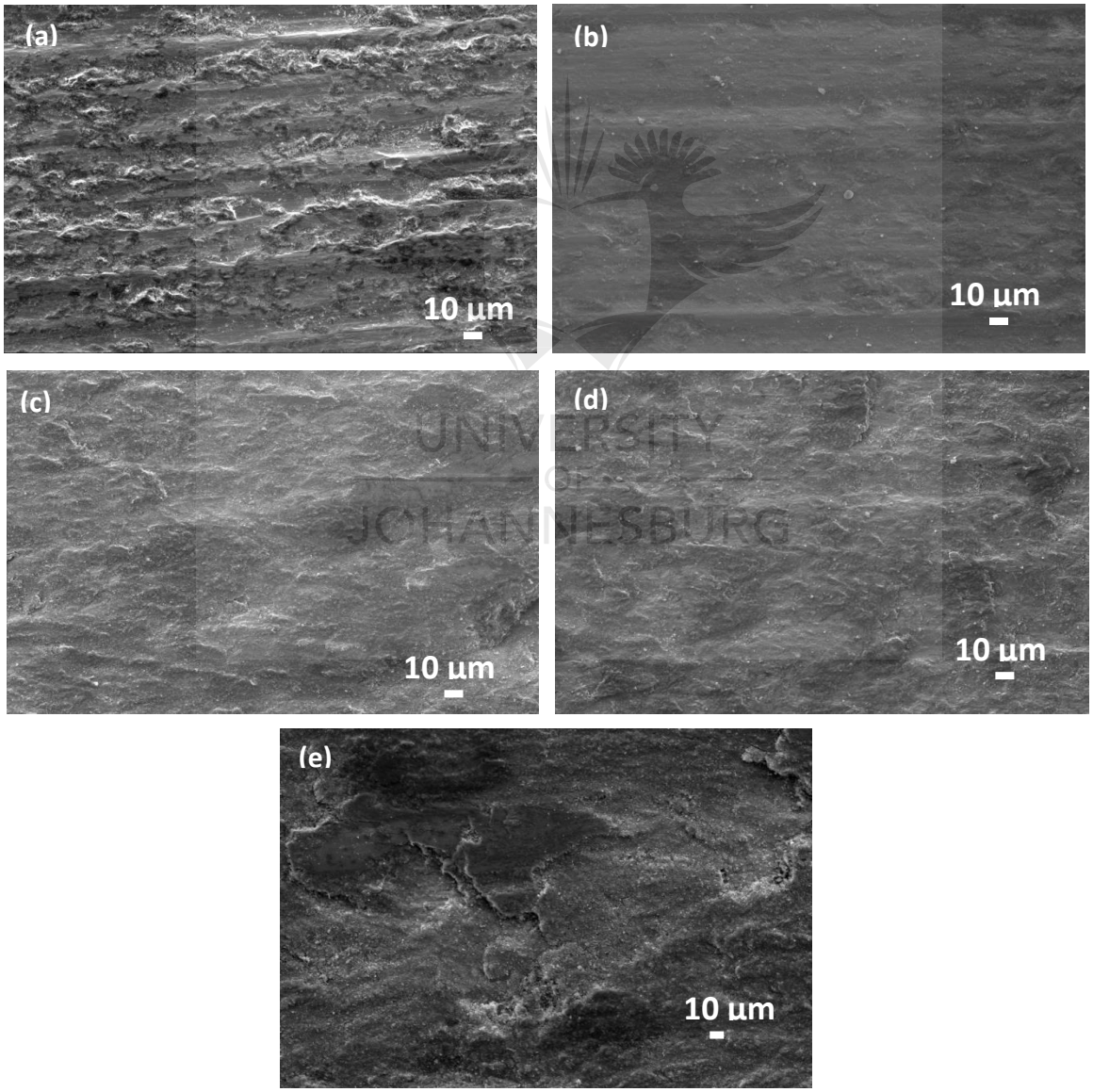

Figure 4.18. SE images of wear tracks of composite under 5 N applied load (a) SAF 2205 (b) SAF 2205 + 2TiN (c) SAF 2205 + 4TiN (d) SAF 2205 + 6TiN (e) SAF 2205 + 8TiN.

The morphology of the worn surface for stainless steel sample also showed the deep plow with scattered wear debris. The deep plow denotes that the wear occurred on the sample by abrasive mechanism, while the scattered wear debris is due to the adhesion wear mechanism. The morphology characteristics were noted to be similar to that conducted at 1 N of applied load. With the addition of nanoparticles of TiN up to 6 % (Fig. 4.18 c-d), less worn and shallow plow build up were observed on the sample surface. This indicates that abrasive wear on the sample but not severely compared to unreinforced stainless steel sample. Therefore, it can be concluded that TiN nanoparticles in form of tribolayers on the top of worn surface in the composite helped to decrease the plastic deformation in the subsurface region and alleviate severe wear. However, with the increase in the TiN content to 8 vol%, the wear conditions become more severe and the particles adhering to the surface are increased by delamination mechanism (Fig. 4.18e). The dominant wear mechanism was severe abrasion, which led to the micro-cracking and ploughing of the surface layers.

CHAPTER 5: CONCLUSIONS AND RECOMMENDATIONS

5.1 Conclusions

This work investigated the effect of nanosized titanium nitride addition on the microstructure, nanoindentation properties and wear behaviour of spark plasma sintered SAF 2205. The results are summarized as follows:

1. The microstructure revealed that the TiN nanoparticles dominated the ferrite/ferrite, ferrite/austenite and austenite/austenite grain boundaries.
2. Nanoindentation results revealed that plastic (H) property, elastic (E) property, the strain-to-break parameter (H/Er) and the resistance to plastic deformation parameter (H^3/Er^2) of the SAF 2205-TiN nanocomposites improved with increasing TiN content.
3. Nano-particles strengthening and grain boundary strengthening were noted to be the dominant strengthening mechanisms which accounted for improved nanohardness and resistance to elastic strain to failure of the composites.
4. With the increase of the TiN content, the micro and nanohardness of composites increased, but there was no change significantly between composites reinforced with 6 wt% and 8 wt% TiN.
5. The coefficient of friction reduces with increase in applied load. Coefficient of friction for the composites were higher than that of the matrix alloy.
6. Increase in applied load increases the volume loss. Also increase in wt.% of TiN nano reinforcement reduces the wear volume. Increase in wear resistance was noted with increase in TiN nanoparticle reinforcements up to 6 % volume fraction.
7. For each of the applied loads the wear track widths were observed to increase with an increase in TiN reinforcements.
8. Assessment of the morphology of the worn surface indicated a mixed mode of adhesive–abrasive wear mechanisms at lower volume fractions of TiN reinforcement. However, for higher volume fraction of TiN, a transition from adhesive–abrasive to predominantly adhesive wear mechanism was noted.
9. The composites possessed excellent wear resistance in terms of wear volume, wear and specific wear rates as compared with the unreinforced stainless steel. Composite with DSS–6 wt% TiN reinforcement shows better wear resistance compared to its matrix alloy and other compositions.

5.2 Recommendations

Maximizing the potentials of dispersion strengthened stainless steels will no doubt be a motivating scheme for materials scientists and engineers to pursue. Further research is required to extend the contribution of this thesis to establish a better understanding of the dispersion of nano TiN particles in duplex stainless steel. Some recommendations to advance the knowledge of the subject are summarized in this section.

1. There is a need for complete understanding of the intrinsic properties (they are determined by the structure at the atomic scale) of the TiN reinforced duplex stainless steels. Although many engineering applications of materials are determined by their properties and are dependent on the materials microstructure but intrinsic properties are considered during materials selection process. These properties influence the electrical, magnetic, dielectric and thermal behaviors of materials. This suggestion for instance, by determining the chemical inertness of TiN reinforced duplex stainless steels at high temperature will enhance its applications in the chemical and metallurgical industries.
2. High temperature nanoindentation and tribology tests should be carried out on the TiN reinforced duplex stainless steels to ascertain the materials behavior (hardness, modulus and wear) at elevated temperatures. Additional data from aqueous and high temperature tribo-corrosion will expand the scope of application of the nanoceramics reinforced DSS 2205.
3. Advanced materials characterization techniques will provide proper analysis and in-depth understanding of the materials microstructure. Thus improving the underlying principles and mechanism governing the behavior of the materials under study. Techniques such as TEM, Raman spectroscopy and EBSD should be carried out in order to understand the dislocation and strengthening mechanism of the TiN reinforced Duplex stainless steel. X-ray microscope and TEM techniques would be suited to study the worn surface of the materials after wear test to identify whether there has been phase transformations and also to determine whether the counter body material worn off or not during testing.
4. Presently, there are limited literatures on the plastic deformability, fracture, creep and fatigue on dispersion strengthened stainless steels. Studies in this direction should be embarked on for a thorough understanding of its mechanical and wear behavior.

CHAPTER 6: REFERENCES

American Society for Testing and Materials. 2005. Test method for wear testing with a pin-on-disk apparatus. ASTM G99-05 standard. Annual book of ASTM standards.

Abdi, S., Khoshkhoo, M.S., Shuleshova, O., Bönisch, M., Calin, M., Schultz, L., Eckert, J., Baró, M., Sort, J. & Gebert, A. 2014. Effect of Nb addition on microstructure evolution and nanomechanical properties of a glass-forming Ti– Zr–Si alloy, *Intermetallics* 46, 156 –163.

Akbarpour, M.R. & Alipour, S. 2017. Wear and friction properties of spark plasma sintered SiC/Cu nanocomposites. *Ceramics International*, 43 (16), 13364-13370.

AlMangour, B., Grzesiak, D. & Yang, J-M. 2017. In-situ formation of novel TiC-particle-reinforced 316L stainless steel bulk-form compo sites by selective laser melting. *Journal of Alloys and Compounds*, 706, 409-418.

Al-Samarai, R.A., Haftirman, K.R.A. & Al-Douri, Y. 2012. Effect of load and sliding speed on wear and friction of aluminum–silicon casting alloy. *International Journal of Science Research Publication*, 2, 1 –4.

Alvarez-Armas. I. 2008. Duplex Stainless Steels: Brief History and Some Recent Alloys. *Recent Patents on Mechanical Engineering 1*, 1, 51-71.

Angerer, P., Yu, L.G., Khor, K.A., Korb, G. & Zalite, I. 2005. Spark-plasma-sintering (SPS) of nanostructured titanium carbonitride powders, *Journal of the European Ceramic Society*, 25, 1919–1927.

Antona, P.I., P. L., & Mapelli, C. 2013. Hot Isostatic Pressing (HIP): the State of the Art and Improvement on Two Steels. *Metallurgical Science and Tecnology*, 19 (2).

Aribo, S., Barker, R., Hu, X. & Neville, A. 2013. Erosion–corrosion behaviour of lean duplex stainless steels in 3.5%NaCl solution. *Wear*, 302, 1602–1608.

Asgari, H. & Mohammadi, M. 2018. Microstructure and mechanical properties of stainless steel CX manufactured by direct metal laser sintering. *Materials Science and Engineering A*, 709, 82-89.

ASTM E2546-07. 2007. Standard Practice for Instrumented Indentation Testing, ASTM International, West Conshohocken, PA, www.astm.org.

ASTM G99-05. 2005. Standard Test Method for Wear Testing with a Pin-on-Disk Apparatus, ASTM International, West Conshohocken, PA, www.astm.org.

Baeslack III, W.A., Duquette, D.J. & Savage, W.F. 1979. The effect of ferrite content on stress corrosion cracking in duplex stainless steel weld metals at room temperature. *Corrosion.* 35 (2), 45-54.

Balancin, O., Hoffmann W.A.M. & Jonas, J.J. 2000. Influence of the microstructure on the flow behavior of duplex stainless steels at high temperatures. *Metallurgical and Materials Transactions A.* 31(2), 1353-1364.

Barber, J.R. & Ciavarella, M. 2009. Contact Mechanics. *International Journal of Solids and Structures,* 37 (1-2), 29-43.

Bellemans, J., Ries, M.D. & Victor, J. 2005. Total knee anthoplasty: A guide to get better performance. *Springer Medizin Verlag Heidelberg,* 90-95.

Bengisu, M.T. & Akay, A. 1991. Stick-Slip oscillations: Dynamics of Friction and Surface Roughness. *Journal of Acoustical Society of America,* 105 (1), 194-205.

Bhattacharya, A. & Singh, P.M. 2007. Stress corrosion cracking of welded 2205 duplex stainless steel in sulfide-containing caustic solution. *Journal of Failure Analysis and Prevention,* 7 (5), 371-377.

Bhowmick, S. & Nowell, M.M. 2014. Mechanical properties of ferrite and austenite phases in duplex steel: A combined EBSD and SEM nanoindentation study, Application note, *Hysitron.*

Black J.T. & Kohser, R.A. 2012. DeGarmo's Materials and Processes in Manufacturing. *Wiley,* 9, 226.

Ed: Blau, P.J. & Shaffer S.J. 2005. 15th Conference on Wear of Materials. Technology and Engineering 259, San Diego, CA, USA, 1-12, 434.

Bowden F.P. & Tabor, D. 1950. *Friction and Lubrication of Solids*. 2. *Clarendon, London.*

Brammer, D.R. & P.J. Hughes, P.J. 1988. The Development and Applications of Duplex Stainless Steel for Control Valve Equipment. *Proceedings of 2nd International Conference on Developments in Valves and Actuators for Fluid Control*. 115-135.

E. Broitman, E. “Indentation hardness measurements at macro-, micro-, and nanoscale: a critical overview.” *Tribology Letter 65,* 1 (2017): 23

D.H. Buckley and R. L. Johnson. “The influence of crystal structure and some properties of hexagonal metals on friction and adhesion.” *Wear 11*, 6 (1968): 405-419.

Bushan, B. (2001) Nano- to microscale wear and mechanical characterization using scanning probe microscopy. Wear. 251 (1-12): 1105-1123.

Campos, M., Bautista, A., Caceres, D., Abenojar, J. & Torralba, J.M. 2003. Study of the interfaces between austenite and ferrite grains in P/M duplex stainless steel, Journal of the European Ceramic Society, 23, 2813-2819.

Cao, Y., Wang, Y.B., An, X.H., Liao, X.Z., Kawasaki, M., Ringer, S.P., Langdon, T.G. & Zhu. Y.T. 2013. Concurrent microsructural evolution of ferrite and austenite in a duplex stainless steel processed by high-pressure torsion, *Acta Materialia*, 63, 16-29.

Chail, C. & P. Kangas, P. 2016. Super and hyper duplex stainless steels: structures, properties and applications. *Procedia Structural Integrity*, 2, 1755-1762.

Chan, W.K. & Tjong, S.C. 2014. Effect of secondary phase precipitation on the corrosion behavior of duplex stainless steels, *Materials,* 7, 5268-5304.

Charles, J. 2008. Duplex Stainless Steels: A Review after ’07 Held in Grado. *Steel Research International*, 79, 6, 455-465.

Charles, J. & Chemelle, P. 2011. The history of duplex developments, nowadays DSS: Properties and duplex market future trends. In *Proceeding of the 8th Duplex Stainless Steels Conference, Beaune, France*, 2.

Chen, J.B., Yang, J., Zhang, Q., Huang, H., Li, H., Tang, H. & Li, C. 2015. Tribological properties of copper-based composites with copper coated NbSe2 and CNT, *Mater. Des*. 75, 24-31.

Chong, D. 1995. Metal injection molding of PH 13-8 Mo stainless steel. *Materials and Manufacturing Processes,* 10 (3), 415-423.

Choudhury, Y. & P. Gupta, P. 2017. Wear Behavior of Composites and Nanocomposites: A New Approach. Recent Trends in Nanomaterials. *In Recent Trends in Nanomaterials Synthesis and Properties*, 29-34.

Cormier, D.H. & West, H. 2004. Characterisation of H13 steel produced via electron beam melting. *Rapid Prototyping Journal*, 10 (1), 35-41.

Costinescu, L., Marin, A., Cojocariu, C. & Munteanu, D. 2011. Testing the mechanical properties of materials at nanoscale; the nanoindentation method. Bulletin of the Transilvania University of Brasov Series I: *Engineering Sciences 4*, 53 (2), 67-74.

Cuardado, N., Casellas, D., Anglada, M. & E. 2012. Jimenez-Pique Evaluation of Fracture Toughness of Small Volumes by Means of Cube-Corner Nanoindentation. *Scripta Materialia*, 66 (9), 670-673.

Cui, W., Qin, G., Duan, J. & Wang, H. 2017. A graded nano-TiN coating on biomedical Ti alloy: low friction coefficient, good bonding and biocompatibility. *Mater. Sci. Eng. C* 71, 520-528.

Dille, J., Areiza, M.C.L., Tavares, S.S.M., Pereira, G.R., De Almeida, L.H. & J. M. A. Rebello, J.M.A. 2017. Microstructural evolution during aging at 800° C and its effect on the magnetic behavior of UNS S32304 lean duplex stainless steel. *Journal of Magnetism and Magnetic Materials*, 426, 102-107.

Dobrzanski, L.A., Brytan, Z., Grande, M.A., Rosso, M. & Pallavicini, E.J. 2005. Properties of vacuum sintered duplex stainless steels. *Jour. Of Ma. Proc. Tech.*, 162-163, 286-292.

Dohda, K., Boher, C., Rezai-Aria F. & Mahayotsanun, N. 2015. Tribology in metal forming at elevated temperatures. *Friction*, 3 (1), 1-27.

Dong, P., Wang, Z., Wang, W., Chen, S. & Zou, J. 2016. Understanding the spark plasma sintering from the view of materials joining. *Scripta Materialia*, 123, 11-121.

Donik, Č., Kocijan, A., Grant, J.T., Jenko, M., Drenik, A. & B. Pihlar, B. 2009. XPS study of duplex stainless steel oxidized by oxygen atoms". *Corrosion Science*, 51 (4), 827-832.

Dowling, N.E. 2012. Mechanical Behaviour of Materials: Engineering Methods for Deformation, *Fracture and Fatigue*, 4, 954.

Dowson, D., Dalmaz, G., Childs, T.H.C., Taylor, C.M. & Godet, M. 1992. Wear Particles: From the Cradle to the Grave, 418-420.

Dubois, J-M. & Esther, B-F. 2014. Friction and solid-solid adhesion on complex metallic alloys. *Science and technology of advanced materials*, 15, 3.

Elmer, J.W., Palmer, T.A. & Eliot, D.S. 2007. Direct observations of sigma phase formation in duplex stainless steels using in-situ synchrotron X-ray diffraction. *Metallurgical and materials transactions A,* 38 (3), 464-475.

Enneti, R.K., Onbattuvelli, V.P. & Atre, S.V. 2012. Powder binder formulation and compound manufacture in metal injection molding (MIM). Handbook of Metal Injection Molding, WoodHead Publishing Limited, 64-92.

Escriba, D.M., Materna-Morris, E., Plaut, R.L & Padilha, A.F. 2009. Chi-phase precipitation in a duplex stainless steel. *Materials Characterization,* 60 (11), 1214-1219.

Fargas, G., Mestra, A. & Maestro, A. 2013. Effect of sigma on the on wear behavior of super duplex stainless steel. *Wear,* 303, 584-590.

Ed: Fox-Rabinovich, G. & Totten, G.E. 2006. Self-Organization During Friction: Advanced Surface-Engineered Materials and Systems Design. *Technology and Engineering,* 197-230, 69-79.

Gadelrab, K.R., Li, G., Chiesa, M. & Souier, T. 2012. Local characterization of austenite and ferrite phases in duplex stainless steel using MFM and Nanoindentation. *Journal of Materials Research,* 27 (12), 1573-1579.

Gao, C. & Liu, A. 2017. Instrumented indentation of fused silica by Berkovich indenter. *Journal of Non-Crystalline Solids.* 475, 151-160.

Golovin, Y.I. 2008. Nanoindentation and mechanical properties of solids in submicrovolumes, thin near-surface layers, and films: a review. *Physics of Solids State,* 50, 2205-2236.

Grooves, M.P. 2007. Fundamentals of Modern Manufacturing: Materials, Processes, and Systems. Wiley & Sons Inc. *Technology and Engineering.* 3.

Guan, D., He, X., Zhang, R., Li, R. & Qu, X. 2018. Tribological and corrosion propert ies of PM 316L matrix composites reinforced by in situ polymer-derived ceramics. *Vacuum* 14 (8), 319 – 326.

Guillonneau, G., Kermouche, G., S. Bec, S. & Loubet, J-L. 2013. Determination of mechanical properties by nanoindentation independently of indentation depth measurement. *Journal of Materials Research,* 27 (19), 2551-2560.

Ed: Gunn, R.N. 1997. Duplex Stainless Steels: Microstructure, Properties and Applications. *Woodhead publishing*, 1997.

Guo, L.Q., Lin, M.C., Qiao, L.J. & Volinsky, A.A. 2013. Ferrite and austenite phase identification in duplex stainless steel using SPM technique. Journal of Applied Surface Science, 287, 499-501.

Guo, H., Chen, W., Shan, Y., Wang, W., Zhang, Z. & Jia, J. 2015. Microstructures and Propeerties of Titanium Nitride Films repared by Pulsd Laser Deposition at Different Substrate Temperatures. *Applied Surface Science*. 357A, 473-478.

Han, Y., Zou, D.N., Chen, Z.Y., Fan, G.W. & Zhang, W. 2011. Investigation on Hot Deformation Behavior of Cr23Ni4N Duplex Stainless Steel Under Medium-High Strain Rates, *Materials Characterization*, 62, 198-203

Hanief, M., & Wani, M.F. 2016. Effect of surface roughness on wear rate during running-in of En31-steel: Model and experimental validation. *Materials Letters* 176, 91-93.

Hanninen, H., Romu, J., Llola, R., Trevo, J. & Laitinen, A. 2001. Effects of Processing and Manufacturing of High Nitrogen-Containing Stainless Steels on Their Mechanical, Corrosion and Wear Properties. *Journal of Materials Processing Technology*, 117, 424-430.

Herrmann, K., Jennett, N.M., Wegener, W., Meneve, J. & K. Hasche. 2000. Progress in determination of the area function of indenters used for nanoindentation. *Thin Solid Films*, 377-378, 394-400.

Hertzman, S. & Charles, J. 2011. On the effect of nitrogen on duplex stainless steels, Revue de Metallurgie, 108, 413-425.

http://www.fct-systeme.de/en/content/Spark_Plasma_Sintertechnologie/~nm.20~nc.40/SPS-Technology.html, accessed on 12/06/2017

http://www.microstartech.com/index/NANOINDENTERS.pdf, accessed: 18/09/2016

http://www.toyo.co.jp/files/user/img/product/microscopy/pdf/5990-4907EN.pdf, Accessed: 18/09/2017.

http://www.futurelabs.co.in/wpcontent/uploads/2014/07/sem.jpg. Accessed on 21/12/2017.

https://www.nickelinstitute.org/~/media/Files/Publications/Typical%20fabrication%20defects.ashx, accessed: 08/09/2016.

Hutchings, I. & Shipway, P. 2017. Tribology: Friction and wear of Engineering Materials, 2.

Hynowska, A., Blanquer, A., Pellicer, E., Fornell, J., Suri~nach, S., Baro, M.D., Gonz Alez, S., Ibanez, E., Barrios, L. & Nogues, C. 2013. Novel Ti-Zr-Hf-Fe nano-structured alloy for biomedical applications. *Materials,* 6, 4930-4945.

Idriss, E.T. & Erkki, J. 2014. A descriptive model of wear evolution in rolling bearings," *Engineering Failure Analysis,* 45, 204-224.

Iqbal, Z., Merah, N., Nouari, S. & Shuaib, A.R. 2017. N. Al-Aqeeli. Investigation of wear characteristics of spark plasma sintered W-25wt%Re alloy and W-25wt%Re-3.2wt%HfC composite. *Tribology International,* 116, 129 –137.

ISO 14577-2:2015 Metallic materials -- Instrumented indentation test for hardness and materials parameters -- Part 2: Verification and calibration of testing machines, https://www.iso.org/standard/56628.html, accessed on 14/09/2017

Jiang, J., Stott, F.H. & Stack, M.M. 1998. The role of triboparticulates in dry sliding wear. *Tribology International*, 31 (5), 245–256.

Jie, Z., Zhang, X., Liu, Q., Yang, S. & Wang, Z. 2016. Effects of Load on Dry Sliding Wear Behavior of Mg–Gd–Zn–Zr Alloys. *Journal of Materials Science & Technology.*

Jin, C.X. & Plucknett, K.P. 2016. Microstructure instability in TiC-316L stainless steel cermets, Int. J. Refract. *Met. Hard Mater*. 58, 74– 83.

Kakas, D., Skoric, B., Mitrovic, S., Babic, M., Terek, P., Miletic, A. & Vilotic, M. 2009. Influence of load and sliding speed oon friction coefficient of IBAD deposited TiN. *Tribology in Industry*, 31, 3-4.

Zoltán, K., Szepvolgyi, J., Kaszuwara, W., Łabędź, O., & Bystrzejewski, M. 2015. Influence of ferrite stabilizing elements and Co on structure and magnetic properties of carbon-encapsulated iron nanoparticles synthesized in thermal plasma jet. *Journal of Alloys and Compounds*, 619, 592-600.

Kato, K. & Adachi, K. 2001. Wear Mechanisms. *Nanomaterials*. CRC Press LLC

Kennedy, F.E. 2001. Frictional Heating and Contact Temperatures: Surface Temperatures and Their Significance, Nanomaterials. *Modern Tribology Handbook*, 1, 235-272.

Kessel, H.U., Hennick, J., Schimdt, J., Weibgarber, T., Kieback, B.F., Herrmann, M. & Rathel, J. 2009. ''FAST'' Field Assisted Sintering Technology- A New Process for the Production of Metallic and Ceramic Sintering Materials, 1-37.

Kessel, H.U., Hennicke, J., Kirchner, R. & Kessel, T.2010. Rapid sintering of novel materials by FAST/SPS—further development to the point of an industrial production process with high cost efficiency. *FCT Systeme GmbH*, Rauenstein, Germany.

Kheradmand, N., Johnsen, R., Olsen, J.S. & and Barnoush, A. 2016. Effect of hydrogen on the hardness of different phases in super duplex stainless steel. *Int. Journal of hydrogen energy*, 41, 704-712.

Kiyohiro, Y., Kuribayashi, Y., Nogami, S., Kasada, R. & Hasegawa, A. 2014. Evaluation of irradiation hardening of proton irradiated stainless steels by nanoindentation. *Journal of Nuclear Materials*, 446, 142-147.

Klar, E. & Samal, P.K. 2007. Powder Metallurgy Stainless steels: Processing, Microstructures, and Properties. *ASM international*, 6-20.

Koch, S., Abad, M.D., Renhart, S., Antrekowitsch, H. & Hosemann, P. 2015. A high temperature nanoindentation study of Al-Cu wrought alloy. *Materials science and Engineering A.* 644, 218-224.

Koppad, P.G., Kashyap, K.T., Shrathinth, V., Shetty, T.A. & Koppad, R.G. 2013. Microstructure and microhardness of carbon nanotube reinforced copper nanocomposites. *Mater. Sci. Technol.* 29, 605-609.

Kovarikova, I., Szewczykova, B., Blasovitis, P., Hodulova, E. & Lechovic, E. 2009. Study and Characteristics of Abrasive Wear Mechanisms. *Material Science and Technology*, 1, 1-8.

Kralik, V. & Nemecek, J. 2014. Comparison of nanoindentation techniques for local mechanical quantification of aluminium alloy. *Materials Science & Engineering A*, 618, 118-128.

Krolczyk, G.M., Nieslony, P. & Legutko, S. 2015. Determination of tool life and research wear during duplex stainless steel turning. *Achieves of Civil and Mechanical Engineering,* 15 (2), 347-354.

Lancaster, J.K. 1967. The influence of substrate hardness on the formation and endurance of molybdenum disulphide films. *Wear,* 10,103–107.

Lancaster, J.K. 1990. The influence of environmental humidity and water on friction, lubrication and wear. *Tribology International, 23* (6), 371-389.

Lasebikan, A.B., Akisanya, A.R. & Deans, W.F. 2013. The Mechanical Behavior of a 25Cr Super duplex stainless steel at elevated temperature. *Journal of materials engineering and performance*, 22 (2), 598-606.

Lawn, B.R. & Cook, R.F. 2012. Probing material properties with sharp indenters: a retrospective. *Journal of Materials Science,* 47 (1), 1-22.

Leu, D.K. 2011. Evaluation of friction coefficient using indentation model of brinell hardness test for sheet metal forming. *Journal of Mechanical Science & Technology,* 25 (6), 509-1517.

Leyland, A. & Matthews, A. 2000. On the significance of the H/E ratio in wear control: a nanocomposite coating approach to optimised tribological behavior. *Wear*, 246, 1–11.

Li, H. & Ngan, H.W. 2003. Size effects of nanoindentation creep. *Journal of Materials Research*, 19 (2), 513-522.

Li, X. & Bhushan, B. 2001. A review of nanoindentation continuous stiffness measurement technique and its application. *Materials Characterisation,* 48, 11-36.

X. Li, D. Diao, And B. Bhushan "Fracture mechanisms of thin amorphous carbon films in nanoindentation*." Acta materialia. 45, 11 (1197)*, 4453-4461.

Lindgren, M., Suihkonen, R. & Vuorinen, J. 2015. Erosive wear of various stainless steel grades used as impeller blade materials in high temperature aqueous slurry. *Wear,* 328-329, 391-400

de Lima, M.S.F. & Sankaré, S. 2014. Microstructure and mechanical behavior of laser additive manufactured AISI 316 stainless steel stringers. *Materials & Design*, 55, 526-532.

R.T. Loto. “Pitting Corrosion Resistance and Inhibition of Lean Austenitic Stainless Steel Alloys”, *In Austenitic Stainless Steels-New Aspects, InTech*, 2017.

Lu, C. 2008. Study on Prediction of Surface Quality in Machining Process. *Journal of Materials Processing Technology 205*, 439-450.

Lundberg, O. 2014. Vibrations Induced by Surface Roughness in Nonlinear Rolling Contacts. *Licentiate Thesis*, Stockholm, Sweden.

Mahzoon, F., Behgazin, S.A., Nahrololoom, M.E. & Javadpour, S. 2012. Study the Fatigue-Wear Behaviour of Plasma Electrolytic Nitrocarburized (PEN/C) 316L Stainless Steel. *JMEPEG*, 21, 1752-1756.

Mallikarjuna, H.M., Ramesh, C.S., Koppad, P.G., Keshavamurthy, R. & Sethuram, D. 2017. Nanoindentation and wear behaviour of copper based hybrid composites reinforced with SiC and MWCNTs synthesized by spark plasma sintering. *Vacuum*, 145, 320-333.

Manda, S.K. 2015. Steel metallurgy: properties, specifications and applications. *McGraw-Hill Education.*

Mariappan, R., Kumaran, S., Rao T.S. & Chandrasekar, S.B. 2011. Microstructure and mechanical properties of duplex stainless steels sintered in different atmospheres. *Powder Metallurgy*, 54 (3), 236-241.

Masanta, M., Shariff, S. & Choudhury, A.R. 2011. Evaluation of modulus of elasticity, nano-hardness and fracture toughness of TiB 2–TiC–Al2O3 composite coating developed by SHS and laser cladding. *Mater. Sci. Eng. A*, 528, 5327–5335.

Masouros, G., Dimarogonas, A. & Lefas, K. 1977. A Model for Wear and Surface Roughness Transients During the Running-In of Bearings. *Wear*, 45, 375-382.

Mencik, J. 2007. Determination of mechanical properties by instrumented indentation. *Meccanica*, 42 (1),19-29.

Ed: Menezes, P.L., Ingole, S.P., Nosonovsky, M., Kailas, S.V., Lovell, M.R. 2013. Tribology for Scientists and Engineers: From Basics to Advanced Concepts. *Friction and Wear*, 43-91,

Michalska, J. & Sozańska, M. 2006. Qualitative and quantitative analysis of σ and χ phases in 2205 duplex stainless steel. *Materials Characterization*, 56 (4), 355-362.

Monclus, M.A., Lotfian, S. & Molina-Aldareguia, J.M. 2014. Tip Shape Effect on Hot Nanoindentation Hardness and Modulus Measurements. *International journal of precision engineering and manufacturing,* 15 (8), 1513-1519.

Moore, D.F. & Hopkins, D.W. 2013. Principles and Applications of Tribology: Pergamon International Library of Science Technology, Engineering and Social tudies: International Series in Materials Science and Technology. *Technology & Engineering*.

Moser, B., Schwaiger, R. & Dao, M. 2007. Size effects on deformation and fracture on nanostructured Metals. *Nanostructured Coatings*, 27-77.

Mouawad, B., Fabregue, D., Perez, M., Blat, M., Delabrouille, F., Domain, C. & Pokor, C. 2014. Sintering of ferritic and austenitic nanopowders using Spark Plasma Sintering. *Revue de Métallurgie–International Journal of Metallurgy*, 111 (5), 305-310.

Mousavi, S.M.R., Abarghouie, Seyed, R.S.M. 2010. Investigation of friction and wear behaviors of 2024 Al/SiCp composite at elevated temperatures. *Journal of Alloy Compounds*, 501, 326–32.

Muñoz, A., Igual, A. & Mischler, S. 2011. Effect of the environment on wear ranking and corrosion of biomedical CoCrMo alloys. *Journal of Materials Science: Materials in Medicine,* 22 (3), 437-450.

Musil, J., Kunc, F., Zeman, H. & Polakova, H. 2002. Relationships between hardness, Young's modulus and elastic recovery in hard nanocomposite coatings. *Surface and Coatings Technology*, 154, 304–313.

Ni, Z.F., Sun, Y.S., Xue, F., Bai, J. & Lu, Y.J. 2011. Microstructure and properties of austenitic stainless steel reinforced with in situ TiC particulate. *Materials and Design,* 32, 1462-1467.

Niu, B., Wang, X.G. & Fan, Z.M. 2013. Tribology characteristics of ex-situ and in-situ tungsten carbide particles reinforced iron matrix composites produced by spark plasma sintering. *Technol. Mater. Sci*., 28, 449 –454.

Nuruzzaman, D.M. & Mohammad, A.C. 2012. Friction and wear of polymer and composites. *Composites and Their Properties*.

Ojala, N., Kati, V., Atte, A., Anu, K., Jussi, M., Olli, O. & Kuokkala, V-T. 2016. Wear performance of quenched wear resistant steels in abrasive slurry erosion. *Wear,* 354, 21-31.

Oke, S.R., Ige, O.O., Falodun, O.E., Obadele, B.A., M.B. Shongwe, M.B. & Olubambi, P.A. 2017. Optimization of process parameters for spark plasma sintering of nano structured SAF 2205 composite. *Journal of Materials Research and Technology*, http://dx.doi.org/10.1016/j.jmrt.2017.03.004.

Oliver, W.C. & Pharr, G.M. 1992. An improved technique for determining hardness and elastic modulus using load and displacement sensing indentation experiments. *Journal of Materials Research*, 7, 1564-1583.

Olsson, J. 2005. Stainless steels for desalination plants. *Desalination, 183* (1-3), 217-225.

Onuoha, C.C., Jin, C.X., Farhat, Z.N., Plucknett, K.P. 2016. The effects of TiC grain size and steel binder content on the reciprocating wear behaviour of TiC-316L stainless steel cermets, *Wear,* 350–351, 116–129.

Outokumpu, O. Handbook of stainless steels, www.outokumpu.com/.../outokumpu-stainless-steel-handbook.pdf, *accessed on 05/12/2017*.

Oyama .S.T. 1996. The chemistry of Transition Metal Carbides and Nitrides: Introduction to the chemistry of transition metal carbides and nitrides. Springer, 1-27.

Zhang, P.F., Chen, J., Su, H-L., Kuo, Y-H., Su, C-L., Chen, Y-H., S-H., Lin, K-J., Hsieh, P-H. & Hwang, W-S. 2016. Effects of rare earth metals on steel microstructures. *Materials,* 9 (6), 417.

Paro, J., Hanninen, H. & Kauppinen, V. 2001. Tool wear and machinability of HIPed P/M and conventional cast duplex stainless steels. *Wear*, 249, 279-284.

Petterson, R. & Jernkontorent. 2013. The two-phase optimization of DSS." *Swedish Steel Producers' Association*.

Phani P.S. & Oliver, W.C. 2016. A direct comparison of high temperature nanoindentation creep and uniaxial creep measurements for commercial purity aluminium. *Acta Materialia, 111,* 31-38.

Pittsburgh. PA. 2014. Practical guidelines for the fabrication of duplex stainless steel.

Pohl, M., Storz, O. & Glogowski, T. 2007. Effect of intermetallic precipitations on the properties of duplex stainless steel. *Materials characterization,* 58 (1), 65-71.

Popovich, A., Sufiiarov, V., Polozov, I., Borisov, E., Masaylo, D. & Orlov, A. 2016. Microstructure and mechanical properties of additive manufactured copper alloy. *Materials Letters,* 179, 38-41.

Rahnejat. H. 2010. Tribology and Dynamics of Engine and Powertrain: Fundamentals, Applications and Future Trends. *Technology and Engineering*, 55-60.

Rao, R.N., Das, S., Mondal, D.P. & Dixit, G. 2001. Dry sliding wear behavior of cast high strength aluminium alloy (Al–Zn–Mg) and hard particle composites. *Wear,* 267, 88–95.

Rokanopoulou, A. & Papadimitrou, G.D. 2011. Titanium carbide/duplex stainless steel (DSS) metal matrix composite coatings prepared by plasma transferred arc (PTA) technique: microstructure and wear properties. *Journal of Coating Technology Research,* 8 (3), 427-437.

Sadeghpour, S., Kermanpur, A. & Najafizadeh, A. 2014. Investigation of the effect of grain size on the strain-induced martensitic transformation in a high-Mn stainless steel using nanoindentation. *Materials Science and Engineering A,* 612, 214-216.

Saeidi, K., Kevetkova, L. Lofaj, F. & Shen, Z. 2016. Novel ferritic stainless steel formed by laser melting from duplex stainless steel powder with advanced mechanical properties and high ductility. *Mat. Sci. and Eng*, 665, 59-65.

Saheb, N., Siddiqui, M.U., Arif, A.F.M., Akhtar, S.S. & Al-Aqeeli, N. 2014. Characterization of nanoreinforcement dispersion in inorganic nanocomposites: A review. *Materials*, 6-7, 4148 -4181.

Saxena, A., Singh, N., Kumar, D. & Gupta, P. 2017. Effect of Ceramic Reinforcement on the Properties of Metal Matrix Nanocomposites. *Materials Today: Proceedings 4*, 4, 5561-5570.

Sahu, J.K., Krupp, U., Ghosh, R.N. & H.J. Christ, H.J. 2009. Effect of 475 ^{o}C embrittlement on the mechanical properties of duplex stainless steel. *Materials Science and Engineering A,* 508, 1-14.

Schwarm, S.C., Kolli, R.P., Aydogan, E., Mburu, S. & Ankem, S. 2017. Characterization of phase properties and deformation in ferritic-austenitic duplex stainless steels by nanoindentation and finite element method. *Materials Science and Engineering: A*, 680, 359-367.

Schuh, C.A., Packard, C.E. & Lund, A.C. 2006. Nanoindentation and Contact-Mode Imaging at High Temperatures. *Journal of Materials Research, 21*, 725-736.

Stone, A. 2006. Practical considerations for successful hardness testing. *Materials Testing and Characterization, 83-85.*

Sequeira, T.P. & D.S. Santos, D.S. 2016. Microstructure, Properties and Hydrogen Embrittlement of a Super Duplex Stainless Steel Produced By Hot Isostatic Pressing. Rio Oil & Gas Expo and Conference, October, 24-27, 2016, in Rio de Janeiro.

Shahdad, S.A., Mccabe, J.F., Bull, S., Rusby, S. & Wassell, R.W. 2007. Hardness measured with traditional Vickers and martens hardness methods. *Dental Materials 23*, 1079-1085.

Sherif, El-Sayed, M., Potgieter, J.H., Comins, J.D., Cornish, L., Olubambi, P.A. & Machio, C.N. 2009. Effects of minor additions of ruthenium on the passivation of duplex stainless-steel corrosion in concentrated hydrochloric acid solutions." *Journal of applied electrochemistry*, 39 (8), 1385.

Shongwe, M.B., Diouf, S., Durowoju, M.O., Olubambi, P.A., Ramakokovhu, M.M. & Obadele, B.A. 2016. A comparative study of spark plasma sintering and hybrid spark plasma sintering of 93W-4.9Ni-2.1Fe heavy alloy. *Int. Journ. of Refr. Met. & Hard Mat.* 55, 16-23.

Sieurin, H. & Sandström, R. 2006. Austenite reformation in the heat-affected zone of duplex stainless steel 2205. *Materials Science and Engineering: A*, 418 (1), 250-256.

Skiba, T., Baufeld, B. & Van der Biest, O. 2009. Microstructure and mechanical properties of stainless steel component manufactured by shaped metal deposition. *ISIJ international*, 49 (10), 1588-1591.

Song, J-F., Low, S., Pitchure, D., Germak, A., Desogus, S., Polzin, T., Yang, H-Q. & Ishida, H. 1998. Establishing a worldwide unified Rockwell hardness scale using standard diamond indenters. *Measurement*, 24, 197-205.

Song, H., Yavas, H., Van Der Giessen, E. & Papanikolaou. 2017. Discrete dislocation dynamics simulations of nanoindentation with pre-stress: hardness and statistics of abrupt plastic events. *Cond. Mat. Matrl. Sci.*

Sotomayor, M.E., Sanz, J., Cervera, A., Levenfeld, B. and Várez, A. 2015. Surface modification of a duplex stainless steel for plastic-metal hybrid parts. *Archives of Materials Science and Engineering*, 72 (2), 86-93.

Sotomayor, M.E., Levenfeld, B. & Várez, A. 2011. Powder injection moulding of premixed ferritic and austenitic stainless steel powders. *Materials Science and Engineering: A*, 528 (9), 3480-3488.

Sotomayor, M.E., de Kloe, R., Levenfeld, B. & Várez, A. 2013. Microstructural study of duplex stainless steels obtained by powder injection moulding. *Journal of Alloys and compounds*, 589, 314-321.

Stefan, J., Kopriva, R., Eliasova, I. & Siegl, J. 2015. Comparison of conventional Mechanical Testing with Innovative Techniques for Determination of Mechanical properties of Nuclear Power Plant components. *Materials, Applied Mechanics and materials,* 84, 452-59.

Straffelini, G., Molinari, A. & Trabucco, D. 2002. Sliding wear of austenitic and austenitic-ferritic stainless steels. *Metallurgical and materials transactions A,* 33 (3), 613-624.

Stolaeski, T. 1999. Tribology in Machine Design. *Technology and Engineering, 20.*

Suarez, M., Fernandez, M.A., Menendez,J.L., Torrecillas, R., Kessel, H.U., Hennicke, J., Kirchner, R. and Kessel, T. 2013. Challenges and Opportunities for Spark Plasma Sintering: A Key Technology for a New Generation of Materials. *In Sintering Applications*. Chapter 13.

Stewart, S. & Ahmed, R. 2002. Rolling contact fatigue of coating surface- A Review. *Wear,* 253 (11-12), 1132-1144.

Stone, A. 2006. Practical considerations for successful hardness testing. *Materials Testing and Characterization*, 83-85.

Sulima, I., Jaworska, I. & Figiel, P. 2014. Influence of processing parameters and different content of TiB 2 ceramics on the properties of composites sintered by high temperature high pressure (HT-HP) method. *Archives of Metallurgy and Materials*, 59 (1), 203-207.

Sulima, I., Klimczyk, P. & Malczewski, P. 2014. Effect of TiB2Particles on the Tribological Properties of Stainless Steel Matrix Composites. *Acta Metall. Sin. (Engl. Lett.)*, 27(1), 12–18.

Tadjiev, D.R., Hand, R.J. & Hayes, S.A. 2010. Calibrating a nanoindenter for very shallow depth indentation using equivalent contact radius. *Philosophical Magazine*, 90 (13), 1819-1832.

Topolska, S., & Łabanowski, J. 2009. Effect of microstructure on impact toughness of duplex and superduplex stainless steels. *Journal of Achievements in Materials and Manufacturing Engineering*, 36 (2), 142-149.

Trenkle, J.C., Packard, C.E. & Schuh, CA. 2010. Hot nanoindentation in inert environments. *Review of Scientific Instruments*, 81 (7).

Turbine Francis Worn.JPG): https://upload.wikimedia.org/wikipedia/commons/d/d7/Turbine Francis_Worn.JPG, accessed on the 09/10/2017.

Utela, B., Storti, D., Anderson, R. & Ganter, M. 2008. A review of process development steps for new material systems in three dimensional printing (3DP). *Journal of Manufacturing Processes*, 10 (2), 96-104.

Varga, M., Flasch, M. & Badisch, E. 2017. Introduction of a novel tribometer especially designed for scratch, adhesion and hardness investigation up to 1000°C. *Proceedings of the Institution of Mechanical Engineers, Part J: Journal of Engineering Tribology*, 231 (4), 469-478.

de Vasconcelos, L.S., Xu, R., Li, J., and Zhao, J. 2016. Grid indentation analysis of mechanical properties of composite electrodes in Li-ion batteries. *Extreme Mechanics Letters*, 9 (3), 495-502.

Voisin, T., Durand, L., Karnatak, N., Gallet, S.L., Thomas, M., Berre, Y.L., Castagne, J-F. & Couret, A. 2013. Temperature control during spark plasma sintering and application to up-scaling and complex shaping. *Journal of Mat. Proc. Tech.*, 213, 269-278.

Voyiadjis, G.Z. & Peters, R. 2009. Size effects in nanoindentation: an experimental and analytical study. *Acta Mechanica*, 21, 131-153.

Wang, Z. 2012. Influences of sample preparation on the indentation size effect and nanoindentation pop-in on nickel. *PhD diss., University of Tennessee*,

http://trace.tennessee.edu/cgi/viewcontent.cgi?article=2482&context=utk_graddiss, accessed on 15/12/2016

Wang, L. & Rokhlin, S.I. 2005. Universal scaling functions for continuous stiffness nanoindentation with sharp indenters." *Int. Journal of Solids & Structures,* 42 (13),n 3807-3832.

Wang, X., Li, Y., Wang, S., Deng, Y., Xing, D. & He, S. 2015. Investigating the Nanomechanical Behaviour of Thermosetting Polymers Using High-Temperature Nanoindentation. *European Polymer Journal,* 70, 360-370.

Wang, M., Wang, T., Song, S., Ravi, M., Liu, R. & S. Ji. Enhanced Multiferroic Properties of YMnO3 Ceramics Fabricated by Spark Plasma Sintering Along with Low-Temperature Solid-State Reaction. *Materials,* 10 (5), 474.

Wen, S. & Huang, P. 2012. Principles of Tribology, *John Wiley & Sons.*

Wheeler, J.M. & Michler, J. 2013. Indenter Materials for High Temperature Nanoindentation. *Review of Scientific Instruments,* 84 (10).

Wheeler, J.M., Armstrong, D.E.J., Heinz, W. & R. Schwaiger, R. 2015. High temperature nanoindentation: The state of the art and future challenges. *Current Opinion in Solid State and Materials Science,* 19 (6), 354-366.

R.J.K. Wood. R.J.K. 2007. Tribo-corrosion of coatings: a review. *Journal of Physics D: Applied Physics, 40* (8).

Wu, L., Guo, X. & Zhang, J. 2014. Abrasive resistant coatings - a review. *Lubricants,* 2, 66-89.

Wu, M-W., Huang, Z-K., Tseng, C-F. & K-S. Hwang, K-S. 2015. Microstructures, mechanical properties, and fracture behaviors of metal-injection molded 17-4PH stainless steel. *Metals and Materials International,* 21 (3), 531.

Wu, H., Zhao, J., Cheng, X., Xia, W., He, A., Yun, J., Huang, S., Wang, L., Huang, H., Jiao, S. & Jiang, Z. 2018. Friction and wear characteristics of TiO2 nano-additive water-based lubricant on ferritic stainless steel. *Tribology International,* 117, 24–38.

Xu, J., Wang, G.D., Lu, X., Liu, L., P. Munroe, P., Xie, Z-H. 2014. Mechanical and corrosion-resistant properties of Ti-Nb-Si-N nanocomposite films prepared by a double glow discharge plasma technique, *Ceram. Int*. 40, 8621-8630.

Yan, F.K., Zhang, B.B., Wang, H.T., Tao, N.R. & Lu, K. 2016. Nanoindentation characterization of nano-twinned grains in an austenitic stainless steel. *Scripta Materialia*, 112, 19-22.

Yilzmaz, O. & Ugla, A.A. 2016. Shaped metal deposition technique in additive manufacturing: A review. *Proceedings of the Institution of Mechanical Engineers, Part B: Journal of Engineering Manufacture,* 230 (10), 1781-1798.

Yunan, P., Ibrahim, K. & Wan Nik W.B. 2009. Effect of pH and Chloride Concentration on the Corrosion of Duplex Stainless Steel, *The Arabian Journal for Science and Engineering,* 34. Number 2C.

Yust. C.S. 1985. Tribology and Wear. *International Metals Reviews,* 30 (1), 141-154.

Zhang, L., Yu, P., Cheng, H., Zhang, H., Diao, H., Shi, Y., Chen, B., P. Chen, P., Feng, R., Bai, J. and Q. Jing, Q. 2016. Nanoindentation Creep Behavior of an Al0. 3CoCrFeNi High-Entropy Alloy. *Metallurgical and Materials Transactions A*, 47(12), 5871-5875.

Zhang, Z., Chen, Y., Zuo, L., Zhang, Y., Qi, Y. & K. Gao, K. 2017. The effect of volume fraction of WC particles on wear behavior of in-situ WC/Fe composites by spark plasma sintering. *International Journal of Refractory Metals & Hard Materials,* 69, 196–208.

Zhang, J. & Meng, Y. 2015. Boundary Lubrication by Adsorption Film. *Friction,* 3 (2) 115-147.

Zhao, Y., Zhang, W., Liu, Z. & Wang, G. 2017. Development of an easy-deformable Cr21 lean duplex stainless steel and the effect of heat treatment on its deformation mechanism. *Materials Science and Engineering: A,* 702, 279-288.

Zimmerman, F.X. & Toops, J. 2008. Hot Isostatic Pressing: Today and Tomorrow. *Avure Technologies, www.avure.com*.

Zmitrowics, A. 2006. Wear patterns and laws of wear: A Review. *Journal of Theoretical and Applied Mechanics,* 44 (2), 219-253.

Zucato, I., Moreira, M.C., Machado, I.F. & Lebrao. S.M.G. 2002. Microstructural characterisation and the effect of phase transformations on toughness of the UNS S31803 duplex stainless steel aged treated at 850^0C. *Materials Research*, 5 (3), 385-389.